Coordination Chemistry Reviews 484 (2023) 215101

Contents lists available at ScienceDirect

Coordination Chemistry Reviews

journal homepage: www.elsevier.com/locate/ccr

Review

Structure-directed growth and morphology of multifunctional metal-organic frameworks

Qi Huang, Yun Yang *, Jinjie Qian *

Key Laboratory of Carbon Materials of Zhejiang Province, College of Chemistry and Materials Engineering, Wenzhou University, Wenzhou, Zhejiang, PR China

ARTICLE INFO

Article history:
Received 24 December 2022
Accepted 28 February 2023
Available online 14 March 2023

Keywords:
Metal-organic framework
Controllable Synthesis
Structure
Morphology
Multifunctionality

ABSTRACT

Metal-organic frameworks (MOFs) have attracted much attention in the whole materials science due to their structural tunability that endows precise size and morphology control. Meanwhile, hierarchical MOFs and their derivatives possess fascinating physicochemical properties with their special morphology, controllable nanostructure, ultra-high porosity, and large specific surface area, which have been widely used in the environment and energy fields. Here, the recent advances in controlled synthesis will be comprehensively introduced, mainly focusing on the transformation of MOF morphology and structure based on the following factors, such as precursors, substrates, and synthesis methods. Furthermore, the progress of relevant MOF applications, including gas storage and separation, dye adsorption, heterogeneous catalysis, and fuel cells, is described to emphasize the intrinsic structure–property relationship. Lastly, the challenges and intractable dilemmas arising in their controlled synthesis and performance applications are also briefly discussed.

© 2023 Elsevier B.V. All rights reserved.

Contents

1. Background . . . 2
2. Tunable structure of MOFs . . . 3
   2.1. Metals . . . 3
   2.2. Ligands . . . 5
   2.3. Secondary building units . . . 6
   2.4. Solvents . . . 7
   2.5. Surfactants . . . 9

Abbreviations: 1D, One-dimensional; AFM, Atomic force microscopy; ATRP, Atom transfer radical polymerization; BBB, Blood-brain barrier; BET, Brunauer-Emmett-Teller; CA, Cyanuric acid; CMC, Carboxymethylcellulose; COFs, Covalent organic frameworks; CO_2RR, CO_2 reduction reaction; CP, Carbon paper; CPL, Cyclopentanol; CTAB, hexadecyltrimethylammonium bromide; CUR, Curcumin; CV, Cyclic voltammetry; CVD, Chemical vapor deposition; DABCO, 1,4-Diazabicyclo[2.2.2]octane; DEF, *N,N*-Diethylformamide; DMF, *N,N*-Dimethylformamide; EBL, Electron-beam lithography; EDS, Energy dispersive X-ray spectroscopy; EtOH, Ethanol; FE, Faraday efficiency; GBM, Glioblastoma multiforme; HAADF-STEM, High-angle annular dark field scanning TEM; H_4ABTC, 3,3′,5,5′-Azobenzenetetracarboxylic acid; H_2BDC, 1,4-Benzenedicarboxylic acid; H_3BO_3, Boric acid; H_4BPTC, Biphenyl-3,3′,5,5′-tetracarboxylic acid; H_3BTB, Benzene-1,3,5-tris(4-benzoic acid); H_3BTC, 1,3,5-Benzenetricarboxylic acid; HdcIm, 4,5-Dichloroimidazole; HER, Hydrogen evolution reaction; HHTP, 2,3,6,7,10,11-Hexahydroxytriphenylene; H_2IPA, Isophthalic acid; H_2NDC, Naphthalene-1,4-dicarboxylatic acid; HOFs, Hydrogen-bonded organic frameworks; HOR, Hydrogen oxidation reaction; IM, Imidazole; L-I, 2,5-Dihydroxyterephthalic acid; L-II, 3,3′-Dihydroxybiphenyl-4,4′-dicarboxylic acid; L-III, 2′,5′-Dimethyl-[1,1′:4′,1″-terphenyl]-3,3″-dihydroxy-4,4″-dicarboxylic acid; L-IV, 2′,2″,5′,5″-Tetramethyl-[1,1′:4′,1″-quaterphenyl]-3,3‴-dihydroxy-4,4‴-dicarboxylic acid; LIB, Lithium-ion battery; LSV, Linear sweep voltammetry; MAB, Metal-air battery; MeCN, Acetonitrile; MeOH, Methanol; MB, Methylene blue; MG, Main group; 2-MI, 2-Methylimidazole; SBUs, Secondary building units; SDS, Sodium dodecyl sulfate; SEM, Scanning electron microscopy; SUL, Sulindac; TAT, Triamterene; TCPP, Meso-tetra(4-carboxyphenyl)porphine; TEM, Transmission electron microscopy; TM, Transition metal; SIB, Sodium-ion battery; MIB, Metal-ion battery; MMA, Methyl methacrylate; MO, Methyl orange; MOFs, Metal-organic frameworks; NMR, Nuclear magnetic resonance; NRR, Nitrogen reduction reaction; NPs, Nanoparticles; OER, Oxygen evolution reaction; ORR, Oxygen reduction reaction; PBA, Prussian blue analogous; PES, Polyethersulfone; PS, Polystyrene spheres; PSM, Post-synthetic modification; PVP, Polyvinylpyrrolidone; RABV, Rabies virus; RhB, Rhodamine B; SLG, Single-layer graphene; TMPBPO, 1,1′-(2,3,5,6-Tetramethyl-1,4-phenylene)bis(methylene)dipyridinium-4-olate; TRD, Truncated rhombic dodecahedral; TPBE, 1,1,2,2-Tetrakis(4′-(pyridin-4-yl)-[1,1′-biphenyl]-4-yl)-ethene; TPEPA, (3S,3′S,3″S,3‴S)-4,4′,4″,4‴-[Adamantane-1,3,5,7-tetrayltetrakis-(phenylene-4,1-diyl)]tetrakis(but-1-yn-3-ol); TPOP, Titanium isopropoxide; XRL, X-ray lithography; XRD, Powder X-ray diffraction; ZAB, Zn-air battery.

* Corresponding authors.
E-mail addresses: bachier@163.com (Y. Yang), jinjieqian@wzu.edu.cn (J. Qian).

https://doi.org/10.1016/j.ccr.2023.215101
0010-8545/© 2023 Elsevier B.V. All rights reserved.

2.6. Others . . . 10
3. Controllable morphology of MOFs . . . 12
3.1. Substrates . . . 13
3.2. Templates . . . 14
3.3. MOF-on-MOFs . . . 14
3.4. Self-assembly . . . 15
3.5. Superstructures . . . 16
4. Novel synthetic strategies of MOFs . . . 18
4.1. Chemical vapor deposition . . . 18
4.2. Electrochemical growth . . . 19
4.3. Spray-drying . . . 20
4.4. Chemical etching . . . 21
4.5. Mechanochemistry . . . 21
4.6. Others . . . 22
5. Relevant applications of MOFs and their derivatives . . . 23
5.1. Gas storage and separation . . . 23
5.2. Dye adsorption and degradation . . . 24
5.3. Electrochemical catalysts . . . 26
5.4. Battery . . . 27
5.5. Heterogeneous catalysts . . . 30
5.6. Drug delivery . . . 31
6. Conclusion and perspectives . . . 31
Declaration of Competing Interest . . . 33
Acknowledgments . . . 33
References . . . 33

1. Background

Back in 1995, Omar M. Yaghi is the first man to report a coordination compound with a two-dimensional (2D) nanostructure constructed from a rigid organic ligand and the transition metal [1]. Since then, the concept of metal–organic frameworks (MOFs) is formally introduced, and a series of IRMOF, ZIF, MIL, NU, DUT, NOTT, UiO, etc. emerge in the following nearly two decades. As an emerging subclass of coordination polymers, MOFs are porous crystalline materials with ordered periodic topology formed by self-assembly of metal-based nodes, such as metal ions and/or metal clusters, also called secondary building units (SBUs), with various organic ligands [2-6]. Furthermore, the structure of MOFs can be induced by internal or external factors to change and eventually form the desired morphology, such as thin films, hollow tubes, etc., for specific fields. Therefore, an in-depth study of the effect on structure and morphology of MOFs will facilitate the facile and controlled synthesis of the desirable crystalline materials.

However, the structural control of MOF materials at multiple-scales remains a huge challenge nowadays, which is the key to translating scientific innovations in coordination chemistry from theory to real-world applications [7]. At the same time, the structural and chemical tunability of a large number of MOFs are associated with a wealth of metal nodes and organic linkers, allowing their synthesis to start with a strategic selection of precursor materials [8]. First of all, metal ions can be derived from easily soluble metal salts or low-solubility metal oxides [9,10]. This part owns various reaction properties due to different atomic radii and charge densities, and thus impacts the way of coordination with bridging linkers, leading to changes in the growth behavior of MOF crystals [11]. Besides, there are a wide variety of organic ligands, mostly based on aromatic carboxylates, which can be further functionalized with acidic groups (–COOH, -SO_3H), basic groups (–NH_2, –NH–), or even different organic compounds, resulting in activities derived from the nature of the grafted moieties [12]. It is well-known that these modified connectors can be used in an one-step synthesis of MOFs that completely or partially substitute the original linkers, which will interfere with the formation of the intended structure and empower different functionality to the target material.[13,14]. On the other hand, the structure-guiding role of inorganic SBUs is crucial for determining the topology of MOFs [15]. The multinuclear nature of SBUs gives a unique skeleton structure and mechanical stability compared to single-metal nodes, and also facilitates the development of MOFs with high porosity [16]. Meanwhile, solvents are also essential for maintaining framework stability in crystal preparation, usually as guest molecules filling the pores of MOFs, and also inducing transformations in morphology and structure of MOFs depending on the different solubility of metal salts and organic ligands [17]. In addition to the appealing influencing factors, altering various factors such as time, temperature, and pressure during the reaction can modulate the overall crystal morphology, optimize the pore structure to increase the accessible surface area, and improve the practical application of MOF-based products [18-20].

Despite the high intrinsic surface area of MOFs, the available region for large-sized molecules is limited to the pore size determined by the crystal structure, and further optimization of morphology can realize the full utilization of MOFs [21,22]. Normally, MOFs exist as polycrystalline micropowders, while they are assembled into specially shaped materials, such as membrane and hollow sphere, leading to unprecedented technological breakthroughs [23,24]. In this regard, the substrate-assisted approach is practical to guiding randomly grown MOF particles into unique and promising nanomaterials by the role of supports [25]. The substrates can be chosen from a wide range of insoluble materials with a specific morphology, such as conductive graphene and dielectric quartz glass, which can guide the formation of nano-thick MOF membranes over their surface in the lattice-matching situation [26,27]. Besides, the soluble substances, including soft-templates (surfactants, colloids) [28,29] and hard-templates (polystyrene spheres, silica spheres),[30,31] can also be selected to provide suitable conditions for the self-assembly process to enrich the pore structures and morphological features of MOFs. Moreover, these emerging MOF-on-MOFs structures synthesized with MOFs as supports will offer greater structural diversity and larger potential for performance enhancement, as the integration of MOFs with different functions will maximize their capabilities and generate

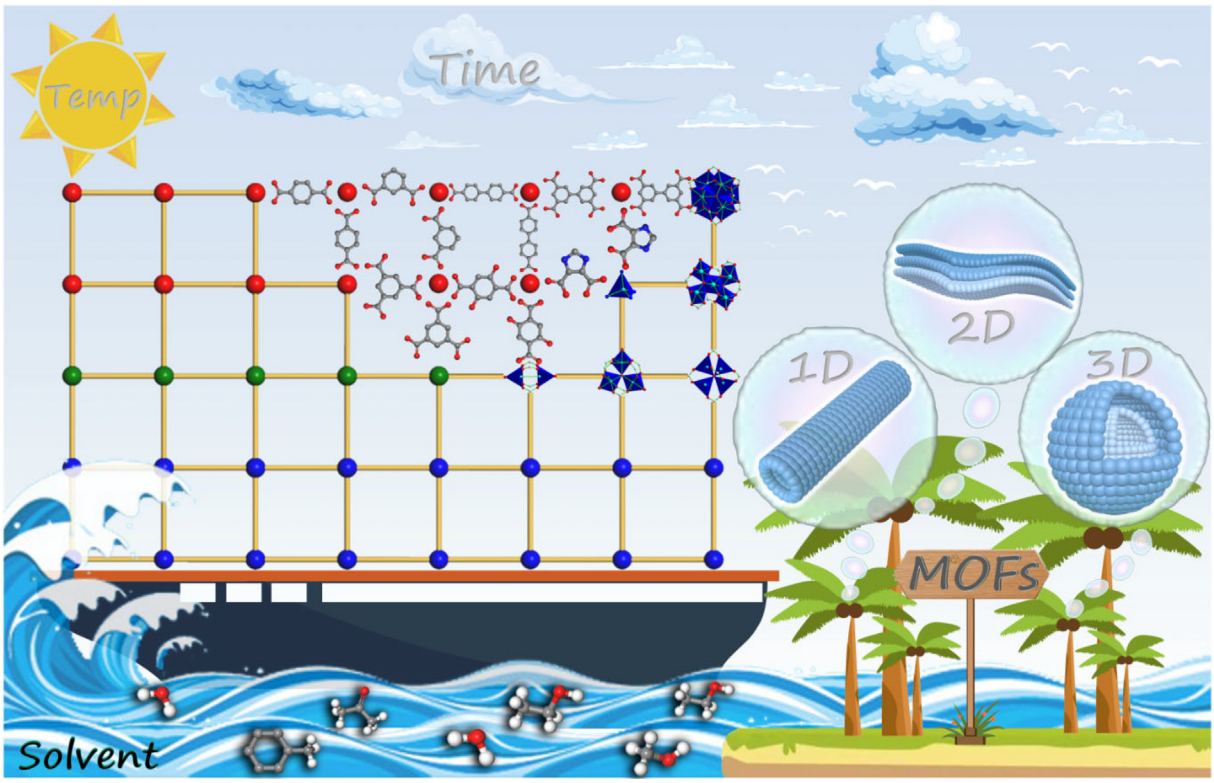

Scheme 1. Illustration for the construction elements of structure-induced MOFs. Here, the sun, clouds, ship, and sea represent the temperature, time, reaction vessel, and solvent, respectively, which are the basic conditions for the synthesis of MOFs. Finally, the crystals with 1D tubular, 2D sheet and 3D spherical morphologies can be synthesized in a controlled manner by changing various metal ions, organic ligands, and synthesis conditions.

unexpected properties [32,33]. At present, the most challenging aspect of MOF-based composites is the inhomogeneity of the composition, but this can be surmounted nicely with the help of well-shaped nanomaterials as a matrix through the bottom-up growth method [34]. Thus, the substrate-assisted synthesis strategy of MOFs provides a flexible way to tune the particle size and morphology, conferring attractive properties and advanced functionality while minimizing the amount of material used for breakthrough performance in environmental protection [35-37].

As for the traditional synthesis techniques like hydrothermal, microwave-assisted, and solvothermal methods, they are always limited in large-scale production, so there is an urgent need to propose innovative strategies to efficiently produce desirable MOF materials in a variety of forms [38]. For example, chemical vapor deposition (CVD) [39], and electrochemically growth strategies [40] can be used to acquire dense MOF films in large quantities, and the universality of the spray-drying method [41] has been testified to be applicable for the preparation of hollow superstructures. Furthermore, desirable hollow structures and multi-metal doped MOFs can be selectively prepared by chemical etching and mechanical grinding, respectively, for a wider range of applications.[42,43]. Ultimately, by selecting the structurally modified and morphologically tuned MOFs with high specific surface area, abundant porosity, and diverse components as precursors [44,45], they can be further transformed into metal oxides [46], metal phosphides [47], and metal carbides [48] with controlled porous structures, high porosity, and exposed active sites, which exhibit important applications in energy engineering [40,49].

In this review, we summarize the structural and morphological control methods of MOFs and several novel synthetic strategies, with particular emphasis on the respective different roles played by intrinsic and extrinsic influences as structure-guiding agents. Starting from the structural adjustment of factors such as metal ions, organic ligands, and solvents, it covers the transformation of single MOFs as well as subsequent MOF composites and provides a comprehensive discussion of the synthesis methods and mechanisms (Scheme 1). Eventually, we detail the key role of morphological and structural conversion of MOFs in the fields of gas storage, dye adsorption, electrochemical catalysis, fuel cells, and so on (Scheme 2). Overall, this review describes the various perspectives that can influence the morphological and structural changes of MOFs to obtain controlled and tunable high-quality crystals for relevant applications, providing a rare opportunity for rational design and utilization of MOFs.

2. Tunable structure of MOFs

It is well known that microporous MOFs are recognized as a subclass of compounds consisting of metal ions or clusters as inorganic SBUs, which are further connected to organic spacers to form different dimension nanostructures [50]. In addition, there are numerous factors such as the used solvent, time, and temperature that can have a significant impact on the morphology and structure of MOFs [51,52]. Therefore, in this section, we will focus on the structural changes and morphological differences of MOFs due to composition modifications for more effective applications in different fields.

2.1. Metals

Undoubtedly, metal centers can pose a significant influence on the overall structure of three-dimensional (3D) framework [53]. It is well-known that the coordination preference of inorganic part determines the size and shape of pores by dictating how many ligands can bind to the metal and in which orientation [54,55].

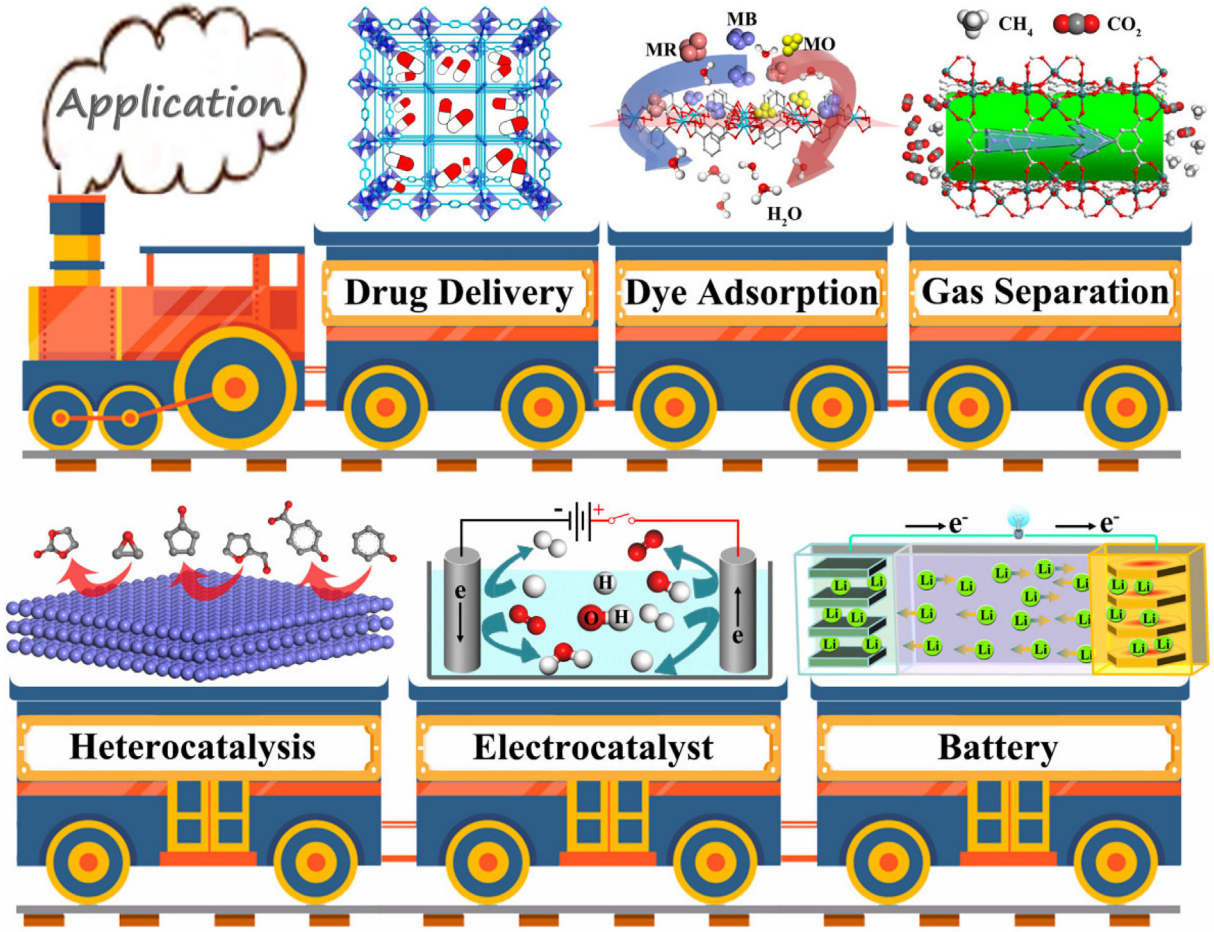

Scheme 2. Schematic illustration of MOFs and their derivatives with different structures and morphologies for energy and environment application, such as drug delivery, dye adsorption, gas separation, heterogeneous catalysis, electrochemical catalyst, and battery.

Under these circumstances, main group (MG) metal elements, including aluminum, gallium, and indium, have been demonstrated to successfully construct various MOF structures [56-58]. However, the MG IIIA metals induce different MOF growth behaviors due to the large difference in ionic radius. Fig. 1**a** shows an epitaxial growth of heterometallic MOFs by using Fe-MIL-88B (CPP-15) as a seed with the addition of Ga(III) and In(III) ions [59]. In this work, the size difference between Ga(III, 76.0 pm) and In(III, 94.0 pm) involved within the Fe-based CPP-15 (Fe(III), 78.5 pm) will give rise to variation in the cell units of the as-obtained heterostructures. Scanning/transmission electron microscopy (SEM/TEM) images reveal the successful preparation of two heterostructured MOF-on-MOFs through an isotropic manner to grow Ga-CPP I (A@B), while a nonisotropic growth creates hybrid In-CPP II (A@C). Therefore, the dissimilar growth behavior on the surface of the CPP-15 seeds can be well explained by the size variation of the metal ions. Furthermore, MIL-96, formed by coordination bonds between 1,3,5-benzenetricarboxylic acid (H_3BTC) and Al (III, 53.5 pm) ions, can induce the change of crystal morphology by using Cu (II, 73.0 pm) salts as structural guiding agents [60]. It is found that Cu ions alter the equilibrium between Al ions and ligands, and restrict the growth direction of MIL-96 without changing the structure. Eventually, the morphology of MIL-96 is transformed from an icosahedral hexagonal spindle to an octahedral hexagonal spindle, while the size is reduced from 10 μm to 1 μm.

Although the radius of transition metal (TM) ions are comparatively similar, especially in Group VIII (Fe(III), 64.5 pm; Co(II), 74.5 pm; Ni(II), 69.0 pm), the introduction of different TM ions could change the structure and morphology of MOFs. In Fig. 1**b**, while Co(II) and Ni(II) ions are simultaneously added into Fe-MIL-101-NH_2, the microstructure of trimetallic CoNiFe-MOF can be conveniently obtained from the original smooth surface to rough, fluffy nanosheet [61]. During the ion exchange process, Ni ions replace part of Fe atoms in the framework, while Co ions etch the surface of Fe-MIL-101-NH_2, and then the dissolved Fe ions are re-coordinated with carboxylate groups to form trimetallic MOF nanosheets. Hence, the mutual function of Co(II) and Ni(II) ions plays an indispensable role in the morphology change of MOF, leading to the two-dimensional (2D) ternary metal MOF layer encapsulated into the 3D MOF octahedral crystal. As for the lanthanide (Ln) metals, the difference in atomic radius between them will be even smaller. Nevertheless, when different Ln metals are combined to generate the MOF-on-MOFs, there are still different growth manners to result in different morphologies. There are a series of single crystals with isomorphic structures from the self-assembly of organic ligand (TMPBPO) with various Ln salts (Ln = Ce, Pr, Nd, Sm, Eu, Gd, Tb) [62]. In Fig. 1**c1-1c3**, bimetallic crystals show distinguishable colors under daylight due to the eye-detectable color difference between Pr, Nd, and Ce cations. As for other mixed-metallic crystals (Fig. 1**c4-1c15**), the multilevel crystals exhibit intrinsic multi-color luminescence, while hybrid-type hetero-Ln-MOF crystals show uniform emission colors (Fig. 1-**c16-1c18**).

Overall, the growth behavior of MOFs can be affected by the size change of metal ions to a certain extent, so the isotropic and/or anisotropic epitaxial growth mode can be precisely controlled by

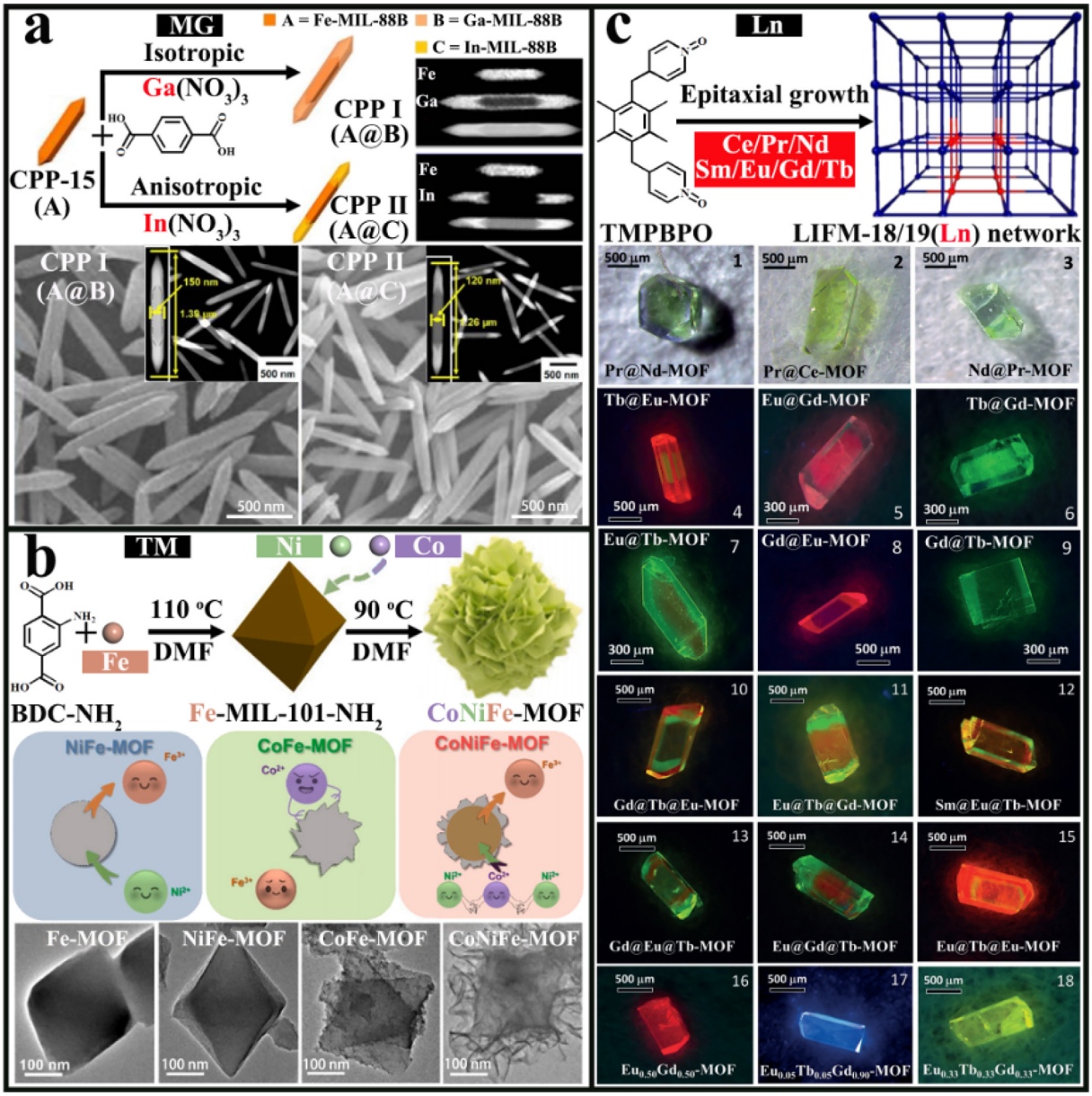

Fig. 1. A) Schematic route to synthesize heterostructured In-/Ga-MOFs governed by the isotropic and anisotropic growth. Reproduced with permission from ref. [59]. Copyright 2013, American Chemical Society. b) Preparation of trimetallic MOF from initial Fe-MOF seed. Reproduced with permission from ref. [61]. Copyright 2021, Elsevier. c) An epitaxial growth of bi-/tri-metallic Ln-MOFs. Reproduced with permission from ref. [62]. Copyright 2017, Wiley-VCH GmbH.

selecting appropriate metal species. For another, the charge difference between different metals will affect the coordination style and thus change the overall structure of the crystals, which deserves more in-depth study [63]. Therefore, the well-designed polymetallic-doped MOF materials own wonderful heterostructure and electronic structure, which is of great significance to the research of multifunctional materials and the optimization of catalytic performance [64,65].

2.2. Ligands

In the composition of MOFs, besides metal ions, organic ligands are another dominant factor in forming the monolithic framework. Meanwhile, we can exchange an existing organic linking group in a prefabricated MOF with a new linker by the post-synthetic modification (PSM), which enables the incorporation of various functional groups into MOFs [66]. The resulting structural and morphological features of MOF particles are closely related to organic linkers with different width and functionality [67-69].

In Fig. 2**a1-2a6**, there are a series of reactions in the presence of In(III) cations, in which various ratios of isophthalic acid (H_2IPA) to terephthalic acid (H_2BDC) have been carried out [70]. The morphology of intermediate MOF particles is highly dependent on the relative amounts of the two organic linkers where the morphology of MOF particles changes with the increase of H_2BDC from microspheres to ovals, angulated ovals, and finally close to hexagonal microrods. On the other hand, when the width of the ligand remains unchanged, altering the substituent groups will also induce unforeseeable changes [71,72]. Fig. 2**a7-2a10** shows that MOFs are constructed from these functionalized H_2BDC ligands, including H_2BDC-Br, naphthalene-1,4-dicarboxylatic acid (H_2NDC), H_2BDC-NO_2 and H_2BDC-NH_2, where they have identical lengths but different widths. It is observed that H_2BDC-Br is added to give microrods without causing too much change, while the

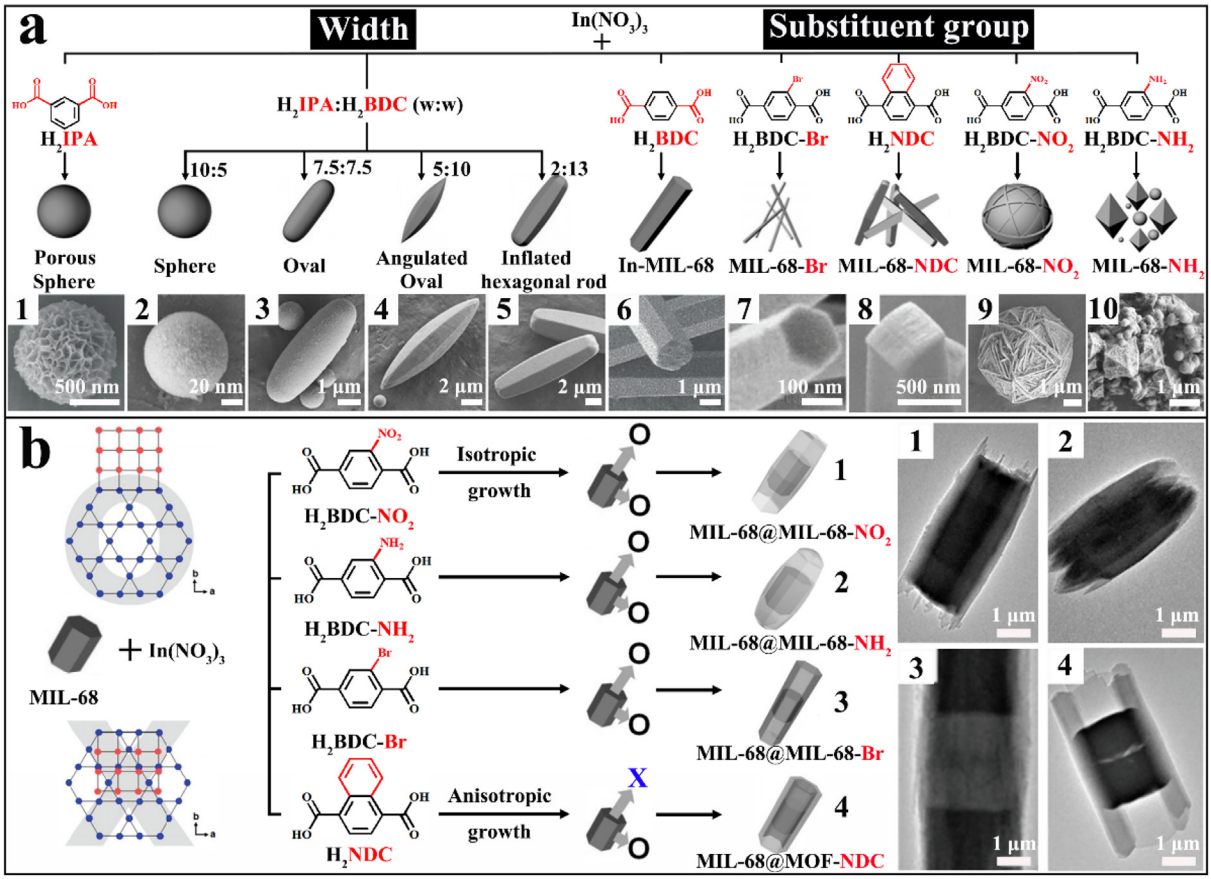

Fig. 2. A) Morphological evolution of MIL-68 formed with different dicarboxylates. Reproduced with permission from ref. [70]. Copyright 2015, Wiley-VCH GmbH. b) The influence of dicarboxylates with different groups on the growth behavior of secondary MOFs. Reproduced with permission from ref. [71,72]. Copyright 2016, 2018, American Chemical Society.

additional large aromatic rings of the H_2NDC building blocks may interrupt MIL-68-like structure, resulting in the formation of thin rods. However, the steric constraints originating from more polar $-NO_2$ and $-NH_2$ cause defects in the structure, thus forming amorphous particles. Because -Br, $-NO_2$, and $-NH_2$ groups exhibit similar molecular sizes, it is predictable that the isotropic growth on MOF template produces core–shell MOF-on-MOFs (MIL-68@MIL-68-Br, MIL-68@MIL-68-NO_2, MIL-68@MIL-68-NH_2, Fig. 2**b**) [70,71]. As for H_2NDC, a type of 3D square nanostructure owns well-matched lattices with the MIL-68 template along the direction of the *a*/*c* axes but shows a largely mismatched lattice in *b* axis. Therefore, it can grow on the six rectangular facets (*ac* plane) but cannot grow on the two hexagonal facets (*ab* plane) of the template to obtain an intriguing MIL-68@MIL-68-NDC.

Depending on the lengths of bridging organic linkers, the growth of secondary MOFs on the spherulite seeds can be completely different (Fig. 3**a**). One fact is that the pore size and porosity of MOF-74 analogues can be systematically expanded by elongating the bridging spacer length (Fig. 3**b**) [73]. However, by utilizing MOF-74-III spherulites as seeds, multiple quaternary architectures with superior hierarchy could be achieved. In Fig. 3**c**, the secondary evolution modes including epitaxial growth of MOF-74-III, plumose superstructures of MOF-74-II and templated evolution of MOF-74-I hollow aggregates are observed when MOF-74-III spherulites are mixed with precursors containing linkers which have either identical or different lengths as a result of the significant difference in the chemical stability of MOFs [74].

As researches find that by adjusting the relative amount of the mixed linkers, substituting ligands with different functional groups, and changing the length of the organic connectors, the evolution process of the crystals can be reasonably designed to obtain unique porous materials with diverse morphologies and multilayered structures [75]. Taking these advantages of the growth strategy using ligand replacement, it is a practical method to improve the crystallinity and porosity of MOF materials, which help to facilitate the encapsulation of guest molecules in porous channels for further applications in drug storage and delivery [76,77].

2.3. Secondary building units

Usually, inorganic–organic SBUs refer to a structural unit formed by stable metal–oxygen/nitrogen bonds with a certain geometric environment, which are conducive to generating more coordination sites and promoting the extension of the overall framework [78,79]. In contrast to the adjustment of inorganic metals and organic ligands, these SBU-regulated frameworks are featured with these following unique advantages: 1) avoid irrational selection of metal centers to form long-range ordered structures; 2) save time in synthesizing organic ligands with specified functional groups; 3) induce various structures of larger pores stemmed from these sophisticated SBUs [80].

In this case, the mononuclear SBU formed by the Cu(II) centers that are coordinated with four pyridine moieties can be further extended to grow achiral yo-yo-like crystals (Fig. 4**a**) [81]. It is amazing that the chiral structure can be triggered through changing the arrangement way of the pyridine groups around the metal ions to create a propeller-shaped conformation. In the micro-computed tomography and SEM images, one single crystal contains

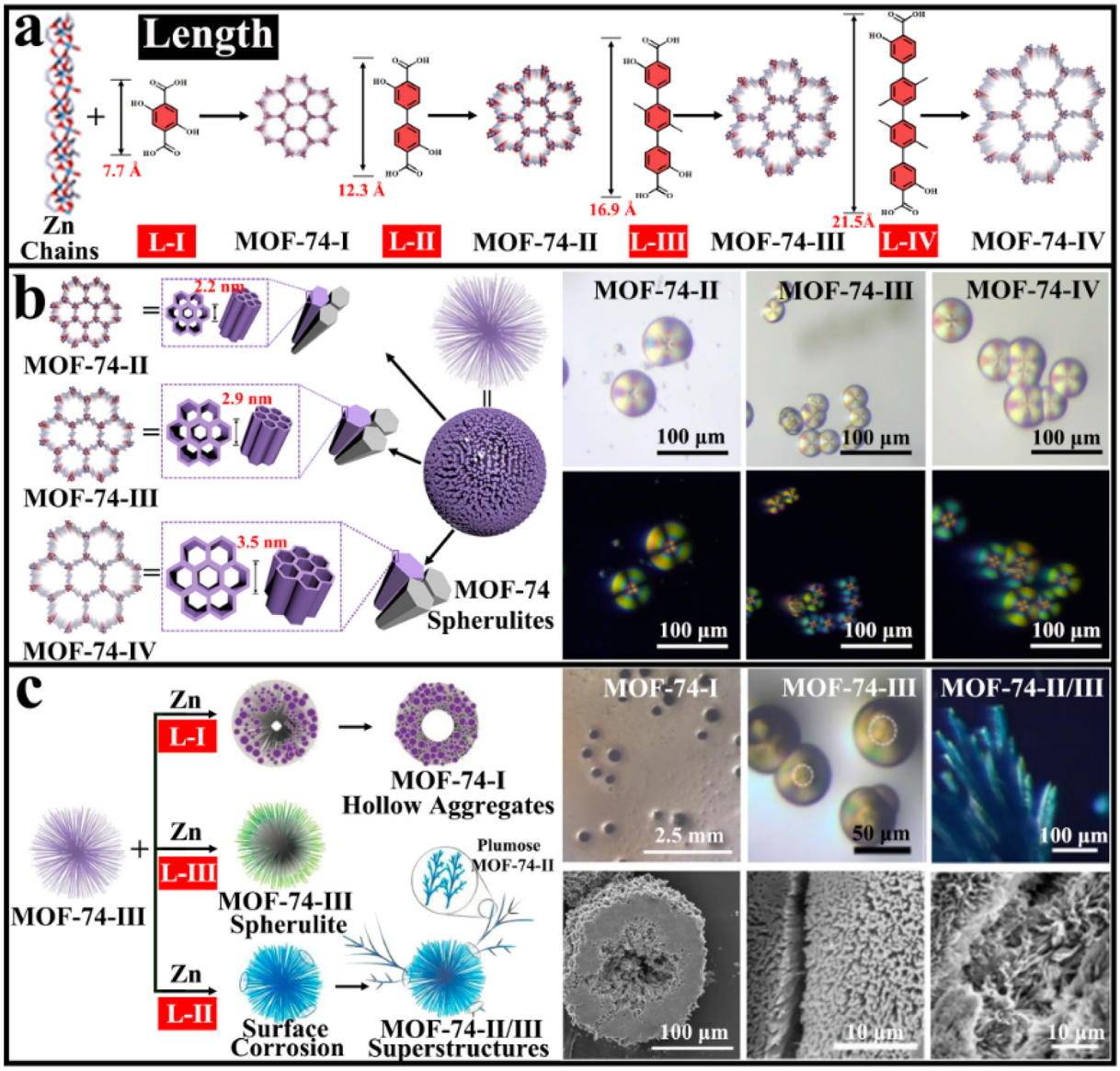

Fig. 3. A) Structures of MOF-74-I-IV and the lengths of corresponding organic building units. b) Isoreticular synthesis of MOF-74 spherulites with tunable pore sizes. Reproduced with permission from ref. [73]. Copyright 2020, Elsevier. c) Diverse secondary growth pathways on the MOF-74-III. Reproduced with permission from ref. [74]. Copyright 2020, Royal Society of Chemistry.

two concave disks with distinct petals and a stigma as a support. Similarly, an achiral FJI-H16 is formed by multinuclear Zn(II)/Cd(II)-O SBUs with benzene-1,3,5-tris(4-benzoic acid) (H_3BTB) [82]. In Fig. 4**b**, it shows that the extra addition of pyridine leads to the formation of chiral FJI-H27 and can further selectively produce FJI-H27(*M*) or FJI-H27(*P*) by controlling its concentration, confirming that pyridine serves as the inducer for transformation of chirality from achiral SBUs. Otherwise, the MOFs with different structures can be further adjusted by the modification of the terminal sites in SBUs. For example, three original –OH/H_2O terminal groups in initial soc-MOF with the trinuclear $Fe_3(\mu_3\text{-}O)(CH_3COO)_6$ can be substituted by three imidazole (IM) molecules to form the soc-MOF-IM (Fig. 4**c**) [83]. However, in the surface and cross-section SEM images and energy-dispersive X-ray spectroscopy (EDS) mapping images, both membranes possess a continuous surface with an average thickness of 20 μm. After adding IM, the pore environmental engineering of Fe-MOFs can be regulated in which pore size can be reduced from 3.9 to 2.5 Å.

Therefore, we can adjust the morphology and structure of MOFs by changing the chirality of SBUs and/or modifying SBUs directly. Especially, with the SBU-decorated engineering, the pores of these modified MOFs can be controlled to play a molecular sieving effect. [84]. However, most of SBUs cannot exist alone and need to be stabilized in a suitable solution, so the added solvent is another key point in the synthesis process.

2.4. Solvents

Solvent, one of the most critical factors during the synthesis of single crystals, greatly affects the nucleation and growth of MOFs for the polarity and solubility of the building blocks [85]. Herein, it can not only act as a reaction medium but also a structure directing agent to modulate the topology of different MOFs [86]. It means that exchanging the solvent interferes with the assembly process to form coordination compounds with various morphologies. Generally speaking, the solvent as guest molecules could play

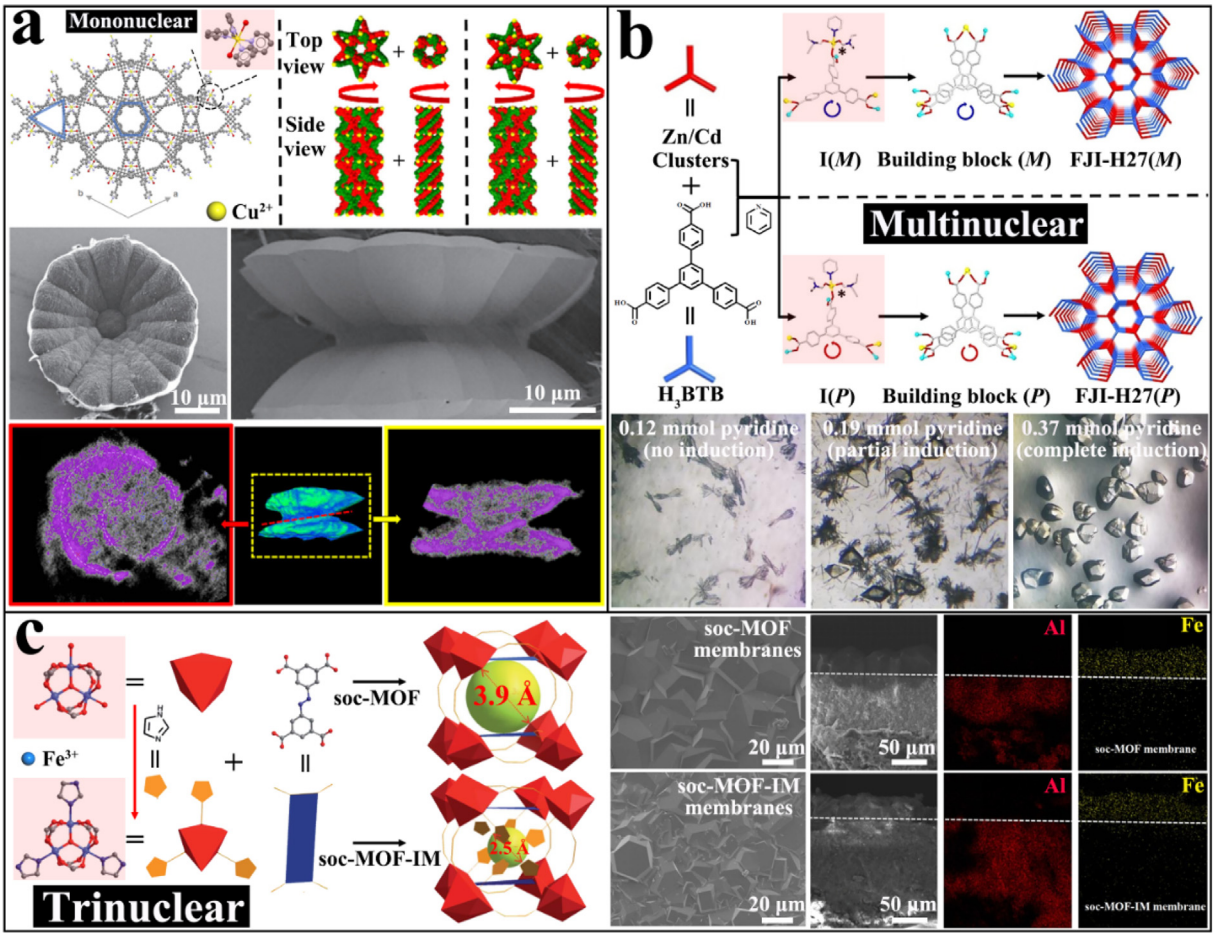

Fig. 4. A) Multidomain morphology in yo-yo-like single crystals. Reproduced with permission from ref. [81]. Copyright 2020, Springer Nature. b) Chiral induction from achiral linkers through a template-driven self-assembly process. Reproduced with permission from ref. [82]. Copyright 2021, Wiley-VCH GmbH. c) The IM-modified SBU to construct soc-MOF-IM. Reproduced with permission from ref. [83]. Copyright 2020, Royal Society of Chemistry.

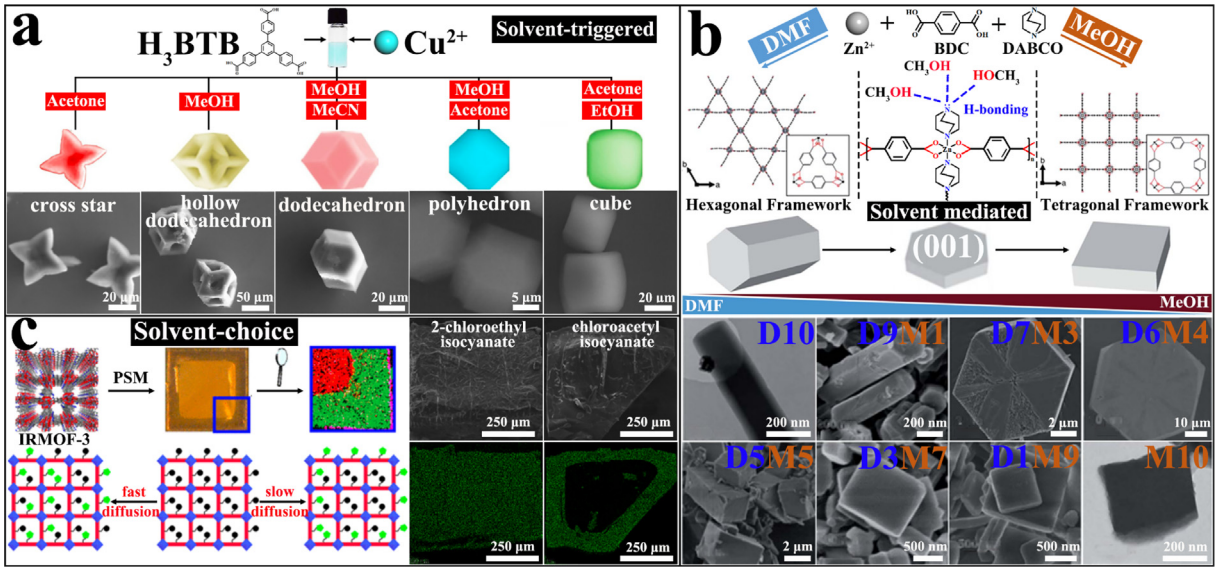

Fig. 5. A) A solvent-triggered method to obtain various Cu-BTB MOFs. Reproduced with permission from ref. [89]. Copyright 2019, Elsevier. b) The solvent-mediated synthesis of ZBD with controlled size and shape. Reproduced with permission from ref. [90]. Copyright 2018, Royal Society of Chemistry. c) The solvent-choice method to regulate the distribution and core–shell microstructure. Reproduced with permission from ref. [91]. Copyright 2021, American Chemical Society.

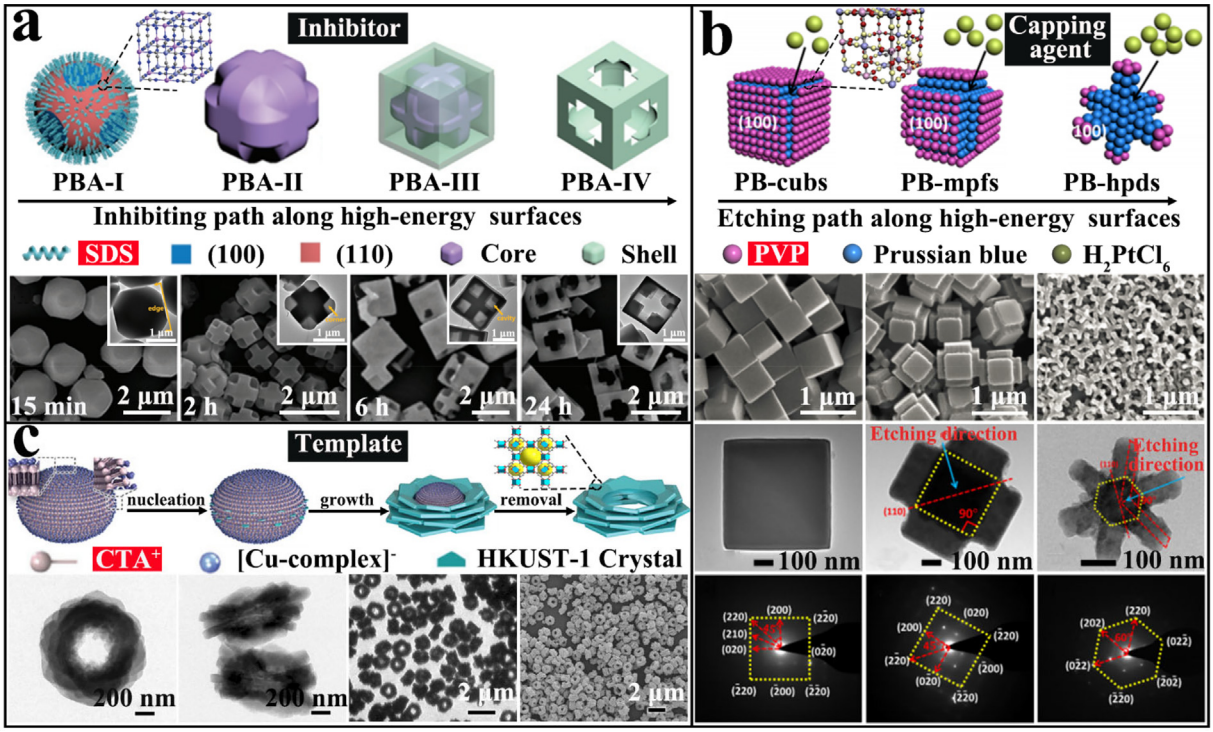

Fig. 6. A) SDS as inhibitor to tune the morphology of MnCoPBA. Reproduced with permission from ref. [98]. Copyright 2020, Wiley-VCH GmbH. b) PVP as capping agent to prevent the etching of microcrystals by H_2PtCl_6. Reproduced with permission from ref. [99]. Copyright 2019, American Chemical Society. c) CTAB to form vesicle template to prepare ring-like crystals. Reproduced with permission from ref. [100]. Copyright 2017, Wiley-VCH GmbH.

the template effect in filling the micropores of crystals, which is an effective means to achieve the desired framework topology [87]. Through understanding the properties of solvent and the formation mechanism, the ideal size and morphology of MOF particles can be designed rationally and synthesized controllably.

A recent work has been reported that solvents play a dominant role in the self-assembly of coordination polymer [88]. It is learned that various organic solvents can dissolve fiber gels and provide a suitable crystal growth environment for MOFs by a solvent-triggered method simultaneously (Fig. 5**a**) [89]. On this occasion, an amorphous metal–organic gel composed of Cu(II) and H_3BTB can be *in situ* transformed into unconventional MOFs with the shapes of cross star and hollow dodecahedron in acetone and methanol (MeOH), respectively. Meanwhile, SEM images reveal that except for the dodecahedron obtained in mixed MeOH-acetonitrile (MeCN) solvents, the gels can also be converted into polyhedron and cube-like crystals in MeOH-acetone and acetone-ethanol (EtOH), respectively. On the other hand, the growth pattern of MOFs can be tuned to some extent by optimizing the ratio of dual-solvent [90]. The polymorphism of a 3D pillar-layer ZBD (Z = $Zn(NO_3)_2$; B = BDC, benzene-1,4-dicarboxylic acid; D = DABCO, 1,4-diazabicyclo[2.2.2]octane) is further controlled by using *N,N*-dimethylformamide (DMF) and MeOH as co-solvent (Fig. 5**b**). Compared to DMF, polar protic MeOH tends to surround the nucleophilic DABCO ligand and forms hydrogen bonds, thus hindering the longitudinal growth of (001) plane to give the plate-like tetragonal framework. As the content of MeOH increases, the anisotropic hexagonal nanorods (D10) gradually turn into hexagonal microplates (D6M4), tetragonal microcubes (D5M5), and finally tetragonal nanoplates (M10). Moreover, the choice of solvent can affect the reaction kinetics of the PSM, resulting in the formation of multifunctional MOFs with different microstructures. The bulk crystal of IRMOF-3 composed of Zn_4O SBU and NH_2-BDC linkers is selected as the research object because its large pores allow a variety of molecules to diffuse efficiently (Fig. 5**c**) [91]. After PSM, SEM-EDS images show more uniform microstructure with 2-chloroethyl isocyanate and core–shell morphology with chloroacetyl isocyanate, which is attributed to the higher reaction rate of chloroacetyl isocyanate with amine functionality. When the reaction rate between the solvent and MOF is quicker than the diffusion rate, the core–shell structure will be formed; otherwise, the uniform structure will be achieved.

By selectively adjusting the types, proportions, and properties of different solvents, the MOFs with different morphologies, sizes, and topological structures can be conveniently synthesized. The as-synthesized MOFs have incomparable performance to ordinary MOFs, which can be thermally converted into carbon nanocomposites with given morphologies applied in energy field [92]. More solvent effect on structure-directed growth and morphology of multifunctional MOFs and their derivatives should be explored in the near future, such as polarity, solubility, stability, etc. [93].

2.5. Surfactants

In general, surfactants are amphiphilic organic compounds composed of hydrophobic groups and hydrophilic groups, and can be dissolved in solution to influence the topological extension [94,95]. On the one hand, the hydrophobic tails of the surfactants are closely linked while the hydrophilic heads come into contact with the surrounding aqueous phase in solution, forming spherical or cylindrical aggregates as templates to provide sites for nucleation [96]. On the other hand, partial cationic surfactants can adsorb on inorganic–organic building blocks with negative charge as capping agents, which prevent the self-assembly process from proceeding normally and inhibit the conventional growth of MOFs [97].

Previously, our group has utilized an ionic surfactant of sodium dodecyl sulfate (SDS) as an inhibitor to regulate the morphology of MnCo-based Prussian blue analogous (MnCoPBA, Fig. 6**a**) [98]. The anionic SDS can selectively adsorb on the high-energy (111) face

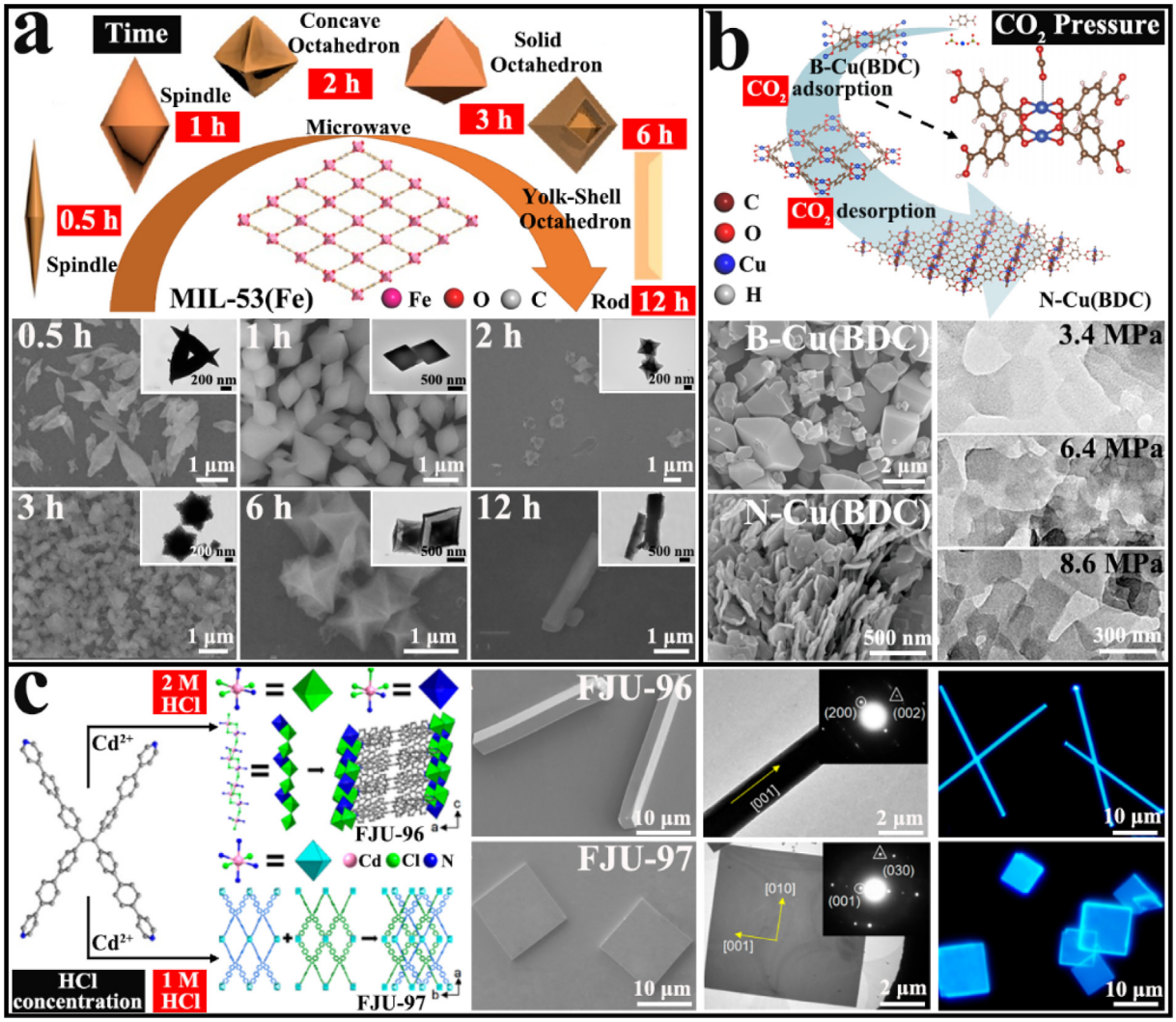

Fig. 7. A) Different MIL-53(Fe) particles synthesized by controlling the reaction time. Reproduced with permission from ref. [108]. Copyright 2017, American Chemical Society. b) The sheet-like Cu(BDC) controlled by adjusting the gas pressure. Reproduced with permission from ref. [109]. Copyright 2020, Springer Nature. c) Different concentrations of HCl added to regulate FJU series. Reproduced with permission from ref. [110]. Copyright 2020, American Chemical Society.

to slow down the degradation rate of the (111) face and control the growth of the (100) face, thus changing the morphology of MnCoPBA crystals from solid sphere (PBA-I) to hollow cube shell (PBA-IV). By comparison, a type of non-ionic surfactant of polyvinylpyrrolidone (PVP) works as the capping agent that reduces the surface energy of (100) face of Prussian blue (PB, Fig. 6**b**) [99]. In this work, H_2PtCl_6 becomes an etchant to corrode the PB microcubes (PB-cubs) along the high-energy edges and corners. As the concentration of H_2PtCl_6 increases, a microcube structure with six protruding faces (PB-mpfs) and a final product with hexapod morphology (PB-hpds) will appear in proper order. Besides, using surfactants as templates is another familiar method for preparing MOFs with ideal morphology. Especially, the hexadecyltrimethylammonium bromide (CTAB) molecules as cationic surfactant readily dissociate into CTA^+ cations in aqueous solution, and their long hydrophobic chains are well stacked to form nano-sized vesicles that electrostatically attract the anionic [Cu-complex]$^-$ intermediate (Fig. 6**c**) [100]. After that, these CTA^+-composed vesicles can serve as templates to provide nucleation sites for efficient growth of MOF crystals and promote nucleating preferentially in the equatorial region to give the ring-like HKUST-1 particles.

According to the properties of surfactants applied to different structures, it will produce the unexpected MOFs with various morphologies [101]. Meanwhile, the crystals with special shape obtained by surfactant-assisted modification could modulate the electronegativity of overall framework to possess markable effects on environmental pollution control [102]. It is worth mentioning that the detailed mechanism to generate intriguing nanostructures and/or superstrutures for multifunctional MOFs is deserved to be under investigation in some cases.

2.6. Others

In addition to these above-mentioned strategies, there are still other approaches to tune structure and composition as well as transform the morphology of MOFs [103,104]. Except for the above factors, other factors such as time, temperature, gas pressure, solution concentration, and the ratio of metal salts to organic ligands may all cause changes in the morphology and structure of porous MOFs [105-107].

Firstly, the reaction time plays a pivotal impact on the formation of crystals. In Fig. 7**a**, by adjusting the microwave irradiation time, spindle, concave octahedron, solid octahedron, yolk-shell

Table 1
The Synthesis of MOFs with Different Morphologies.

MOF	Morphology	Metal ion	Organic linker	Solvent	Synthesis strategy	**Ref.**
CPP-15	Nanorod	Fe^{3+}	H_2BDC	DMF + MeCN	120 °C, 40 min	[59]
CPP I/II	Core-shell nanorod	Ga^{3+}/In^{3+}		DMF	CPP-15, 100 °C, 20 min	
Fe-MOF	Octahedron	Fe^{3+}	$H_2BDC-NH_2$	DMF	115 °C, 20 h	[61]
NiFe/CoFe/CoNiFe-MOF	Octahedron/Concaved octahedron/Nanosheet	$Ni^{2+}/Co^{2+}/Co^{2+}+Ni^{2+}$	/		Fe-MOF, 90 °C, 48 h	
Hierarchical Ln-MOF	Core-shell/Striped bulk	Ln^{3+}	TMPBPO	Acetone + H_2O	Room temperature, 5 days	[62]
In-MIL-68	Amorphous spherical / Sphere/Oval/Angulated oval/Inflated hexagonal rod/Hexagonal rod	In^{3+}	$H_2IPA:H_2BDC$ = 1:0/ 10:5/7.5:7.5/5:10/ 2:13/0:1	DMF	140 °C, 20 min	[70]
MIL-68-Br/NDC/NO_2/ NH_2	Hexagonal rod/ Rectangular rod/Walnuts/ Octahedron and sphere	In^{3+}	H_2BDC-Br/NDC/ NO_2/NH_2	DMF	100 °C, 20 min/ 40 min	[71,72]
MOF-74-I/II/III/IV	Hollow aggregate/ Spherulite	Zn^{2+}	L-I/II/III/IV	EtOH + H_2O + DMF	100 °C, 24 h	[73,74]
Yo-yo like MOF	Yo-yo like chiral cylinder	Cu^{2+}	TPEPA	DMF + $CHCl_3$	Room temperature, 2 days	[81]
FJI-H16	Bulk	$Cd^{2+}+Zn^{2+}$	H_3BTB	DEF + EtOH	85 °C, 3 days	[82]
FJI-H27	Chiral bulk				Pyridine, 85 °C, 3 days	
soc-MOF/soc-MOF-IM	Membrane	Fe^{3+}	H_4ABTC/ H_4ABTC + IM	HAc + DMF	150 °C, 12 h	[83]
Cu-MOF	Cross star/Hollow dodecahedron/ Dodecahedron/ Polyhedron/Cube	Cu^{2+}	H_3BTB	Acetone/MeOH/ MeOH + MeCN/ Acetone + MeOH/ Acetone + EtOH	25 °C, 7 days	[89]
ZBDh/ZBDt	Hexagonal rod/Tetragonal plate	Zn^{2+}	H_2BDC + DABCO	DMF/MeOH	Room temperature, 2 days	[90]
PBA-I/II/III/IV	Solid sphere/Truncated cube/Cuboidal shell/Cube	Mn^{2+}	$K_3[Co(CN)_6]$	H_2O	SDS, 70 °C, 15 min/ 2h/6h/24 h	[98]
PB-cubs/mpfs/hpds	Microcube/Protrusive face/ Hexapod	Fe^{3+}	$K_4Fe(CN)_6$	HCl + H_2O	PVP, 85 °C, 24 h	[99]
HKUST-1-R	Ring-like sheet	Cu^{2+}	H_3BTC	H_2O + TEA	CTAB, room temperature, 30 min	[100]
MIL-53–0.5/1/2/3/6/ 12	Spindle/Spindle/Concave octahedron/Solid octahedron/Yolk-shell octahedron/Rod	Fe^{3+}	H_2BDC	DMF	150 °C, 0.5 h/1h/2h/ 3h/6h/12 h/	[108]
B/N-Cu(BDC)	Bulk/Nanosheet	Cu^{2+}	H_2BDC	DMF	CO_2, 100 °C, 24 h	[109]
FJU-96/97	Microwires/Microplate	Cd^{2+}	TPBE	DMF + H_2O + HCl (2 M)/ (1 M)	65 °C, 12 h	[110]
Ni-CAT-1	Film	Ni^{2+}	HHTP	H_2O	SLG, 85 °C, 12 h	[111]
Cu_2(TCPP)	Film	Cu^{2+}	TCPP	H_2O + $NH_3{\cdot}H_2O$	Quartz glass, 60 °C, 30 min	[112]
Co/CoNi/CoFe/NiFe-BDC	Flower-like nanosheet	$Co^{2+}/Ni^{2+}/Fe^{3+}$	H_2(BDC)	DMF + MeCN	CMC, seed-secondary growth	[113]
SOM-ZIF-8	Truncated rhombic dodecahedra	Zn^{2+}	2-MI	MeOH	PS, room temperature, 24 h	[114]
ZIF-8	Hollow spherical	Zn^{2+}	2-MI	MeOH	Colloid, room temperature, 1 h	[115]
PCN-74	Microfiber	Zn^{2+}	L-II	EtOH + H_2O + DEF	100 °C, 2 h	[116]
MOF-74-II	Hollow tube				PCN-74, 100 °C, 24 h	
InOF-1	Micro-rod	In^{3+}	H_4BPTC	DMF + H_2O + HNO_3 + TEA	CTAB, 140 °C, 30 min	[117]
InOF-1@ ZIF-67	Sugar-gourd-like rod	Co^{2+}	2-MI	MeOH	InOF-1, PVP, 70 °C, 20 min	
MIL-125	Cake-like bulk	Ti^{4+}	Aminoterephthalate	DMF + MeOH	150 °C, 24 h	[118]
MIL-125@ ZIF-67/MIL-125@ZIF-67@ZIF-8	Sandwich cookie	Co^{2+}/Zn^{2+}	2-MI	MeOH	MIL-125/MIL-125@ZIF-67, room temperature, 4 h	
1l-ZIF-8	Solid dodecahedron	Zn^{2+}	2-MI	MeOH	Room temperature, 1 min	[119]
2/6/8l-ZIFs(8)	Multiple core–shell dodecahedron	$Co^{2+}+Zn^{2+}$			ZIF-8, room temperature, 24 h	
ZIF-8-PMMA	Multilayer film	/	/	MeOH	ZIF-8, liquid–air interface technique	[120]
ZIF-8-gel	Thin membrane	/	/	MeOH	ZIF-8, vaporization-gelation method	[121]
Zn-MOF-74	Sphere	Zn^{2+}	L-I	MeOH	Ultrasonication, 30 min	[122]
SS-MOFNR	Chestnut-shell-like sphere	/	/	H_2O	Zn-MOF-74, urea, 175 °C, 24 h	

(*continued on next page*)

Table 1 (*continued*)

MOF	Morphology	Metal ion	Organic linker	Solvent	Synthesis strategy	Ref.
ZIF-8	Polyhedron	Zn^{2+}	2-MI	MeOH	120 °C, 3 h	[123]
SS-MOFNS	Sheet-like sphere	/	/	MeOH	ZIF-8, H_3BO_3, 175 °C, 24 h	
TRD/TD ZIF-8	Truncated rhombic dodecahedron/Rhombic dodecahedron	Zn^{2+}	2-MI	H_2O	Room temperature, 15 min/2h	[124]
UiO-66	Octahedron	Zr^{4+}	H_2BDC	DMF	120 °C, 12 h	
ZIF-71/72	Film	Zn^{2+}	HdcIm	DMF + EtOH/H_2O	CVD	[125]
Cu-BTC	Film	Cu^{2+}	H_3BTC	EtOH + H_2O	PES, electrochemically growth	[126]
HKUST-1/Cu-bdc/ MIL-88A/MIL-88B/ MOF-74/MOF-14/ NOTT-100/UiO-66	Hollow sphere	Cu^{2+}/Cu^{2+}/Fe^{3+}/Fe^{3+}/Zn^{2+}/ Cu^{2+}/Cu^{2+}/Zr^{4+}	H_3BTC/H_2BDC/ Fumaric acid/2-Amino-bdc/L-l/ H_3BTB/H_4BPTC/ H_2BDC	DMF + EtOH + H_2O/DMF/ DMF/DMF/DMF + H_2O/ DMF + EtOH + H_2O/ DMF + H_2O/DMF	Spray-drying synthesis	[127]
tZIF-67	Hollow truncated dodecahedron	/	/	EtOH	ZIF-67, CA, 60 °C, 24 h	[128]
HE-ZIF-BM/ST	Bulk	Zn^{2+}+Cd^{2+}+Cu^{2+}+Co^{2+}+Ni^{2+}	2-MI	Solvent-free/MeOH	Ball grinding, 2 h/ 90 °C, 24 h	[129]
ST/MF-ZrBTB	Bulk/Nanosheet	Zr^{4+}	H_3BTB	DMF	130 °C, 96 h/ Microdroplet flow reaction, formic acid, 130 °C, 32 min	[130]

octahedron, and nanorod of Fe-based MOFs, MIL-53(Fe), can be achieved successively [108]. Secondly, gas molecules behave in a way similar to surfactants as a capping agent to effectively control the directional growth of frameworks [109]. In the presence of CO_2, the coordination growth process of Cu(II) and H_2BDC is severely limited to form nanosheet-like N-Cu(BDC) whose thickness decreases with CO_2 pressure, while bulk B-Cu(BDC) will be formed without CO_2 (Fig. 7**b**). At high pressures, CO_2 is easily soluble in organic solvents and prevents Cu(BDC) from stacking vertically due to its ability to interact with the coordination unsaturated Cu sites. Furthermore, the coordination mode of MOFs can be altered by employing the halogen atoms to facilitate nucleation of crystals. By changing the concentration of HCl, one-dimensional (1D) microwire FJU-96 and 2D microdisk FJU-97 are easily synthesized (Fig. 7**c**) [110]. At a high HCl concentration, these Cd-O-Cd chains are induced to stack along the [0 0 1] direction to form 1D rods. On the contrary, low-concentration HCl can promote the extension of organic molecules along the [0 0 1] and [0 1 0] directions (Table 1).

By artificially changing these external influencing factors, the preparation of MOF materials with special morphology becomes facile, rapid, and high-efficiency, and the as-obtained metal–organic hybrid compounds are endowed with advantages in the many fields [131]. There is no doubt about the morphological adjustments caused by structural changes, but optimizing the shape of MOFs without changing the overall frames is another meaningful operation that can broaden their applications (Table 2).

3. Controllable morphology of MOFs

Although changing the internal influencing factors of MOFs can significantly adjust the structure and morphology of MOFs and

Table 2
The environmental protection and energy storage performance of MOFs and their derivatives.

Materials	Applications	Performance	Ref.
In-MIL-68	N_2/CO_2 sorption	BET surface areas: 1208 m^2 g^{-1}	[70]
HKUST-1	H_2 storage	store 46 g L^{-1} H_2 at 50 bar and 77 K	[132]
DUT-23	CH_4 storage	373 cm^3(STP) cm^{-3}	[132]
soc-MOF-IM	H_2/CO_2 separation	S_{H2}/S_{CO2} = 0.00535, D_{H2}/D_{CO2} = 8911	[83]
PB-hpss	RhB degradation	removal efficiency: 97.1%	[99]
M/HKUST-1-R	Dye adsorption	adsorption efficiency of the MB: 90%	[100]
Ag-MOF	Dye adsorption	adsorption efficiency of the MB: 98%	[133]
UiO-66(Zr)	Dye adsorption	the removal of crystal violet, malachite green, alizarin green, and MO are 58.80%, 64.82%, 61.61%, and 21.12%, respectively	[134]
CoP-InNC@CNT	HER	the overpotentials at 10 mA cm^{-2} reach 153 and 159 mV in 0.5 M H_2SO_4 and 1.0 M KOH, respectively	[117]
$CoNiFeO_x$-NC	OER	overpotential at 50 mA cm^{-2}: 265 mV, Tafel slope: 64.05 mV dec^{-1}	[61]
PBA-III-700	ORR	half-wave potential: 0.801 V, diffusion-limited current density: 5.36 mA cm^{-2}, Tafel slope: 47.5 mV dec^{-1}	[98]
MFM-220-p/CP	CO_2RR	total current density: 23 mA cm^{-2}, $FE_{formate}$ at 1.1 V vs. RHE: 90.4%	[135]
Fe_2O_3-2	LIB	discharge and charge capacity: 1456 and 1048 mAh g^{-1}	[108]
Fe_7S_8/C@ZnS/N-C@C	SIB	reversible capacity of 364.7 mAh g^{-1} after 10,000 cycles at current density of 5.0 A g^{-1}	[136]
NiFe-MOF NSs@CQDs-COOH	ZAB	open-circuit voltage: 1.42 V, specific capacity: 895.5 mAh g_{Zn}^{-1}	[137]
LH-Co@NC	Hydrogenation	CPL selectivity at 160 °C: 97%	[119]
CuBDC/CMC	Cycloaddition	the yield of phenyl cyclic carbonate: 91.5 %	[113]
Pd@InOF-1	Suzuki-Miyaura coupling reaction	isolated yields: 90%	[138]
MOF-5	Drug delivery	encapsulate CUR, SUL, TAT	[139]
MILB@LR	Drug delivery	encapsulate OXA	[140]

improve the application value in various fields, this will also be limited by their intrinsic structures. For example, MOFs generally are in the form of powder particles, which hinders the rapid mass transfer and seriously limits their practical application [141]. By contrast, MOF films can overcome this defect well because of their complete structure and continuity [142]. Therefore, other external factors should be considered such as the substrate effect that can be well explained by the changes in the kinetic process, due to specific surface properties [143]. For this purpose, several synthetic methods have been developed to prepare MOFs with special morphology [144].

3.1. Substrates

Firstly, the facile growth of MOFs on the substrates by means of *ex-situ* methods is regarded as a good choice to synthesize crystals with perfect morphology and appropriate size according to the properties of corresponding materials [145]. Surprisingly, ultrathin single-layer graphene (SLG) with high conductivity and transparency can be expected to become the substrate to facilitate the formation of 2D MOF films [111]. Ni-CAT-1-on-SLG can be efficiently synthesized by the coordination reaction of 2,3,6,7,10,11-hexahydroxytriphenylene (HHTP) and Ni(II) cations on SLG by wet chemistry (Fig. 8**a**). Here, the Ni-CAT-1 displays an extended hexagonal frame, and the triphenylene unit from the organic linker constitutes strong π-π stacking. Therefore, these obtained SEM images show dense accumulation of Ni-CAT-1 crystals on SLG layer to generate ultra-thin films with an average thickness of 25 nm. On the other hand, SLG owns high permeability, nanoporosity, and molecular sieving function, which becomes promising for gas separation [146]. The functional group modification of SLG surface not only allows better dispersion in solution, but also induces nucleation of metal–organic units.[147]. In addition, the development of synthetic methods that can prepare graphene on a large scale can largely improve the possibility for synthesizing 2D MOF films.

In addition to conductive substrates, the dielectric and hydrophilic substrates are also suitable for the growth of MOF films (Fig. 8**b**) [112], in which the highly hydrophilic material is conductive to the diffusion of solvent on the substrate surface. Then the microporous interface of the two substrates stacked face to face will form the capillary effect that inhales trace Cu ions. Finally, the Cu_2(TCPP) membrane is formed on the functionalized substrate because the low nucleation density is favorable for the expansion of thin films. Through the high-resolution atomic force microscopy (AFM) and cryogenic TEM, the obtained MOF film exhibits high crystallinity with obvious internally ordered architecture.

Besides, aerogels can also become ideal supports to fabricate MOF films owing to their rich porous structure, flexibility, and high stability [113]. Here, the available carboxymethylcellulose (CMC) is employed as the carrier, where H_2BDC can be seeded on as the following nucleation site and a small amount of metal ion solution can be sprayed to inhibit homogeneous nucleation (Fig. 8**c**). Subse-

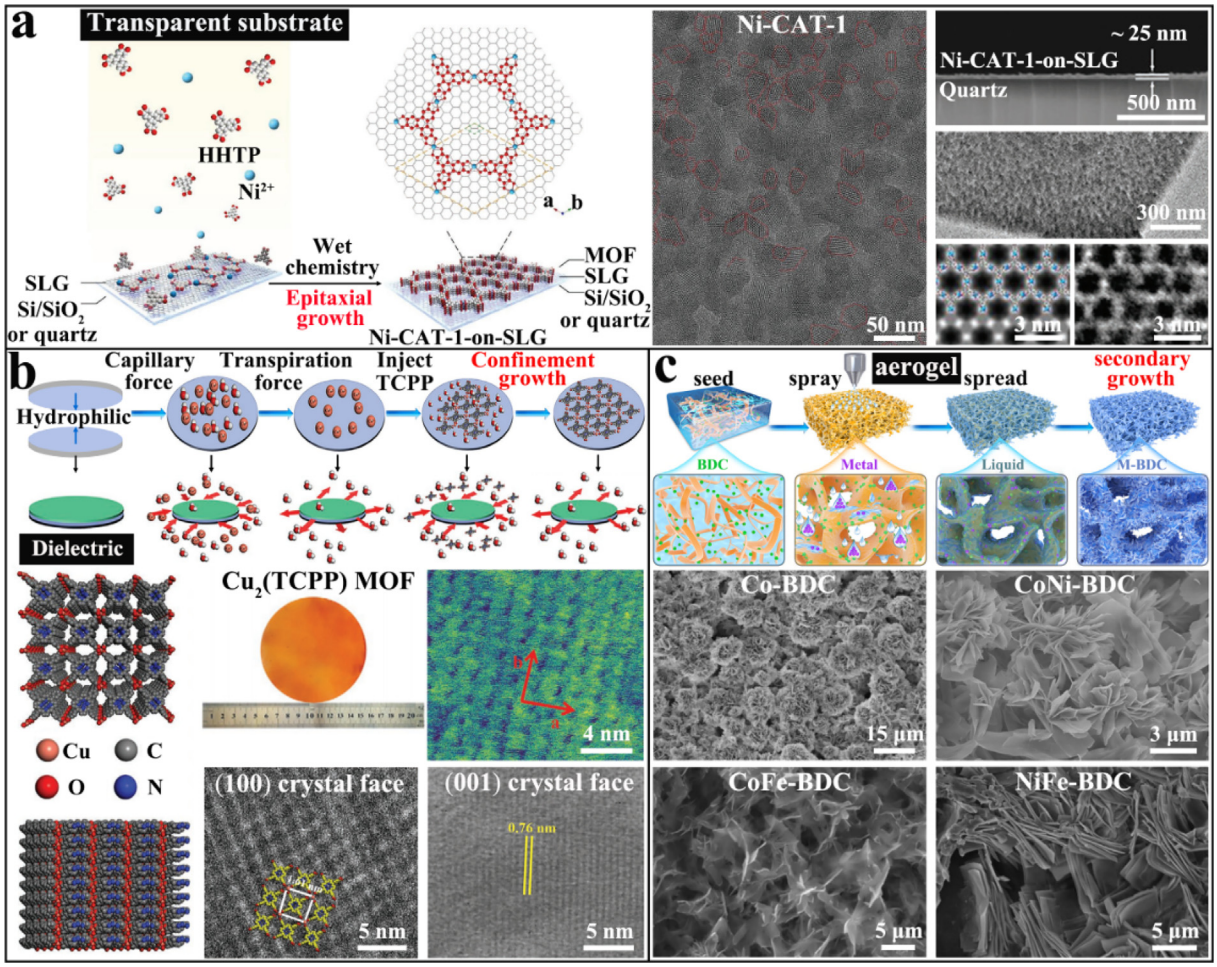

Fig. 8. A) Epitaxial growth of Ni-CAT-1 on slg transparent substrate. Reproduced with permission from ref. [111]. Copyright 2020, Wiley-VCH GmbH. b) Wafer-scale Cu_2(TCPP) films grown on dielectric substrate. Reproduced with permission from ref. [112]. Copyright 2021, Wiley-VCH GmbH. c) Preparation of 2D coordination polymer films on aerogel. Reproduced with permission from ref. [113]. Copyright 2021, Wiley-VCH GmbH.

quently, uniform flower-like MOF films of Co-BDC are further grown on the substrate via soaking process. To demonstrate the universality of the strategy, a series of 2D nanosheet-like CoNi-BDC, CoFe-BDC, and NiFe-BDC films can conveniently be prepared on the aerogel walls. And CMC can also be used as a template to anchor ZIF-L nanosheets, of which not only improves the processability and applicability of ZIF-L, but also provides a highly 3D porous structure, contributing to enhance catalytic activity [148]. Moreover, because of the weak interfacial bonding between MOFs and substrates and the lack of regulation of ionic sites, crystals tend to detach from the composite membrane plate and cannot precisely regulate the crystal structure. However, using 2,2,6,6-tetramethylpiperidyl-1-oxyl-oxidized algae cellulose nanofibers as substrates allows the precisely control of site chelation of metal ions and subsequent firm entanglement of assembled MOF crystals [149]. Thus, low-cost and diverse aerogels are expected to be promising substrates for modulating the morphology and structure of MOFs for a wider range of practical applications.

It is also worth mentioning that low nucleation density is favorable for the formation of 2D nanosized films, which is a key factor to achieve large-scale production [150]. The excellent structure of MOFs combined with the special properties of the substrates can improve the performed activity, so the structural design is of great significance with the rational choice of versatile substrates [151].

3.2. Templates

On the other hand, some special substrates, such as polystyrene sphere (PS) [152], silicon dioxide [153], metal oxide [154], and spherical colloid [155], can also be used as templates to prepare nanomaterials with controlled morphology and hierarchical structure [156]. Among them, PS has the advantages of transparency, good moldability, high rigidity, excellent electrical insulation, and low price. Besdies, these selected templates can be simply removed or degraded during or after chemical reactions, the as-synthesized product will maintain the shape of the template [157]. Furthermore, by choosing the befitting MOF precursors to grow on the particular templates, MOF crystals with definite composition and structure can be efficiently constructed. Such as colloidal particles have a better spherical shape, can continuously change shape to oblong or oblong-elliptical by a fixed volume, and the colloidal suspension of monodisperse spherical particles can adsorb metal ions by electrostatic attraction and provide nucleation sites thus being used as a substrate for the synthesis of novel MOFs.

For instance, a highly ordered PS monomer that can be removed after the reaction is applied as a hard template to regulate the MOF appearance [114]. In Fig. 9**a, a** type of macro-microporous SOM-ZIF-8 single crystals with a tetrakaidecahedron morphology is obtained. SEM images show that the orientation of ordered macropores of the (100) and (111) faces crystal is well-matched with those of 3D ordered PS template, proving that the synthesized hierarchical materials completely inherit the appearance of PS monoliths (Fig. 9**a1-9a5**), while a truncated rhombic dodecahedron is obtained without PS spheres (Fig. 9**a6**). However, the molecular structure of PS contains benzene rings, which are rigid and have poor adhesion to polar substances. Thus, modifiers need to be added to treat them to cross-link each other to form ester polymers, improve the adhesion to polar substances, and promote the nucleation growth of MOFs.

On the other hand, the spherical colloids can behave as soft template to fabricate MOFs, because they will be consumed in the reaction process. For example, metal sulfates are insoluble in alcohols, but $ZnSO_4$ is slightly soluble in MeOH and *in-situ* generates spherical colloidal components due to self-aggregation effect [115]. Subsequently, when a MeOH solution of 2-methylimidazole (2-MI) is added, the well-defined hollow spherical ZIF-8 colloidosomes are obtained gradually (Fig. 9**b**). And the self-templating method, also known as the self-sacrificing method, is regarded as a more feasible approach that can also be utilized to efficiently synthesize hollow MOF crystallites. With this method, a hollow tubular structure of MOF-74-II with high crystallinity is synthesized based on the initial PCN-74 microfiber (Fig. 9**c**) [116]. PCN-74 is structurally labile in the absence of solvents and can be gradually transformed into needle-like MOF-74-II through a highly reversible coordination bond recombination. More importantly, in the process of epitaxial growth, the microfiber template would restrict the movement of MOF-74-II needles to form a crystalline hollow tubule ultimately.

In general, MOF materials prepared by the template-assisted method can retain the morphology of the supporting templates to a large extent. The hierarchically porous nature and directional multi-channel superstructure have shown great potential in gas transport, sensing, and electrochemistry [158]. This will be helpful to provide reference for the growth and evolution mechanism of MOFs in dynamic control. Moreover, to satisfy manufacturing requirements, the 3D hybrid MOF-on-MOF heterogeneous architecture is formed by introducing MOFs with different functions into the modular MOF matrix, creating a novel multifunctional platform. Thus, MOFs themselves can also be considered as a template on which another MOF can be grown, constituting multifunctional MOF-on-MOF heterostructures to widen their research field [159].

3.3. MOF-on-MOFs

Actually, MOF-on-MOF heterostructures are regarded as a kind of composite materials derived from the bottom MOFs as templates in popular sense [160]. Here, the basal MOFs can not only provide nucleation sites to induce the formation of the upper MOFs on their surface, but also become suitable precursors to promote the epitaxial growth of homogeneous crystals directly [161]. Considering that single MOF cannot achieve the desired effect on account of its limited functionality, the multifunctional MOF-on-MOFs can be designed by adding secondary MOFs [162–165]. Therefore, the intriguing MOF-on-MOF system can greatly enhance the application performance with hierarchical porosity and precisely controllable interface [166,167].

Previously, our group has prepared an indium-based InOF-1 with a rod-like morphology and hierarchical structure, which becomes an excellent template to easily absorb free Co(II) ions owing to the large specific surface area and 1D channel structure [117]. Followed by adding 2-MI ligands, it would rapidly coordinate with metals so that the formed densely packed ZIF-67 particles will tightly wrap on the InOF-1 precursors, thus constituting the binary InOF-1@ZIF-67 (Fig. 10**a**). Compared with the binary structures, the ternary MOF-on-MOFs mainly depend on the selection of suitable MOFs and the interaction between the base building blocks and the superstructure units. There is a Ti-based MIL-125 as the host material which is conducive to inducing the growth of the guest MOFs (Fig. 10**b**) [118]. As a result of the rapid nucleation of Co(II) ion and 2-MI and the weaker electrostatic repulsion on the (001) face of MIL-125, the ZIF-67 particles will uniformly grow onto the initial MOF to give a binary MIL-125@ZIF-67. As detected by high-angle annular dark field scanning TEM (HAADF-STEM) and element mapping, the shape of MOF-on-MOFs exhibits a sandwich cookie with two Co-rich layers (Fig. 10**b1**). After that, this binary MIL-125@ZIF-67 is further modified by extra ZIF-8 layers to form the unconventional ternary MIL-125@ZIF-67@ZIF-8 (Fig. 10**b2**). Furthermore, due to the same structural and topological characteristics, the ZIF-67 layer can be heterogeneously nucleated and grown on the surface of ZIF-8 in an epitaxial manner (Fig. 10**c**).[119] Thus the alternating growth of ZIF-8 layer and

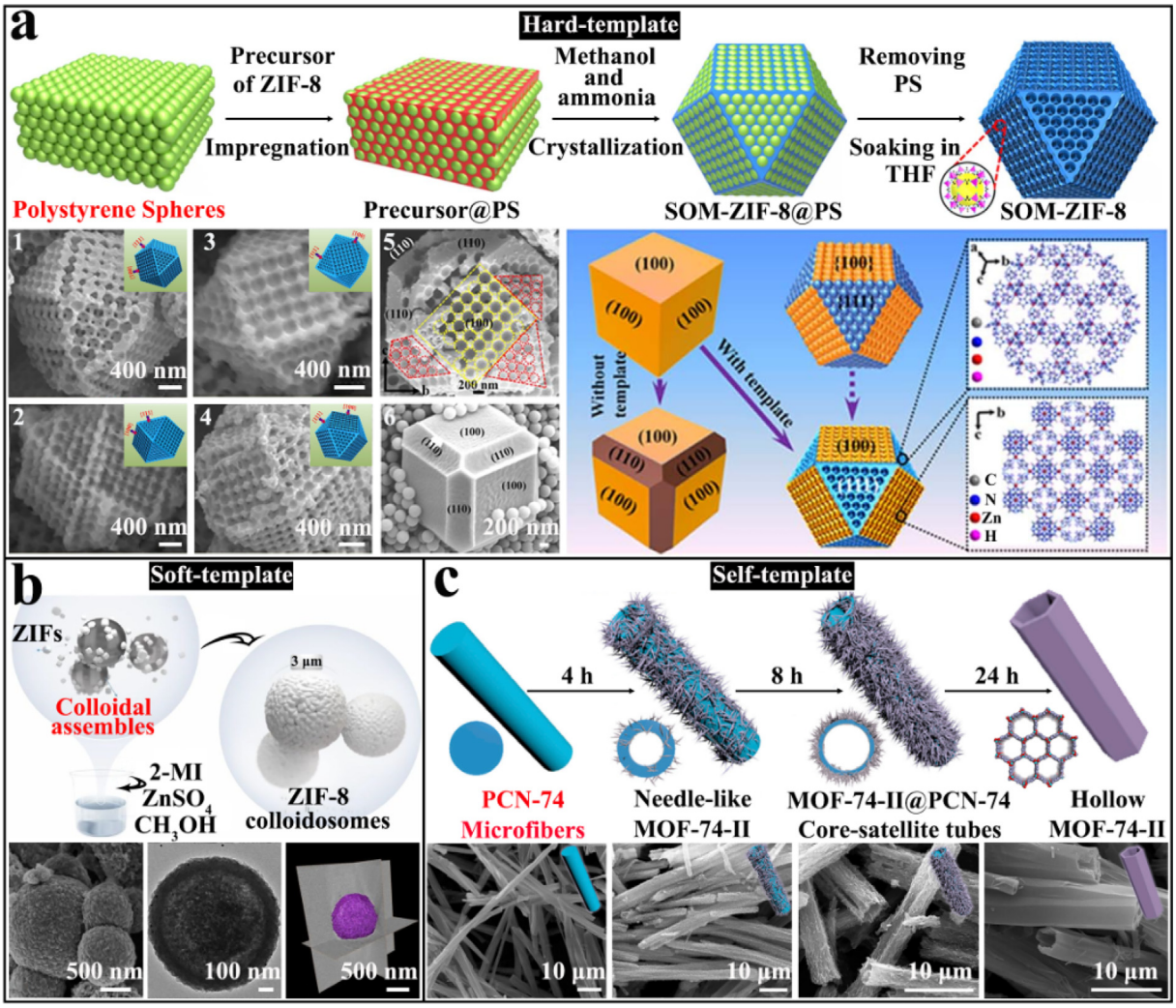

Fig. 9. A) 3D ordered PS hard-template to constitute SOM-ZIF-8 crystals with a tetrakaidecahedron morphology [114] b) An emulsion-free preparation of ZIF-8 colloidosomes. Reproduced with permission from ref. [115]. Copyright 2020, Royal Society of Chemistry. c) Hollow MOF-74-II tubes grown by self-template method. Reproduced with permission from ref. [116]. Copyright 2019, Elsevier.

ZIF-67 layer can be realized by repeating the step-by-step crystal growth process to have ZIF-67-on-ZIF-8 series with multiple core–shell structure (2/4/6/8l-ZIFs(8)).

Different types of multiple MOF-on-MOF hybrids can be synthesized by selecting appropriate MOF precursors, and the morphology and collocation of the whole frame can be precisely controlled. Compared with single MOF blocks, hierarchical MOF system shows higher catalytic performance due to the complexity of their structure and composition [168]. In particular, the unique structural transformation and the tunability of the chemical composition of multifunctional MOFs in the pyrolytic process make it possible to efficiently control the morphology and active sites of their derivatives, which significantly improves the performed properties [169].

3.4. Self-assembly

Compared to the intricate synthesis mechanism of MOF-on-MOFs, the direct use of prefabricated MOF particles to self-assemble into a controlled morphology is more easily grasped. As the self-assembly of organic ligands and inorganic metals is dynamically limited by the topological structure and cannot grow continuously, only forming individually dispersed crystal particles eventually [170]. Therefore, if these discrete MOF particles can be self-assembled again and arranged into ordered nanostructures, their various applications will be greatly promoted.

By surfactant-assisted modification, monodisperse ZIF-8 particles can be used to construct the self-assembled MOF monolayers (SAMM) using a liquid–air interface technique (Fig. 11**a**) [120]. Before the self-assembly process, it first uses imidazolium groups (his-BiB) to conduct post-synthetic exchange reaction on the MOF precursors, which are subsequently combined with methyl methacrylate (MMA) to form core–shell ZIF-8 (ZIF-8-PMMA) through atom transfer radical polymerization (ATRP). Then, the ZIF-8-PMMA is fused with the adjacent particles by evaporation-induced interfacial assembly at the liquid–gas interface, resulting in the formation of a continuous and compact SAMM film (Fig. 11**-a1-11a3**). This film can be neatly stacked alternately with the PMMA or superimposed with each other to form the hetero-/homo-multilayer films (Fig. 11**a4-11a5**). Meanwhile, the obtained flexible SAMM film can cover the SiO_2 particles and create a self-standing film with iridescence on the wire ring (Fig. 11**a6-11a7**). In addition, MOF particles can also be converted into free-standing MOF-gel membrane using a relatively simple vaporization-gelation method (Fig. 11**b**) [121]. In this case, the ZIF-8 wet gel is first cast on the glass substrate and then self-

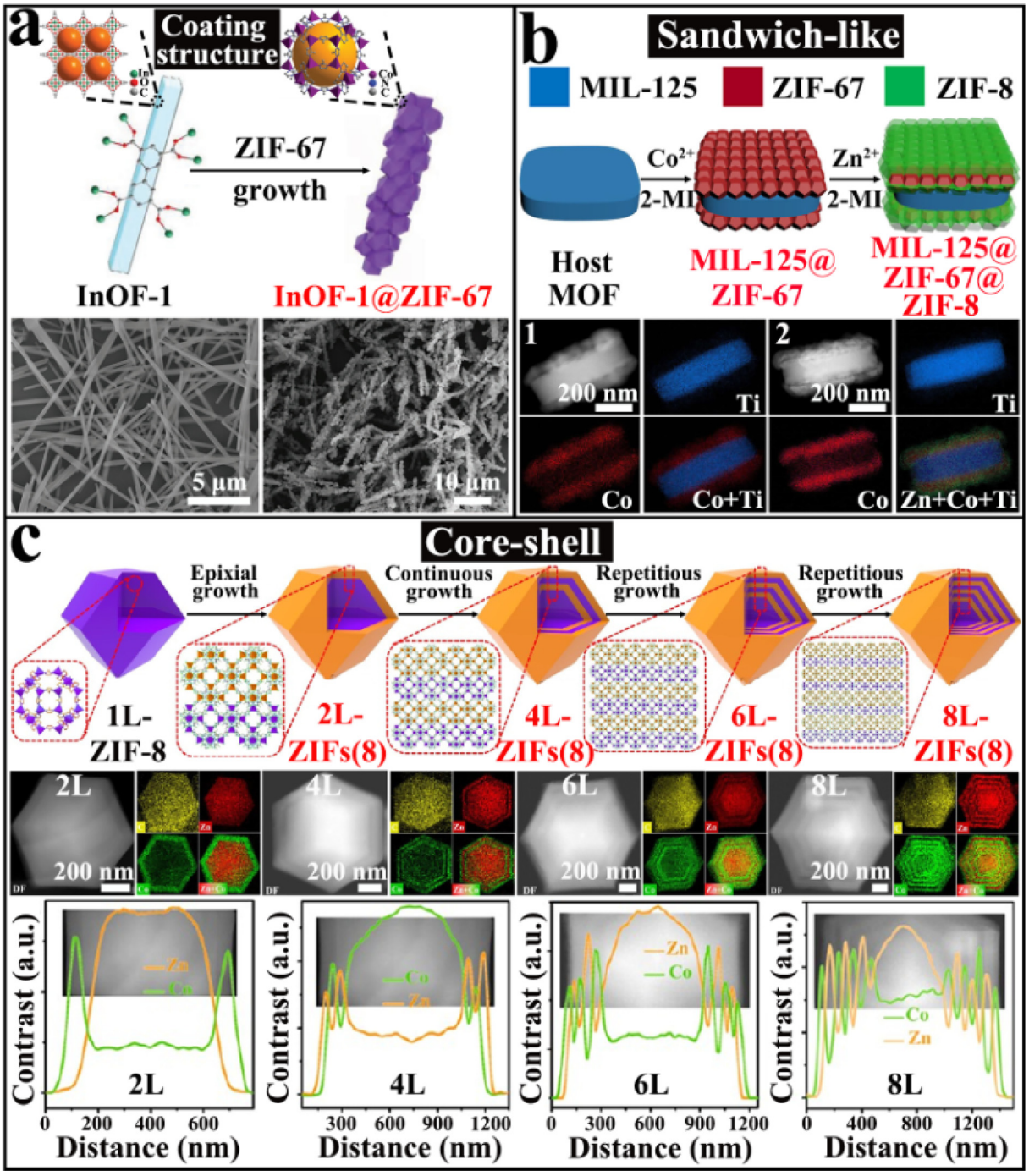

Fig. 10. A) The synthesis process of binary InOF-1@ZIF-67. Reproduced with permission from ref. [117]. Copyright 2020, Wiley-VCH GmbH. b) Selective growth of ternary MOF-on-MOF heterostructures. Reproduced with permission from ref. [118]. Copyright 2020, Springer Nature. c) Controllable synthesis of the multilayer-ZIFs. Reproduced with permission from ref. [119]. Copyright 2019, American Chemical Society.

assembled during the evaporation process to form a dense and intact MOF-gel film. SEM images show that the made MOF-gel film composed by the ZIF-8 nanoparticles (NPs) exhibit a smooth surface and a thickness of around 30 μm.

Under these circumstances, self-assembled MOF membranes are intrinsically endowed with a high MOF loading and great porosity inherited from the microporous MOF precursors. Therefore, they can give full play to potential advantages of the corresponding MOFs as one type of battery separators [171]. Due to the diversity of MOFs with different pore sizes and channels, it is possible to optimize their structure, composition, and property of the self-assembled MOF membranes [172].

3.5. Superstructures

Surprisingly, with the self-assembly method, these simple MOF building blocks can be further transformed into well-ordered superstructures [173]. Generally speaking, superstructure, some composite structures with higher complexity than the original structure, can be formed on the basis of a certain structural level,

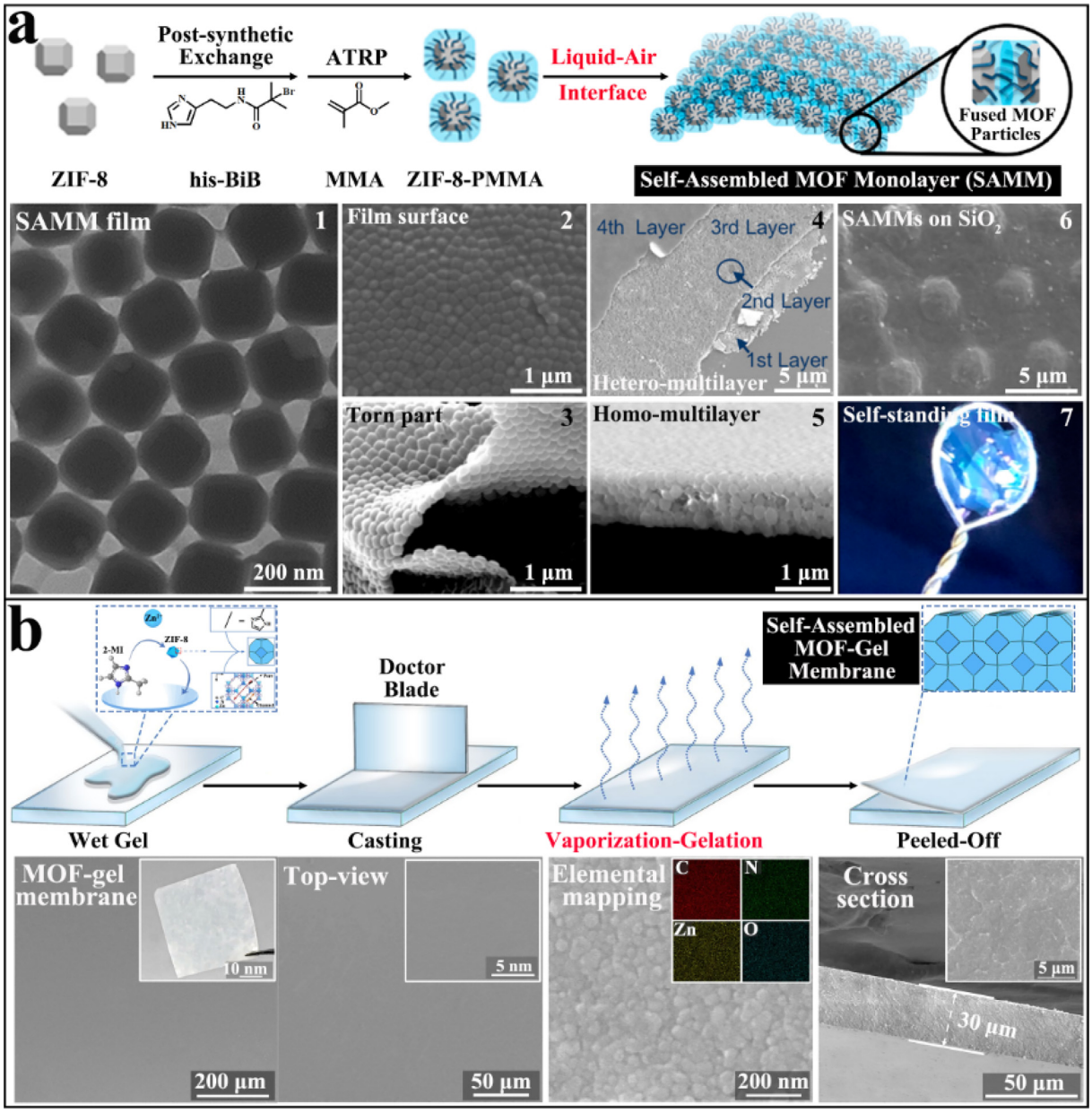

Fig. 11. A) SAMM film using ZIF-8-PMMA precursors. Reproduced with permission from ref. [120]. Copyright 2019, American Chemical Society. b) The vaporization-gelation method to obtain the self-assembled ZIF-8-gel film [121].

arousing great interest in optics, catalysis, and energy-related fields [174,175]. More recently, the self-assembly of uniformly shaped spherical colloidal particles and polyhedral MOF crystals has been demonstrated as a viable strategy to constitute a series of long-range ordered stacking superstructures [176].

Owing to the superior flexibility of MOF nanorods, they will help to form spherical superstructures with spatial order and nanoscale precision. For example, 1D nanorods prepared with crystalline Zn-MOF-74 NPs and urea can be assembled into highly uniform spherical superstructure of MOF nanorods (SS-MOFNR) (Fig. 12**a**) [122]. During the hydrothermal transformation, the slow dissolution of Zn-MOF-74 precursor provides low-concentration metal and ligand, which greatly reduces the nucleation rate and facilitates forming rod-like MOF. Meanwhile, urea as an effective modulator results in the formation of 3D chestnut-shell-like SS-MOFNR. Finally, Zn-MOF-74-derived 1D nanorods are closely and orderly arranged and extend outward to form a spherical superstructure with a large cavity. Under the similar mechanism, the polyhedral ZIF-8 particles react with boric acid (H_3BO_3) to give a spherical superstructure composed of MOF nanosheets (SS-MOFNS) (Fig. 12**b**) [123]. The difference is that H_3BO_3 not only dissolves MOF precursors as an etching agent but also participates in the coordination to transform the topological structure. Furthermore, by controlling the amount of CTAB, ZIF-8 nanocubes will gradually evolve into truncated rhombic dodecahedral (TRD) particles with truncation (t) = 0.69 and 0.57 since they can be selectively attached to the (100) face. It finally turns into the thermodynamically more stable rhombic dodecahedral particles (Fig. 12**c**) [124]. With evaporation in colloidal solution, these uniform MOF particles, including ZIF-8 and UiO-66, are induced by strong van der Waals forces to self-assemble into ordered MOF superstructures.

The advantage of the MOF superstructure is that its appearance and composition can be optimized by adjusting the morphology

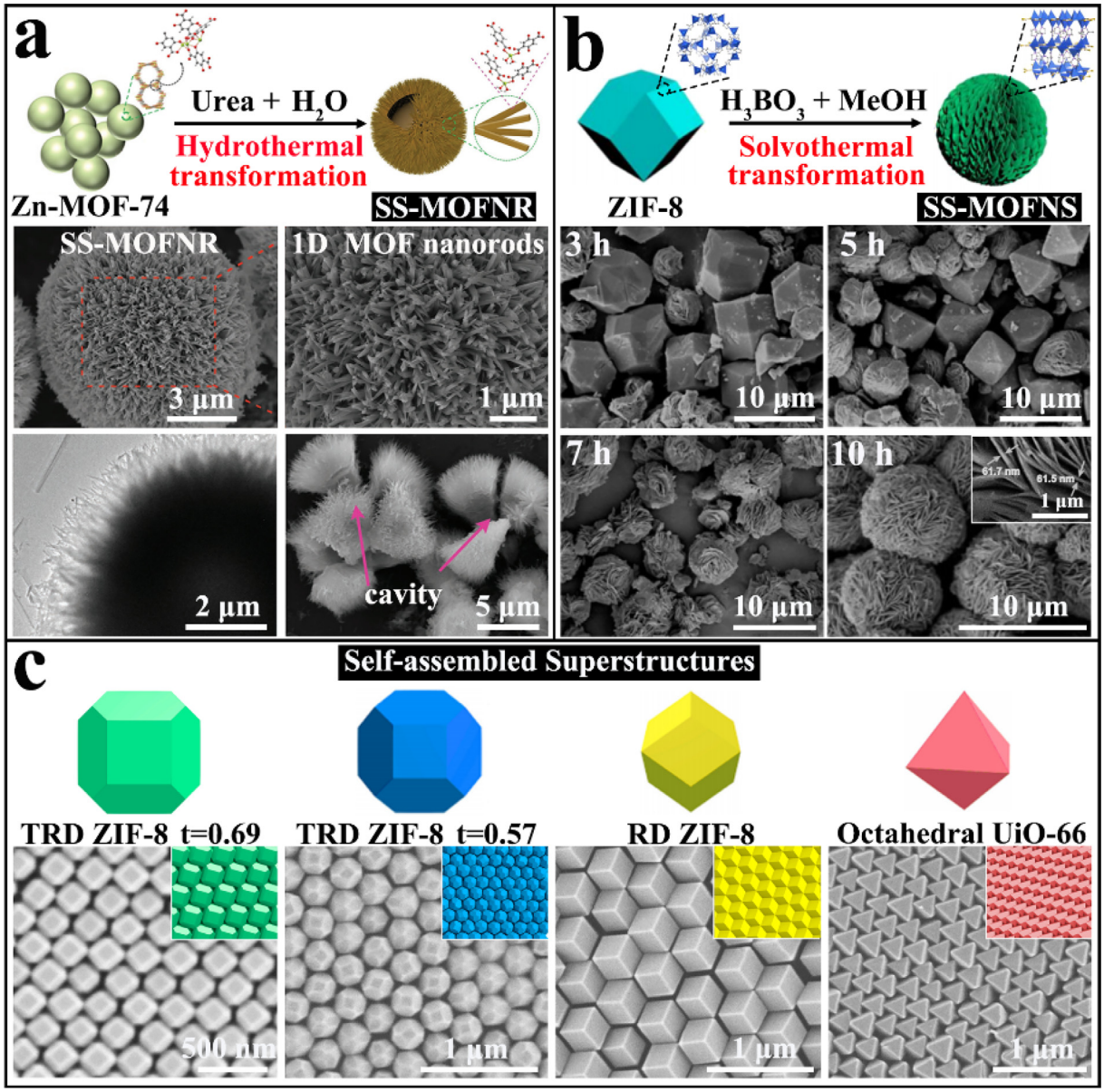

Fig. 12. A) 1D Zn-MOF-74 nanorods to form a hollow spherical superstructure. Reproduced with permission from ref.[122]. Copyright 2019, Wiley-VCH GmbH. b) ZIF-8-derived homogeneous spherical superstructure. Reproduced with permission from ref. [123]. Copyright 2020, American Chemical Society. c) Various homogeneous MOF particles self-assembled into different 3D superstructures [124].

and size of the used MOFs. By chemical transformation, highly uniform 3D spherical superstructures composed of 1D anisotropic MOF nanorods or 2D anisotropic MOF nanosheets can be conveniently obtained [177,178]. Meanwhile, the polyhedral MOF particles with good dispersion, uniform shape, and high colloid stability can also be self-assembled into 3D ordered superstructures [179,180]. These above methods not only provide a new way for the preparation of MOF superstructures, but also provide new ideas for the development of MOF nanomaterials and their derivatives in energy storage, catalysis, and other related fields.

4. Novel synthetic strategies of MOFs

In addition to changing the necessary factors for the production of MOFs, the morphology and structure of MOFs can also be adjusted by using different synthetic strategies [181]. Generally, most of MOF materials can be obtained by conventional methods where the nucleation occurs and crystal grows in a homogeneous solution [182]. For example, in the synthesis of porous MOFs for gas storage and separation, a useful method is to use these metal-binding solvents, such as water [183]. In these cases, when the solvent is evacuated, the exposed metal sites from the desolvated MOFs can easily and selectively combine with the target gas molecules [184]. Although the hydrothermal or solvothermal synthesis have been demonstrated as the most common and effective approach to synthesize structurally stable crystals in the laboratory [185], the use of MOFs for commercialization requires the further development of new synthesis methods at a large scale.

4.1. Chemical vapor deposition

Through CVD, smooth and defect-free MOF films can be effectively deposited on the substrate, which has attracted much attention [186]. This MOF-CVD method consists of two steps: I) metal

oxide layers are first deposited; II) these layers are exposed to sublimate ligand molecules, inducing phase transformation into the MOF lattice (Fig. 13**a**) [125]. The introduction of solvents with favorable hydrogen bond acceptors, such as DMF or EtOH, will contribute to stabilizing the porous structure and promoting the formation of crystallized ZIF-71 during the reaction between ZnO and 4,5-dichloroimidazole (HdcIm) vapor (Fig. 13**b**). On the contrary, while the added solvent is changed to H_2O vapor, it will evolve into amorphous ZIF-72. And SEM images show that the two kinds of topologically controlled ZIF crystals are assembled into dense and uniform MOF films (Fig. 13**c, 13d**).

In recent years, the CVD growth of MOFs is a rapidly developing field, and crystals such as ZIF-8, ZIF-67, MOF-5, CuBDC, CuCDC, and HKUST-1 have been successfully synthesized by this method one after another [187,188]. In contrast to the solvothermal, CVD allows the facile synthesis of porous MOFs under solvent-free and catalyst-free conditions. For example, the zeolitic imidazolate framework (MAF-6), which consists of 2-ethylimidazolate linkers and Zn^{2+} ions, is not easily synthesized in solution due to its substable nature [189]. On the other hand, the methylene group of 2-ethylimidazole enhances the volatility of the organic linker, hence giving it well suited for gas–solid reactions with ZnO. Thus, the film deposition of MAF-6 can be achieved completely from the gas phase synthesis when ZnO is vaporized with 2-ethylimidazole and without any solvent addition at any stage. Another work has showed that the MOF-CVD process relies on the solvent-thermal conversion of the atomic layer deposited oxide to MOF [190]. However, in the absence of solvent, when the ZnO precursors are fully exposed to the vapor of the protonated 2-MI linkers can conveniently form even ZIF-8 membranes, which is used to prepare gas separation membranes, sensors and energy storage devices.

The reasonable utilization of MOF-CVD method has exerted great research value in changing the morphology and structure of MOFs. During the formation of MOF films, the introduction of solvent steam in MOF-CVD process can control the polymorphism of MOFs and form more uniform films. For CVD preparation, some important parameters that should be especially paid attention to include the flowing speed of vapor, temperature, pressure, supporting substrate, etc. [191]. Meanwhile, the MOFs in thin-film form can retain the original structure of MOFs, with high porosity and large specific surface area more conducive to gas storage and screening.

4.2. Electrochemical growth

Based on the structural advantages of porous MOF films, the *in-situ* electrochemical growth is recently proposed [192]. These advantages of electrochemistry-assisted interfacial growth MOF membranes are as follows: 1) less time consuming and no needs of high-temperature and high-pressure conditions; 2) no limitation of solvent types; 3) easy realization of precise control and real-time monitoring of MOF synthesis [193]. Therefore, this synthesis strategy is expected to achieve interfacial synthesis of MOFs on porous polymer substrates, reduce the difficulty of synthesis, and expand the application range of MOF/polymer composite membranes [194].

In the process of electrochemical preparation of HKUST-1 film, the H_3BTC solution, Cu plate, and porous polyethersulfone (PES) covered Cu plate are used as the electrolyte, cathode, and anode, respectively (Fig. 14**a**) [126]. During the anode reaction, the precipitation rate of Cu(II) cations can be adjusted by controlling the current intensity, while the precipitation of hydrogen promotes

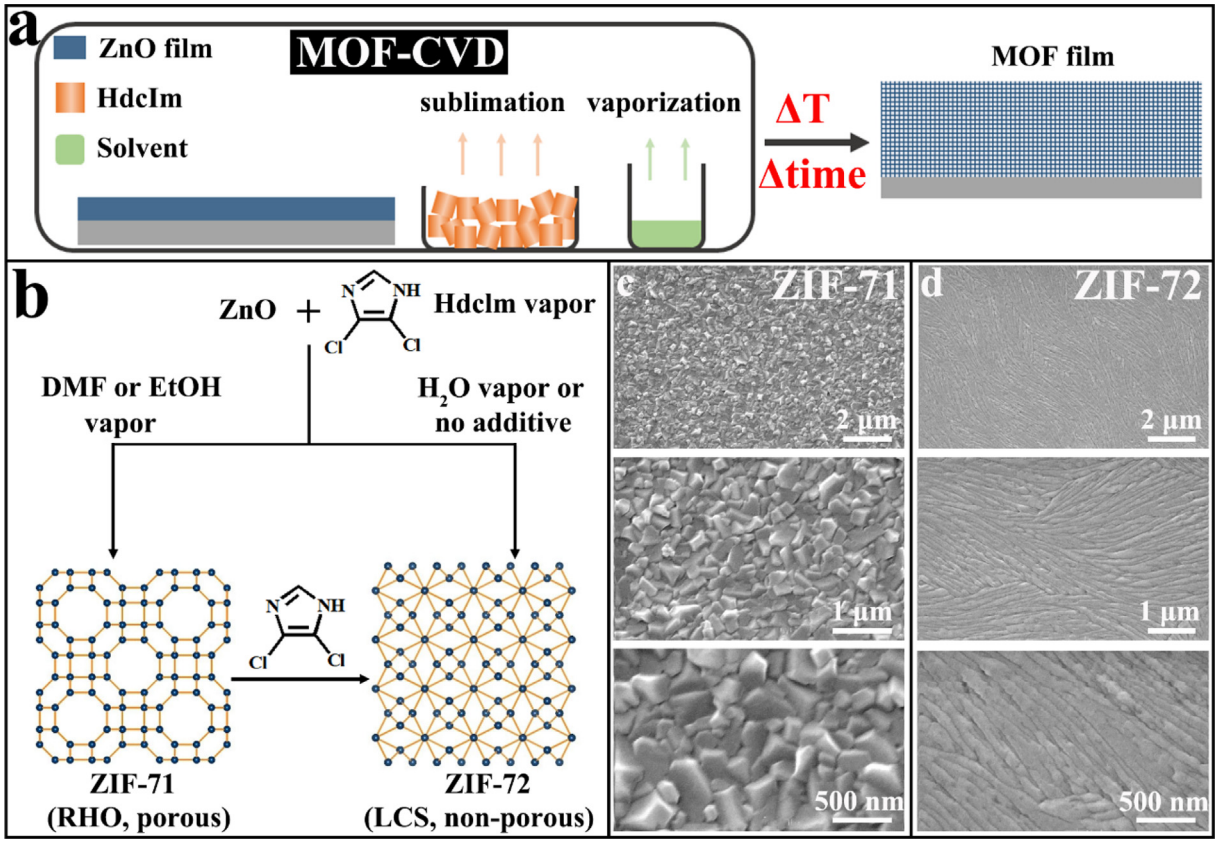

Fig. 13. A) Schematic illustration of MOF-CVD growth of MOF film. Reproduced with permission from ref. [125]. Copyright 2021, Wiley-VCH GmbH. b) Solvent vapor-mediated topology control during the formation of ZIFs. c, d) SEM images of ZIF-71 and ZIF-72 films.

the deprotonation of organic ligands, thus facilitating the growth of MOFs. Combined with SEM images and element mapping analysis, it can be proved that the irregular polyhedral crystals are densely stacked to form a continuous and complete Cu-BTC/PES membrane (Fig. 14**b-14h**). The combination of polymers and MOFs not only gives play to the porous structure characteristics of polymer supports, but also makes full use of the absorption ability of MOFs. The as-prepared MOF/polymer membrane have great advantages in dye adsorption and many other applications [195,196].

In addition to the anodic dissolution strategy described above, there are cathodic deposition and electrophoretic deposition methods in the preparation of MOF films by electrochemical deposition [197]. Firstly, in the cathodic deposition strategy, both metal ions and organic ligands are dissolved in the solvent, and reduction reactions occur near the conductive substrate to promote ligands deprotonation, and eventually nucleation and crystal growth on the substrate. This cathodic deposition method can be used to fabricate ZIF-8 membranes, using water as the solvent and obtaining low defect density membranes without any pre-synthesis treatment, which show excellent performance in C_3H_6/C_3H_8 separation.[198]. Besides, in the electrophoretic deposition strategy, charged particles are driven by an electric field toward the conductive matrix and eventually form a thin film on the substrate. For instance, 2D $Ni_3(HITP)_2$ nanosheets can be deposited on nickel foam using an electrophoretic deposition method for the facile preparation of supercapacitor and exhibits excellent electrochemical properties in Na_2SO_4 electrolyte [199].

4.3. Spray-drying

Considering the unconventional nanometer effect, the nanoscale MOFs often have a higher range of applications and better performance than micron-level MOFs [200]. Although the traditional solvothermal method can efficiently produce the ultrafine MOFs, the synthetic method with adjustable composition and uniform size distribution of nanometer MOF is still a difficult and demanding task [201]. With the in-depth research, the spray-drying technology acts as a kind of general cost-effective method that can be used in the rapid, large-scale synthesis and self-assembly of MOF nanocrystals [202].

By atomizing the solution containing metal ions and organic ligands, the efficient nucleation and crystallization will occur on the surface of the formed micro-droplets, and the hollow spherical nanosized MOF superstructures can be created conveniently (Fig. 15) [127]. Primarily, the solvent of atomized droplets begins to evaporate and induce the diffusion of the internal precursors to the surface under the heating action of circulating airflow. With the solvent evaporation, the concentration of precursors will gradually increase until the initial crystallization, and they eventually assemble into the 3D spherical nanoscale complexes when the liquid disappears completely. At the same time, by adjusting the operating parameters, such as gas temperature and airflow rate, the hollow nanosized MOF materials with ideal size and structure can be selectively prepared. According to this novel method, several hollow nanoscale MOFs, including HKUST-1, Cu-bdc, MIL-88A, MIL-88B, MOF-74, MOF-14, NOTT-100, and UiO-66 crystals, can be conveniently synthesized to verify its practicality and universality.

In this context, the convenient preparation of hollow MOFs would show better application in guest molecule adsorption because of their unique nanostructures and large cavity. The emerging spray-drying technology can realize the large-scale production of nanoscale MOF nanomaterials and greatly reduce the synthetic cost and production time. Finally, it is worth noting that another satisfactory advantage of spray-drying is to recycle a large number of used solvent that can protect the environment to a large extent [203]. Among them, hollow MOFs have been proved to be promising candidates for electrolytes as well as catalysts in a variety of applications [204,205].

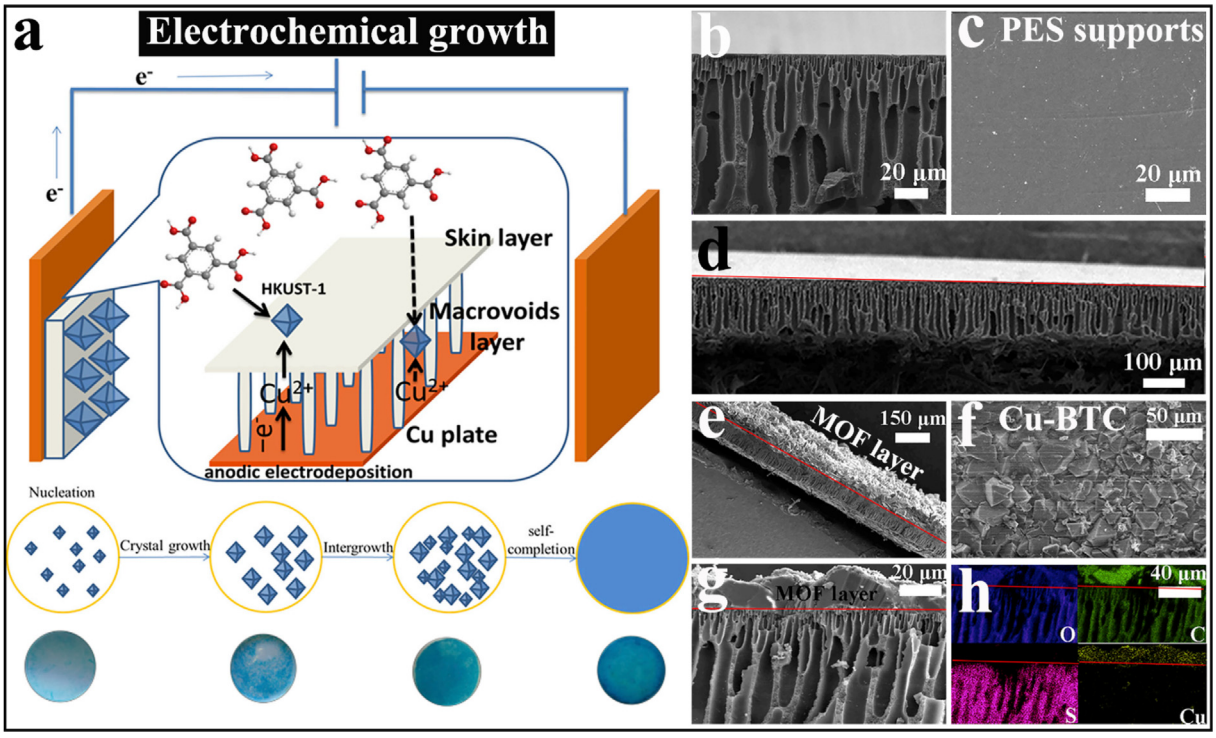

Fig. 14. A) Electrochemistry assisted interfacial growth of HKUST-1 membrane. Reproduced with permission from ref. [126]. Copyright 2019, Elsevier. b-d) SEM images of PES supports. e-g) SEM images and h) Element mapping images of the obtained MOF/PES film.

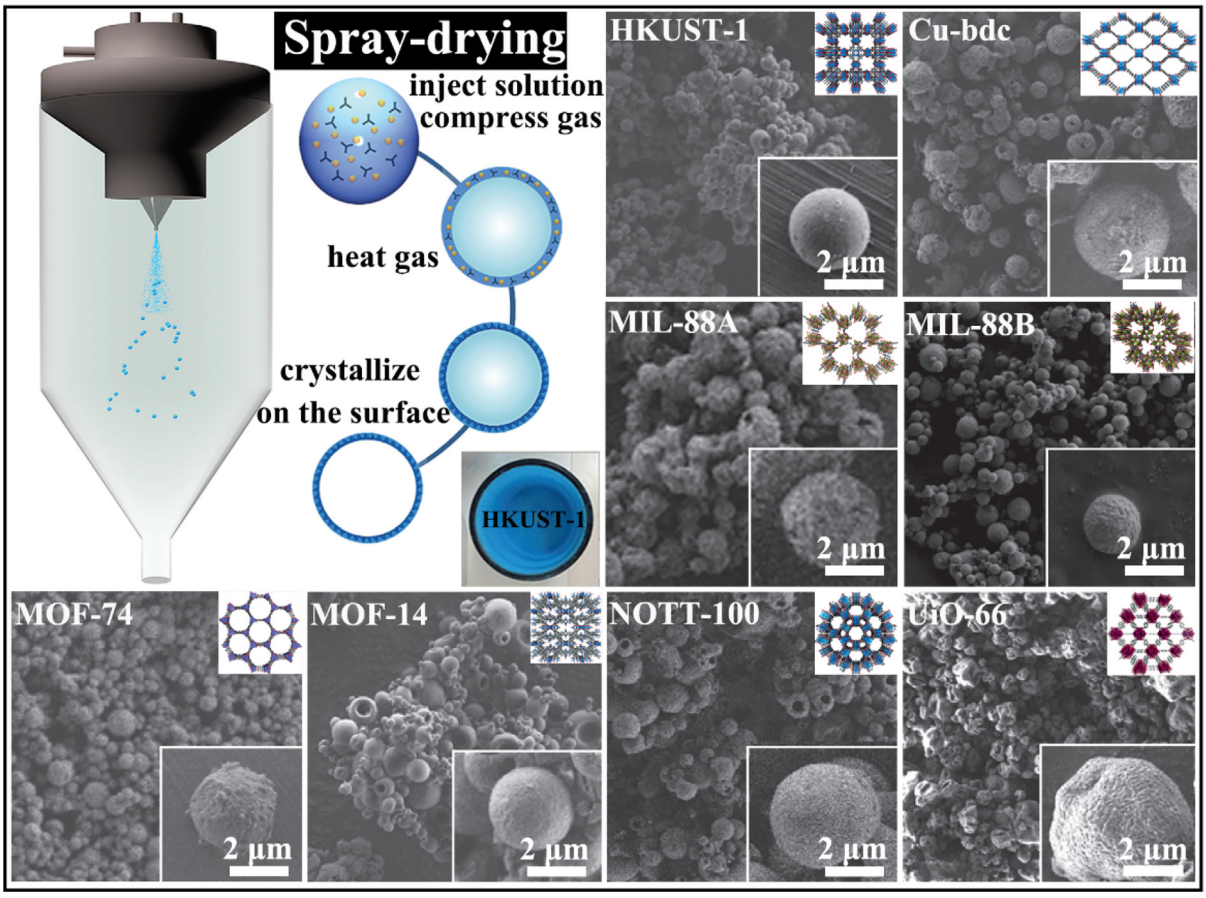

Fig. 15. A series of hollow MOF superstructures synthesized by spray-drying [127].

4.4. Chemical etching

Recently, hollow MOF materials can be conveniently obtained by anisotropic chemical etching, which exhibit the well-defined geometry with controllable or selectively etched facets [206,207]. However, it remains a huge challenge to prepare the MOF crystals with hollow structure and excellent geometrical shape with the rational design and facile synthesis. In Fig. 16**a, 16b, a** type of truncated rhombic dodecahedron ZIF-67 (tZIF-67) is synthesized, which is further transformed into a unique hollow framework via combining the anisotropic surface modification and etching strategies [128]. Due to the steric hindrance effect of the (100) face, the cyanuric acid (CA) molecules are more likely to bond with the (110) plane, thereby protecting them from etching in the following stage. Subsequently, the protons released from CA could competitively break the coordination bond to cause the inside-out selective etching of (100) face (Fig. 16**c**). Furthermore, the added metal salt, such as H_2PtCl_6, not only can play the role of etching agent as Lewis acid, but also can be used as a doping agent to diversify the composition of the final product. And the SEM and TEM images show that H_2PtCl_6 also selectively etches the (100) face of tZIF-67 and gives rise to six square pits on the surface, which suggests that the etching reaction with metal salt is conducted outside-in (Fig. 16**d**).

Typically, hollow nanostructures can be prepared with MOFs as templates since weak metal–organic coordination bonds are prone to be broken when reacting with metal salts. The kinetics of shell layer formation and template removal can be controlled by regulating the concentration of MOF precursors and metal salts, which will lead to the formation of hollow layered double hydroxides on the MOF surfaces [42]. In addition, a wet chemical process can be used to control the anisotropic etching of ZIF-8 and ZIF-67 crystals [208]. Because the exposed crystal faces, edges, and vertices of MOFs own different chemical compositions, and etching process preferentially occurs in the crystal orientation where metal–ligand bonds are abundant and on the high-dimensional number of crystal surfaces [209]. Therefore, the solubilization rate of the metal ions can be regulated by adjusting the pH of etchants, which ultimately converts these porous MOFs uniformly into a hollow morphology.

In general, these nanomaterials with hollow morphology have recently attracted significant research interest for various applications on account of their unique nanostructures and intrinsic physical and chemical properties. It deserves more efforts to the development of hollow MOFs and their derivatives with the simple and effective chemical etching. Moreover, the acidity/alkalinity of the etchant and its affinity to different crystal planes within various MOFs should be under an in-depth investigation [210,211].

4.5. Mechanochemistry

On the other hand, when different types of inorganic species are deliberately or randomly combined into the lattice of MOF structures, more metal centers will be inserted to make this kind of polymetallic MOFs have more unique properties [212]. It is well known that mechanochemistry is recognized as a powerful tool for the facile preparation of various porous nanomaterials, and ball milling is the most common method [213,214]. In the process of

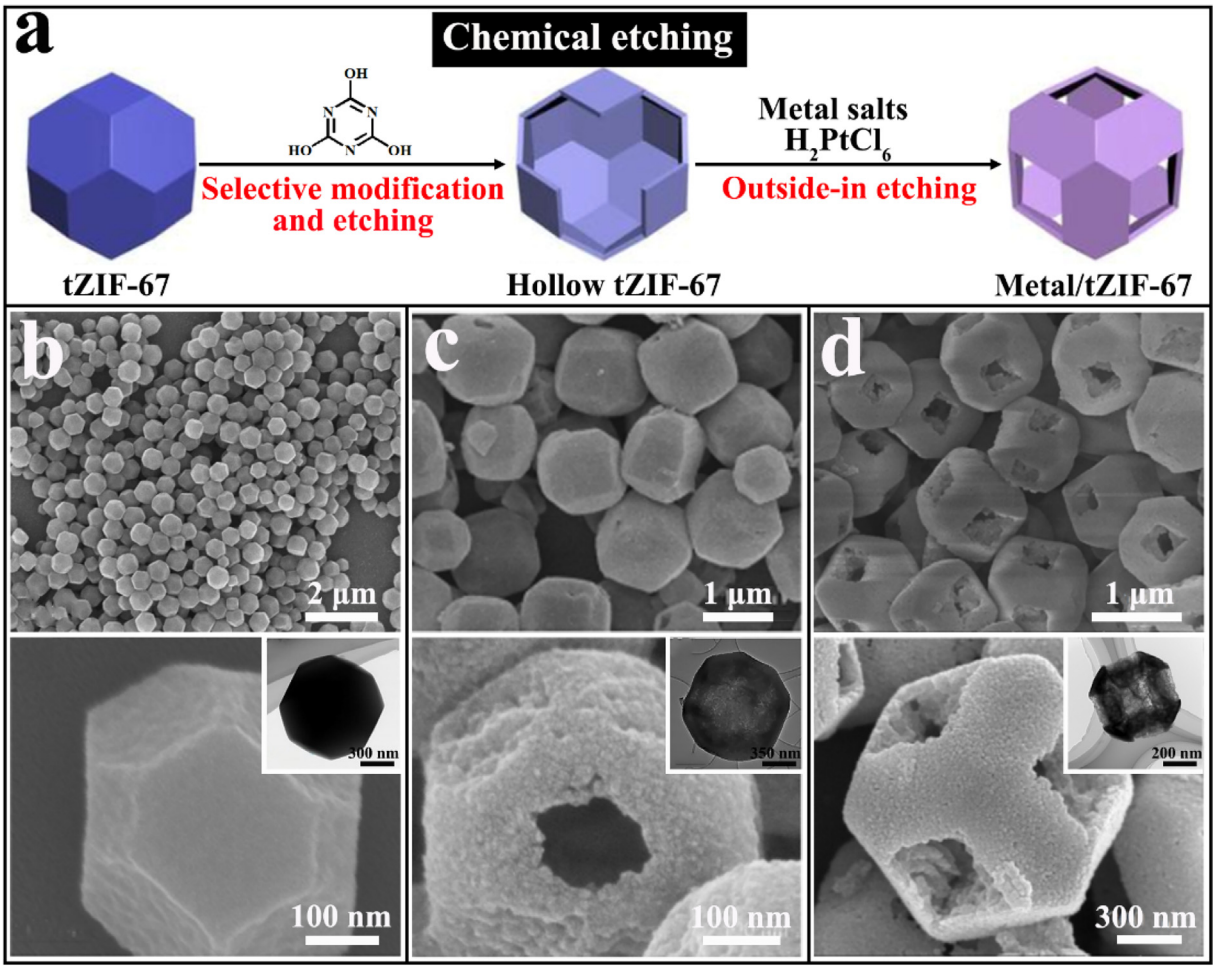

Fig. 16. A) Hollow MOFs by anisotropic chemical etching. Reproduced with permission from ref. [128]. Copyright 2021, Wiley-VCH GmbH. The SEM images for b) tZIF-67, c) hollow tZIF-67, and d) Metal/tZIF-67.

ball grinding, local short-range heating is used to induce the formation of high-entropy MOFs [129]. The rapid development of high-entropy materials provides the possibility to obtain MOF materials that constitute two or more inorganic SBUs [215,216].

In this context, one high-entropy ZIF (HE-ZIF-BM) containing five metal species is prepared by long-time powerful ball milling of Zn(II)/Cu(II)/Cd(II)/Ni(II)/Co(II) based metal salts together with an excess of 2-MI ligand (Fig. 17**a-17b**) [129]. It shows that the synthesized HE-ZIF-BM owns similar crystal structure, Brunauer-Emmett-Teller (BET) specific surface area, and pore width in comparison with the HE-ZIF-ST obtained by a traditional solvothermal approach (Fig. 17**c-17e**). In this case, compared to single-metal ZIF material, the five metal ions play a synergistic role and have stronger catalytic conversion of CO_2 to carbonate in HE-ZIF material.

Moreover, ball milling is well-known for the solvent-free, and can be used to encapsulate various nanosized particles when combined with porous MOFs. For example, since bulky and rigid fullerenes are soluble only in nonpolar solvents, while MOFs are unstable in most solvents, encapsulation of fullerenes into MOFs by solvent-based methods is obviously a great challenge. However, the problem of solvent selection is not only avoided when preparing MOFs by the ball milling, but also fullerenes can be completely encapsulated within the crystal voids [217]. Besides, a series of enzymes, such as β-glucosidase, invertase, β-galactosidase, and catalase, can be efficiently included in ZIF-8, UiO-66-NH_2, or Zn-MOF-74 by mechanochemistry, thus preserving the biological activity of the enzymes to a large extent [213]. Furthermore, it is feasible to wrap metal NPs with MOFs and prevent the aggregation of metal NPs on the crystal surface with assistance of the ball grinding method [218]. Therefore, the preparation of MOFs by mechanochemical method presents the following advantages: 1) no solvent is needed enabling the synthesis process to be safe and pollution-free; 2) the problem of uneven growth of MOFs in solution can be avoided; 3) more kinds of functional NPs can be coated to form MOF composites without destroying the overall crystal structure.

4.6. Others

To expand their application range, the facile preparation of various MOF materials with varied shapes and tunable structures is highly desired. For instance, when MOF is combined with 3D printing technology [219], the hierarchical integration of functional nanoscale MOF materials can be achieved. Meanwhile, a continuous and facile bottom-up method is utilized to obtain ultrathin 2D metal–organic nanosheets directly through the novel microdroplet flow reaction [220]. In addition to these above-mentioned novel methods, there are more and more emerging synthesis methods that have also been developed to date [221–224].

In Fig. 18**a, 3D** Ln-MOFs-assembled optical platforms with tunable colors and morphology features are successfully constructed using a direct ink writing [225]. At first, the mellitic acid with high connectivity and hydrophilic sodium alginate are mixed together to obtain the fine precursor inks. After that, the ink can be loaded

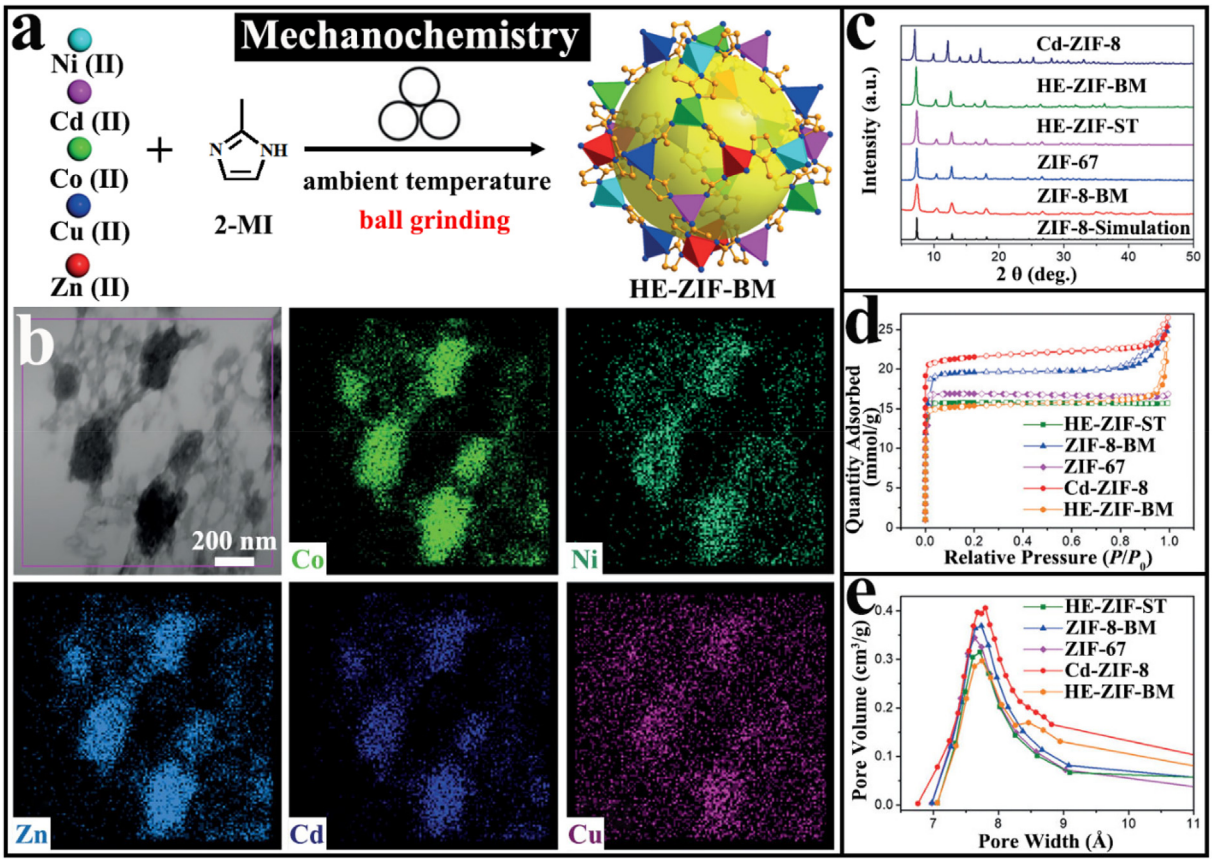

Fig. 17. A) The synthesis of HE-ZIF by ball milling. b) TEM image and EDS elemental mapping images. Reproduced with permission from ref. [129]. Copyright 2019, Wiley-VCH GmbH. c) PXRD patterns, d) N_2 isotherms, and e) BJH PSD curves of ZIF-8 derivatives.

into a 3D printing workstation to produce variously shaped materials (Fig. 18**a1-18a6**). Meanwhile, the emergence of microdroplet flow technology has also witnessed a breakthrough in the production of ultra-thin MOF nanosheets (Fig. 18**b**) [130]. In this case, the 2D ZrBTB affected by van der Waals interaction and interlayer hydrogen bonding will generate 3D blocky crystals by solvothermal method (ST-ZrBTB). However, in the microdroplet flow reaction process, it is beneficial to restrict the growth of crystal along the vertical direction to form the ultra-thin 2D nanosheets (MF-ZrBTB). Clearly, the collected SEM, HRTEM and AFM images show that the as-synthesized 2D MF-ZrBTB nanosheets exhibit well-dispersion and distinct wrinkle with an average thickness of 3 nm. Furthermore, the traditional X-ray and electron-beam lithography (XRL and EBL) can be further utilized to achieve resistance-free lithography of MOFs at the small scale and fabricate highly permeable materials with controlled morphologies (Fig. 18**c**) [226].

5. Relevant applications of MOFs and their derivatives

Thanks to the unique morphology, adjustable nanostructure, abundant active site, diverse pore environment, and large specific surface area, MOF materials have attracted numerous attention in the fields of environmental protection and energy conservation, including gas storage and separation, heterogeneous catalysis, drug delivery and release, etc. [227–229]. Moreover, because metal ions and organic ligands are regularly and orderly arranged in the crystals, MOF materials can also be utilized as appropriate precursors or sacrificial templates for the facile preparation of multifunctional nanomaterials with intricate structure, tunable composition, and uniform distribution of components [230]. Through calcination in different atmospheres, such as argon or air, MOFs can be thermally transformed into porous metal oxides, metal phosphides, and metal carbides with certain structures, which not only inherit the special morphology of precursors but also exploit innovative functional applications in more scientific fields.

5.1. Gas storage and separation

In order to meet the demand for clean energy and the reduction of greenhouse gas emissions, the H_2 storage, as well as CO_2 capture and sequestration, remains a great challenge. MOFs are a unique class of porous materials that have attracted extensive scientific interest for gas storage and separation applications [231,232]. To improve the adsorption capacity, different types of MOFs have been prepared to face the sustainability issues with great environmental benefits [233]. Although MOFs, COFs (covalent organic frameworks) and HOFs (hydrogen-bonded organic frameworks) are all crystalline materials, they structurally differ in structure due to various bonding modes. For example, HOFs are slightly less designable and unstable due to weak bond orientation. In contrast, MOFs are ligated by metal ions and organic ligands, which becomes more stable. Also, MOFs can be modified to have more flexible structures, thus showing significantly better performance than COFs and HOFs in terms of gas separation, energy storage and other related applications.

After structural modification, the performance and application of MOF nanomaterials can be improved. For example, in the mixed-ligand system, sphere (10:5), oval (7.5:7.5, 6.5:8.5), angulated oval (5:10, 3.5:11.5), and inflated hexagonal rod-like (2:13) In-based MOF particles can be obtained by adjusting the ratio of

H_2IPA and H_2BDC linker (Fig. 19**a-19f**) [70]. It is proved that the morphology structure and porosity of the resulting products are closely related to the relative amounts of the two organic linkers, which greatly affect the gas adsorption performance. Clearly, the N_2 and CO_2 adsorption capacity could be improved gradually with the increase of H_2BDC connector (Fig. 19**g-19h**). Meanwhile, the development of novel porous MOFs for transporting H_2 and CH_4 which are considered as the sustainable energy carrier and alternative to fossil fuels is of great intergenerational importance. At present, the HKUST-1 monoliths as the best-in-class densified MOF could store 46 g L^{-1} H_2 at 50 bar and 77 K, and delivers 42 g L^{-1} H_2 at the same operating pressures [132]. Besides, after a large-scale computational screening of 5446 MOFs, DUT-23(Cu) and DUT-23(Co) exhibit higher working capacities towards the natural gas than other porous materials, and exceed the airborne CH_4 storage and release performance targets set by advanced research projects agency-energy [234]. Moreover, MOFs with porous properties can be applied to adsorb greenhouse gases to ameliorate global climate issues, which is also worthy of further study and discussion.

To achieve better gas separation effect, the pore environment can be further optimized by decorating the SBUs of MOF, so that the obtained materials can selectively sieve gas molecules. Inspired by this, the IM ligand is chosen to modify the $Fe_3(\mu_3\text{-}O)(CH_3COO)_6$ of soc-MOF to construct the stable and microporous soc-MOF-IM membrane (Fig. 19**i-19j**) [83]. Due to the introduction of IM, the diffusion path of small H_2 molecules do not change, while the further diffusion of larger CO_2 is hindered (Fig. 19**k**). Furthermore, the H_2/CO_2 selectivity of soc-MOF-IM membrane is significantly higher than that of unmodified membrane, indicating that a suitable pore environment is a key factor for efficient gas separation, especially in the pore structure of MOFs (Fig. 19**l-19n**). However, when several gas molecules are close in size, as in the case of light hydrocarbon mixtures (C_2H_2, C_2H_4, C_2H_6, C_3H_8), more efficient methods are required for the precise detection and monitoring. For example, Raman spectroscopy isotherm is analyzed to investigate the interaction of MOFs with adsorbed gaseous guests, thus determining the independent adsorption contribution of each component in the gas mixture and facilitating the initial screening of adsorbents in the separation [235]. Unfortunately, it remains a puzzle to regulate the internal structure of the MOFs to achieve a satisfactory separation.

5.2. Dye adsorption and degradation

On the other hand, the rapid development of industry has produced many organic pollutants that cause increasingly serious environmental pollution. There is a strong demand to develop a novel technology to decompose organic pollutants into harmless carbon dioxide and water. In recent years, PB nanocrystals with different sizes and morphologies have been synthesized to over-

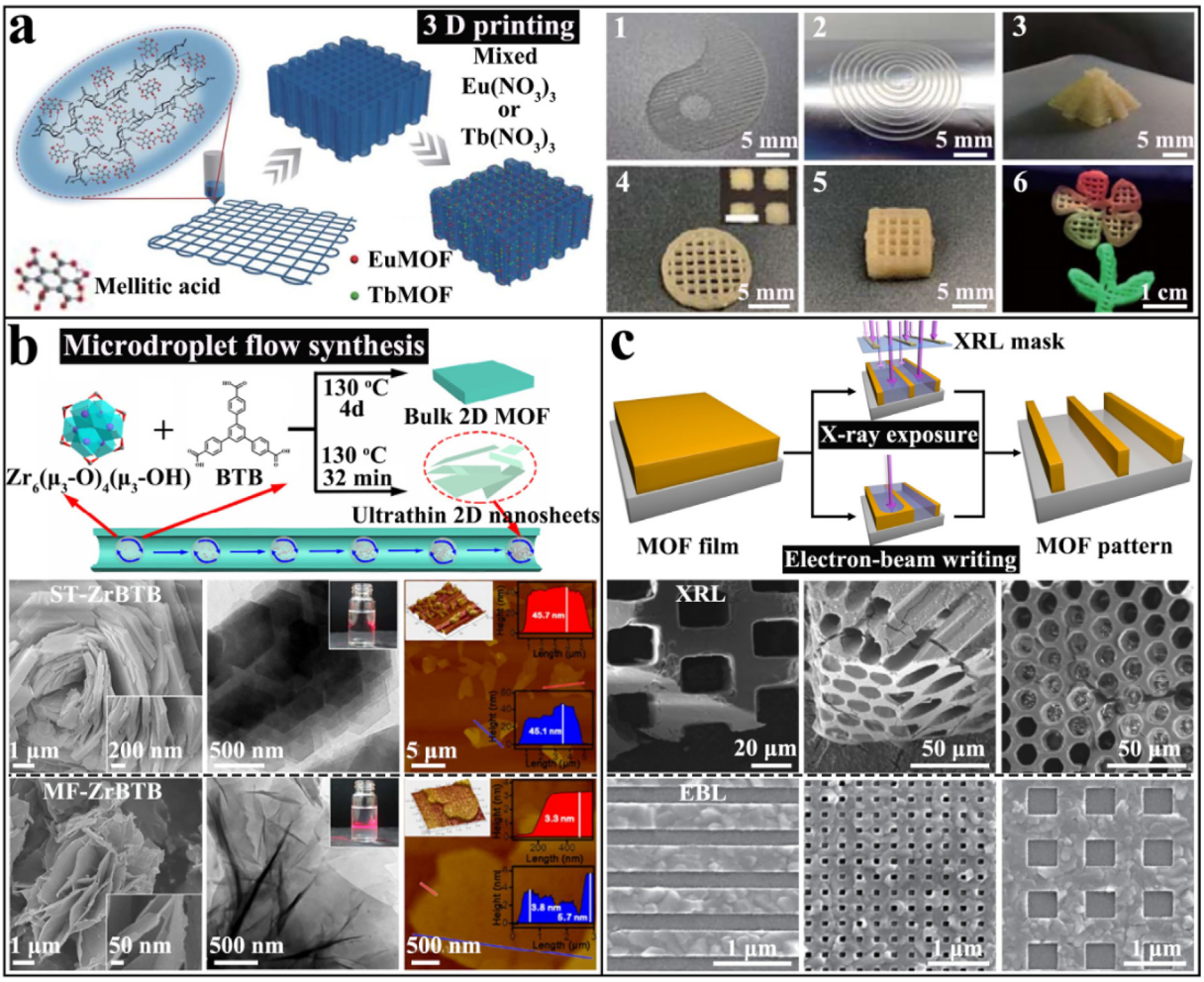

Fig. 18. A) Schematic illustration of controlled assembly in 3D printing. Reproduced with permission from ref. [225]. Copyright 2021, Springer Nature. b) The process of 2D MF-ZrBTB through microdroplet flow reaction technology. Reproduced with permission from ref. [130]. Copyright 2018, American Chemical Society. c) Direct patterning of MOF films by XRL and EBL.[226].

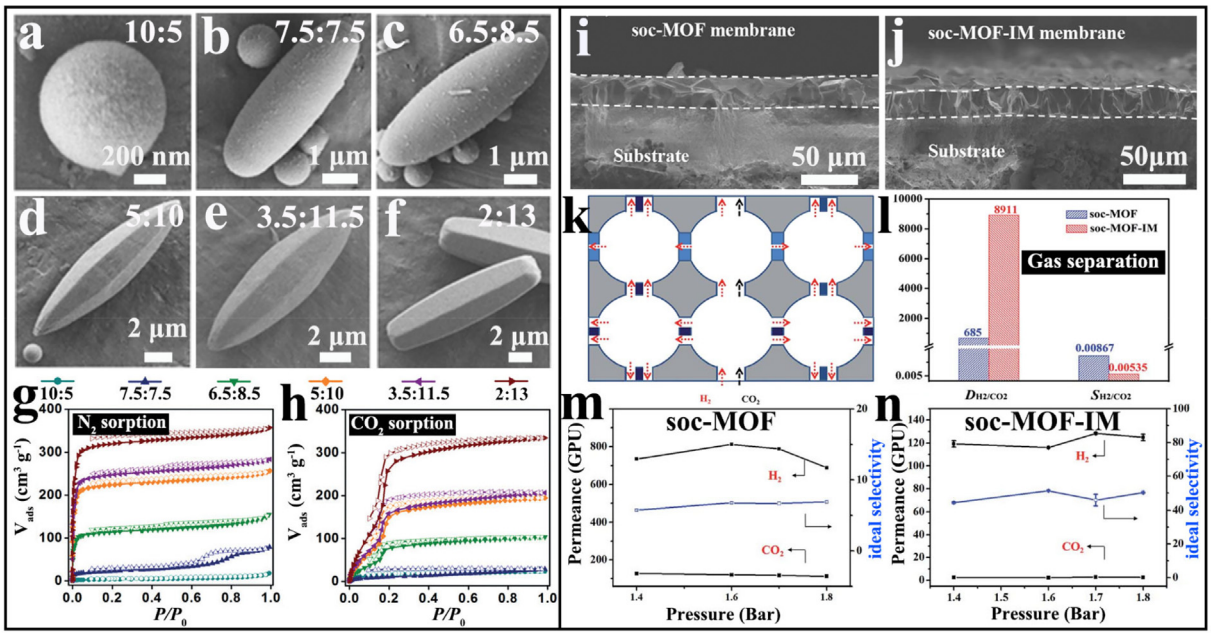

Fig. 19. A-f) SEM images of the morphological evolution of In-MOF particles in various ratios of H_2IPA and H_2BDC. Reproduced with permission from ref. [70]. Copyright 2015, Wiley-VCH GmbH. g/h) N_2/CO_2 isotherms. SEM images of the i/j) soc-MOF/soc-MOF-IM membranes. Reproduced with permission from ref. [83]. Copyright 2020, Royal Society of Chemistry. k) Gas diffusion diagram of H_2 and CO_2. l) The D_{H2}/D_{CO2} and S_{H2}/S_{CO2} of soc-MOF and soc-MOF-IM membranes. Gas permeation properties of the m/n) soc-MOF/soc-MOF-IM membranes.

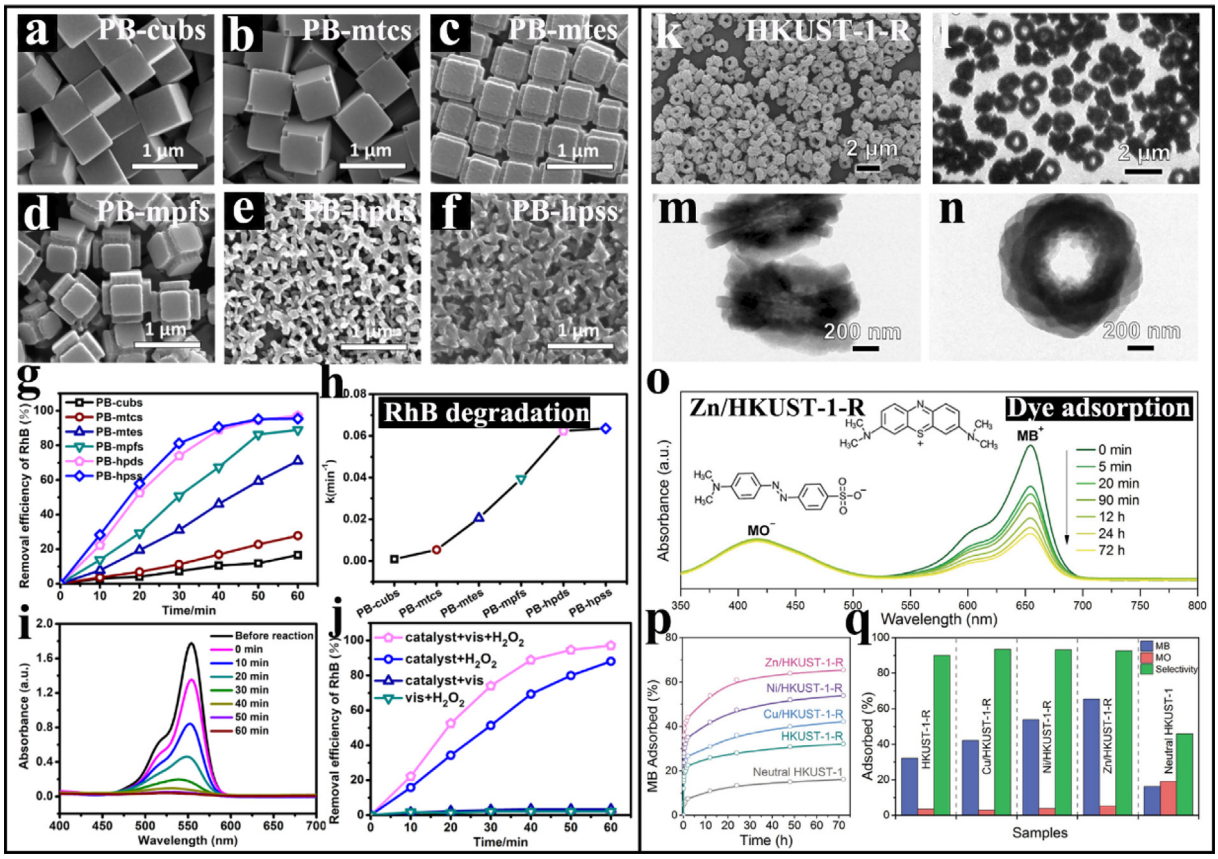

Fig. 20. A-f) SEM images of different PB microcrystals. g) their removal efficiencies of RhB. Reproduced with permission from ref. [99]. Copyright 2019, American Chemical Society. h) Reaction rate constants and i) UV–vis spectra of RhB degradation with PB-hpds. j) Photo-Fenton activities of PB-hpds. k) SEM and l-n) TEM images of Zn/HKUST-1-R. Reproduced with permission from ref. [100]. Copyright 2017, Wiley-VCH GmbH. o) UV–vis absorption spectra of MO and MB over time. p) Percentage of MB adsorbed over time. q) Dye adsorption performance.

come these difficult problems. A series of PB microcrystals ranging from cubes to hexapod stars are prepared by adjusting the concentration of H_2PtCl_6 (Fig. 20**a-20f**) [99]. They can be used as photo-Fenton catalyst to degrade the RhB due to their high specific surface area and exposed Fe^{III}-NC active sites. The removal efficiency of cube-like PB to RhB is calculated to be only 16.6% after one hour, while PB-hpds have a significantly higher removal efficiency of 97.1% (Fig. 20**g**). As the etching degree of H_2PtCl_6 deepens, the specific surface area of PB increases rapidly, which is conducive to the exposure of active sites, and the corresponding kinetic constants rise gradually (Fig. 20**h**). By UV–vis spectrum analysis, the concentration of RhB is reduced over time in the presence of PB-hpds microcrystals, and complete degradation is achieved after 60 min (Fig. 20**i**). Finally, the catalytic performance of PB-hpds in different reaction systems is investigated, and results show that when PB-hpds and H_2O_2 coexist, the degradation efficiency of RhB is significantly improved (Fig. 20**j**).

Moreover, ion exchange is an effective method to adjust the structure of MOFs to improve their adsorption performance for dyes. One type of anionic HKUST-1-R with hierarchical ring structure is synthesized by using CTAB as template, which consists of numerous 2D nanoplates stacked together and clustered in the center of the cavity, allowing cationic interaction and thus obtaining mesoporous materials (M/HKUST-1-R, M = Ca, Cd, Ce, Co, Li, Mn, Na, Ni, or Zn) (Fig. 20**k-20n**) [100]. In the dye adsorption, the UV–vis absorption peak of methylene blue (MB) decreases with time, while the absorption peak of methyl orange (MO) remains relatively constant, which proves the selective adsorption of cationic dyes through cation exchange (Fig. 20**o**). At the same time, the non-porosity of neutral HKUST-1 shows a significantly lower adsorption capacity (Fig. 20**p**). More importantly, the anionic frameworks of HKUST-1-R and M/HKUST-1-R provide selective adsorption of the cationic MB, with an efficiency up to 90%, which cannot be achieved within pristine HKUST-1 (Fig. 20**q**). Similarly, another research work reports the removal of MB by Ag-MOF immobilized on graphene oxide at more than 98% under monolayer adsorption with electrostatic interactions [133]. Furthermore, an NH_2-functionalized UiO-66(Zr) could become a carrier for fixing laccase, which improve the pH stability of free laccase and affinity for the dyes, and the removal of crystal violet, malachite green, alizarin green, and MO are as high as 58.80%, 64.82%, 61.61%, and 21.12%, respectively [134]. However, it is well-known that MOFs are prone to decompose in aqueous solutions, especially in acidic and alkaline mediums, so improving the water stability of MOFs could grant more possibilities in dye adsorption and degradation applications.

Therefore, it is very important to control the structure and morphology of MOFs, which can not only enhance the performance but also expand the application range. It is obvious that they have outstanding contribution in reducing greenhouse gas emissions and can effectively protect the environment [236]. Moreover, the significance of MOF morphology control goes far beyond this and will have excellent performance in the energy fields [237].

5.3. Electrochemical catalysts

In recent years, the crisis of traditional energy shortage is becoming more and more prominent, and the development of new energy sources can alleviate the problem to a limited extent, which is of great significance to energy saving and emission reduction [238]. In the field of electrochemical energy storage and conversion, the sustainable and environmentally friendly energy conversion technologies, such as overall water splitting, metal-air batteries, and fuel cells, can effectively overcome the problem of future energy shortages [239]. In the water splitting [240], hydrogen evolution reaction (HER) [241] and oxygen evolution reaction (OER) [242] are two important half reactions, while oxygen reduction reaction (ORR) [243] plays an important role in fuel cell and metal-air batteries. However, its sluggish reaction kinetics severely restricts the efficiency of electrochemical process, and thus electrocatalysts with high catalytic activity are demanded to reduce the energy barrier and enhance the reaction rate [244]. In this case, the MOF-derived electrocatalysts with designated structures and diversified morphologies have large specific surface area, exposed active sites, and open pore structures, which can shorten the mass and charge transfer distance to speed up the electrochemical reaction [245].

The CoP-InNC@CNT is prepared by phosphorization from the sugar-gourd-like InOF-1@ZIF-67 [117]. Their SEM and TEM images show a large number of carbon nanotubes coated with fine CoP particles that are wrapped around the rough surface of the nanocomposite (Fig. 21**a-21b**). Meanwhile, the abundant mesoporous structure of CoP-InNC@CNT compounds are conducive to promoting the charge and mass transfer during electrocatalysis. By analyzing the linear sweep voltammetry (LSV) curves, it can be concluded that the overpotentials of the CoP-InNC@CNT electrocatalyst reach 153 and 159 mV in 0.5 M H_2SO_4 and 1.0 M KOH, respectively (Fig. 21**c-21d**). The corresponding Tafel slopes (62 and 56 mV dec^{-1}) are significantly lower than those of control samples, including CoPInNC (65 and 78 mV dec^{-1}), CoInNC@CNT (106 and 122 mV dec^{-1}), CoInNC (116 and 147 mV dec^{-1}), and InNC (257 and 201 mV dec^{-1}) (Fig. 21**e-21f**), indicating that the MOF-derived catalyst owns more active sites and porous structures.

In order to obtain excellent OER catalyst, by calcination of CoNiFe-MOF in air, the spinel oxide-carbonitride hybrid ($CoNiFeO_x$-NC) with multi-layer structures is obtained (Fig. 21**g**) [61]. The microstructure of trimetallic spinel oxides, including $NiFe_2O_4$, γ-Fe_2O_3 species and amorphous carbon structure, is further confirmed by HRTEM (Fig. 21**h**). In the OER test, the optimal $CoNiFeO_x$-NC electrocatalyst gives an outstanding overpotential of 265 mV at 50 mA cm^{-2} with an excellent Tafel slope of 64.05 mV dec^{-1} as a result of the enhancement of reaction kinetics after adding Co and Ni (Fig. 21**i, 21j**). Besides, the carbonitride provides a stable skeleton and large specific surface area for the uniform distribution of $CoNiFeO_x$ active sites that greatly improves its OER property. When exploring the relationship between electronic structure in different spinel oxides and OER mechanism, the third reaction step owns the largest energy barrier as the rate-determining step (Fig. 21**k-21 l**). However, the free energy of Co-$NiFe_2O_4$ (1 1 0) at the third step drops significantly, which means that it requires a lower overpotential for OER. Therefore, the well-designed $CoNiFeO_x$ electrocatalyst is intrinsically endowed with excellent performance in alkaline OER.

In terms of ORR applications, the research work on MOF-derived carbon materials for ORR applications is also greatly appreciated [246]. Hence, a series of carbon nanomaterials (PBA-I/II/III/IV-700) with Mn_2Co_2C NPs and specific morphologies are prepared by calcining the SDS modified MnCoPBA crystals (Fig. 22**a1-22a4**) [98]. Due to the unique morphology of PBA-III-700 favorable for ion/electron transport in the carbon layer, it possesses a good half-wave potential of 0.801 V, a large diffusion-limited current density of 5.36 mA cm^{-2}, and the lowest Tafel slope of 47.5 mV dec^{-1} close to Pt/C (0.821 V, 5.32 mA cm^{-2}, and 67.2 mV dec^{-1}) (Fig. 22**b-22c**). Although PBA-III-700 exhibits superior stability compared to the Pt/C, it still does not meet industry standards (Fig. 22**d**). In general, the reasons for poor stability are related to the deactivation of active sites, including the carbon corrosion, dissolution of metal atoms, Osterwald ripening, agglomeration, particle detachment, etc. [247]. Therefore, it remains a challenge to seek for suitable MOF precursors to obtain carbon carriers that can effectively stabilize catalytic sites for practical applications.

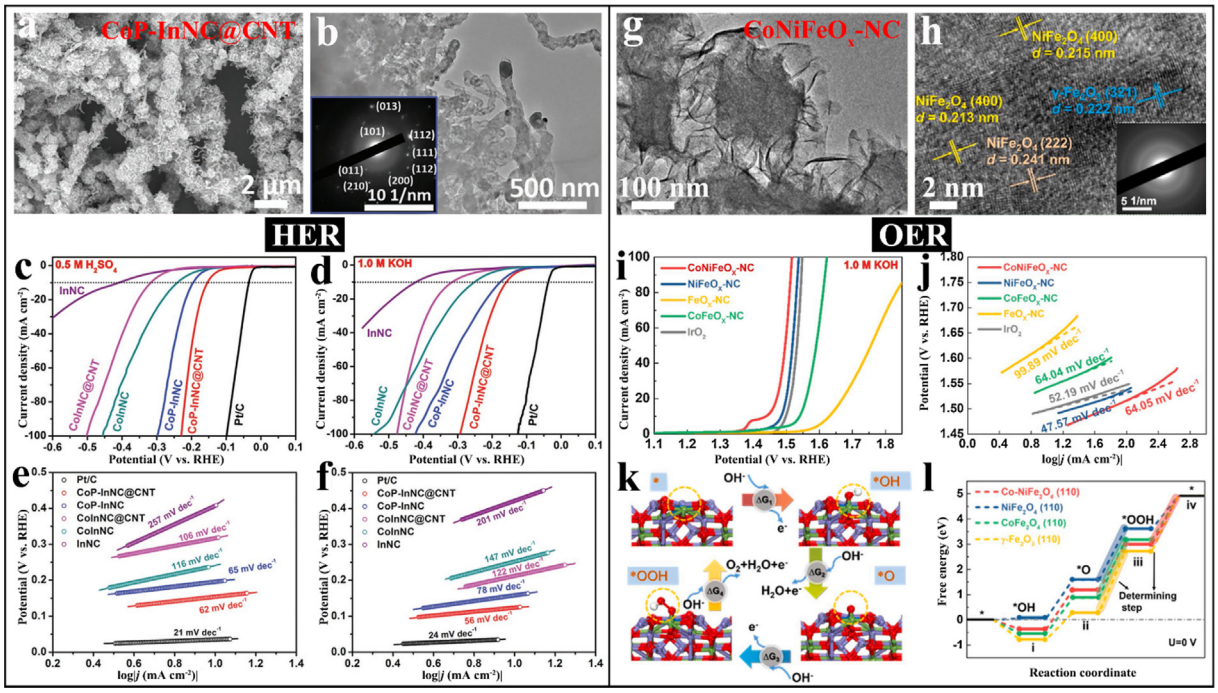

Fig. 21. a/b) SEM/TEM images of CoP-InNC@CNT. Reproduced with permission from ref. [117]. Copyright 2020, Wiley-VCH GmbH. c-d) LSV curves and e-f) Tafel slopes of various samples. g/h) TEM/HRTEM images of $CoNiFeO_x$-NC. Reproduced with permission from ref. [61]. Copyright 2021, Elsevier. i) LSV curves and j) Tafel slopes of different samples. k) Schematic diagram of four-electron transfer mechanism. l) Gibbs free energy for the spinel oxides.

Besides, the reduction of CO_2 to fuels or chemical feedstocks by electrochemical methods is a highly desirable carbon neutral process. Also, HER is the main competing side reaction in the electrochemical CO_2 reduction reaction (CO_2RR), and the inhibition of hydrogen precipitation will greatly increase the Faraday efficiency (FE) of the formed carbon-based products. Three structurally different Bi-MOFs, namely MFM-220, MFM-221, and MFM-222, with different porosity are applied in a comprehensive study of the reduction of CO_2 to formate (Fig. 22**e1-22e3**).[135]. The as-synthesized MFM-220-p/CP (p = potential; CP = carbon paper) with the highest porosity shows the best catalytic performance for CO_2-RR, with a total current density of 23 mA cm^{-2} and $FE_{formate}$ of 90.4% at 1.1 V vs. RHE (Fig. 22**f-22 g**). This study demonstrates the important role of the porosity of MOFs in their evolution into CO_2 reduction electrocatalysts. However, the stability of this CO_2RR catalyst is not as satisfactory as that of the ORR catalyst mentioned above, indicating that the long-term stability effect should be taken into account along with the catalytic performance in the practical electrolysis (Fig. 22**h**).

Moreover, the electrocatalytic reaction also includes the hydrogen oxidation reaction (HOR) which is an important anodic half-reaction driving fuel cell and the nitrogen reduction reaction (NRR) which is a key step in the electrochemical ammonia production. Until now, there is still controversy about the mechanism and catalytic pathway of HOR and NRR, causing few relevant MOFs to be reported in this aspect. Although, it is reasonable to believe that MOFs with their unique charm and advantages will be used in more fields and play an excellent performance.

5.4. Battery

The development of metal-ion battery (MIB) is of great significance in the field of electrochemical energy storage [248]. To improve the battery performance, it is necessary to design and construct electrode materials with a novel nanostructure, and hollow metal oxides originated from the MOFs with unique composition and flexible structure have low mass density, excellent stability, and large surface area, which can be explored and applied as the anode materials of battery [249]. For example, by air-calcining the MIL-53(Fe) to adjust the morphology, the obtained transition metal oxides with different shapes, such as porous spindle-like Fe_2O_3-0.5, can be well used in lithium-ion battery (LIB, Fig. 23**a1-23a6**) [108]. Then, the as-synthesized hollow Fe_2O_3-2 is prepared as the anode of LIB for cyclic voltammetry (CV) experiment, where the obvious change of valence state of Fe ions is observed during the first CV scan that is consistent with the result of charge–discharge curve under 100 mA g^{-1} (Fig. 23**b, 23c**). Compared with the same series of products, Fe_2O_3-2 exhibits the largest initial discharge and charge capacity of 1456 and 1048 mAh g^{-1}, respectively, in the cycle performance test at 1 A g^{-1} (Fig. 23**d**). When the cycling performance is carried out at a constant current density of 0.1 A g^{-1}, the reversible charging capacity of Fe_2O_3-2 is smooth and steady during the 200 cycles, mainly due to its porous yolk-shell structure with larger surface area and more active sites for lithium storage (Fig. 23**e**).

In recent decades, sodium-ion battery (SIB) has also been widely studied owing to abundant sodium resources and low cost. Meanwhile, MOFs with core–shell structure can be prepared as carbon-based bimetallic sulfide with high active cores, abundant interfaces, and strong mechanical strength, thus extremely potential for large-scale energy storage [250]. Thus, the okra-like Fe_7S_8/C@ZnS/N-C@C (Fig. 23**g1-23g4**) with layered core–shell structure is designed and synthesized by high-temperature calcination of a MOF-on-MOF hybrid structure of MIL-53@ZIF-8@RF (Fig. 23**f1-23f4**) with a MIL-53 core, ZIF-8 shell and resorcinol–formaldehyde coating [136]. While the Fe_7S_8/C@ZnS/N-C@C is acted as an anode catalyst for SIB, the carbon layer not only facilitates the promotion of Na^+ transport, but also limits the aggregation of active sites. *Ex situ* powder X-ray diffraction (XRD) tests are performed in different charging/discharging states, and it is found that Fe_7S_8 would be converted to Na_2FeS_2, Fe, Zn, Na_2S, and $NaZn_{13}$ in order with the gradual decrease of the discharging voltage (Fig. 23**h**). However,

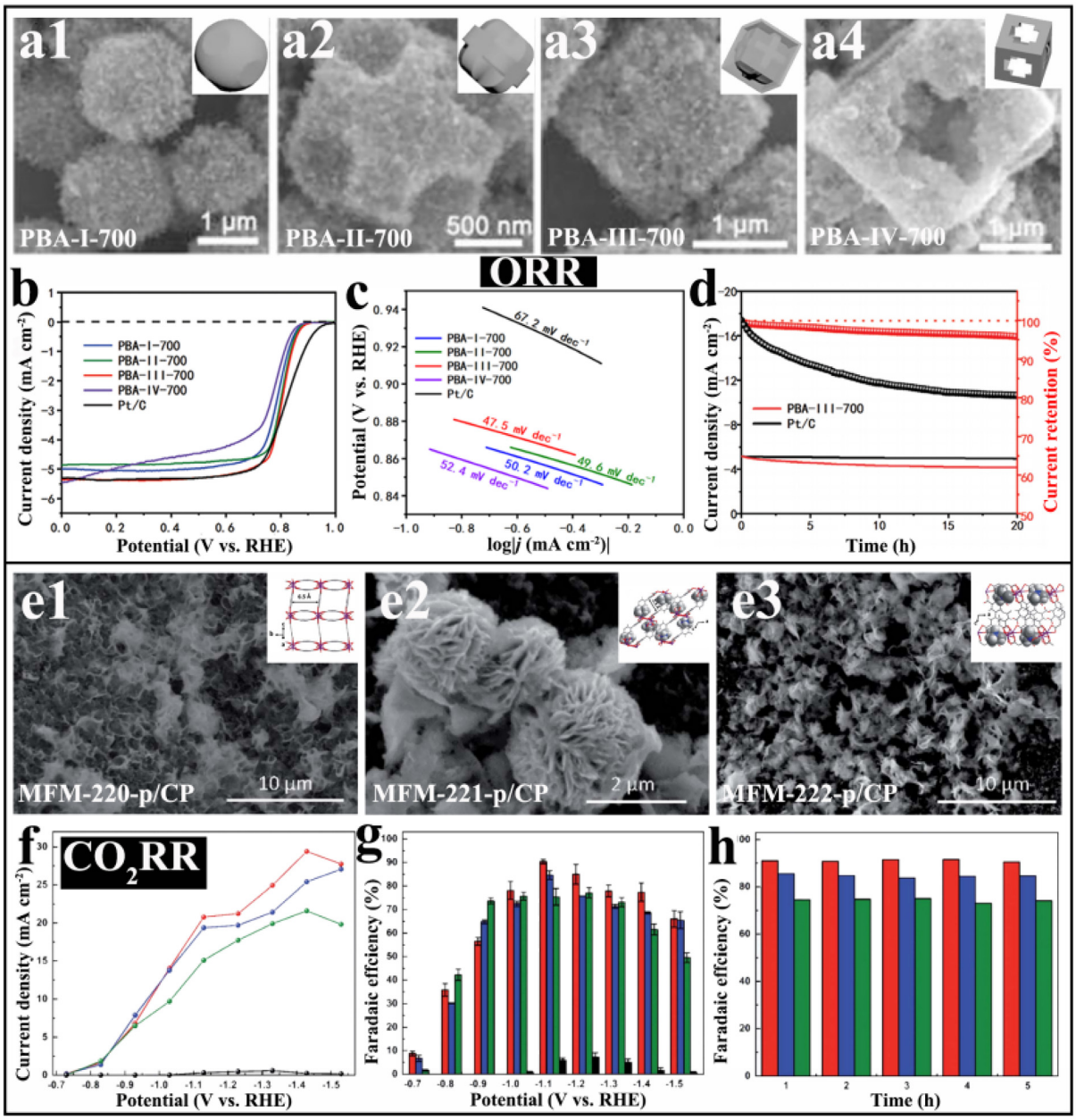

Fig. 22. a1-a4) SEM images and schematic diagrams of the PBA-I/II/III/IV-700. Reproduced with permission from ref. [98]. Copyright 2020, Wiley-VCH GmbH. b) LSV curves, c) Tafel slopes, and d) long-time stability for ORR. e1-e3) SEM images of MFM-220-p/CP, MFM-221-p/CP, and MFM-222-p/CP. Reproduced with permission from ref. [135]. Copyright 2022, Royal Society of Chemistry. f-h) CO_2RR catalytic performance of MFM-220-p/CP (red lines or column), MFM-221-p/CP (blue lines or column), MFM-222-p/CP (green lines or column), and CP (black lines or column) in 0.1 M $KHCO_3$. (For interpretation of the references to color in this figure legend, the reader is referred to the web version of this article.)

the Na_2FeS_2 peaks still present in the fully charged state to confirm that the reaction could not be restored to the Fe_7S_8 phase (Fig. 23**i**). The schematic diagram depicted in Fig. 23**j** further illustrates that the stepwise sodization/desodiation reactions at different positions will form a homogeneous solid state interface layer and gradually release the strain, ensuring its cyclic stability. Therefore, by structural design and composition optimization of MOF precursors, core–shell hybrids with different layer chemistry and metal sulfides with large energy band gap differences can not only accelerate sodium storage kinetics but also provide combined advantages in terms of cycling stability and ion/electron transport.

Meanwhile, as the theory of gas diffusion electrode is further complicated, metal-air batteries (MAB) with oxygen in air as positive electrode, such as zinc-air batteries (ZAB), aluminum-air batteries, magnesium-air batteries, etc., are widely researched and developed. As a high-performance emerging green energy, MAB is regarded as an ideal product to replace traditional batteries because of its low cost, no pollution, and high specific energy. In a meaningful research work, the layer spacing of NiFe-MOF is expanded using carboxylated carbon quantum dots (CQDs-COOH), and effectively inducing the formation of 2D NiFe-MOF nanosheets by electron-withdrawing-COOH groups, which increases the positive charge on the active sites and improves the electrocatalytic performance [137]. When NiFe-MOF NSs@CQDs-COOH is applied as a cathode catalyst in a rechargeable ZAB, it shows excellent performance with an open-circuit voltage of 1.42 V and a specific capacity of 895.5 mAh g_{Zn}^{-1}. In addition, several works in our group have also shown that MOF-derived carbon

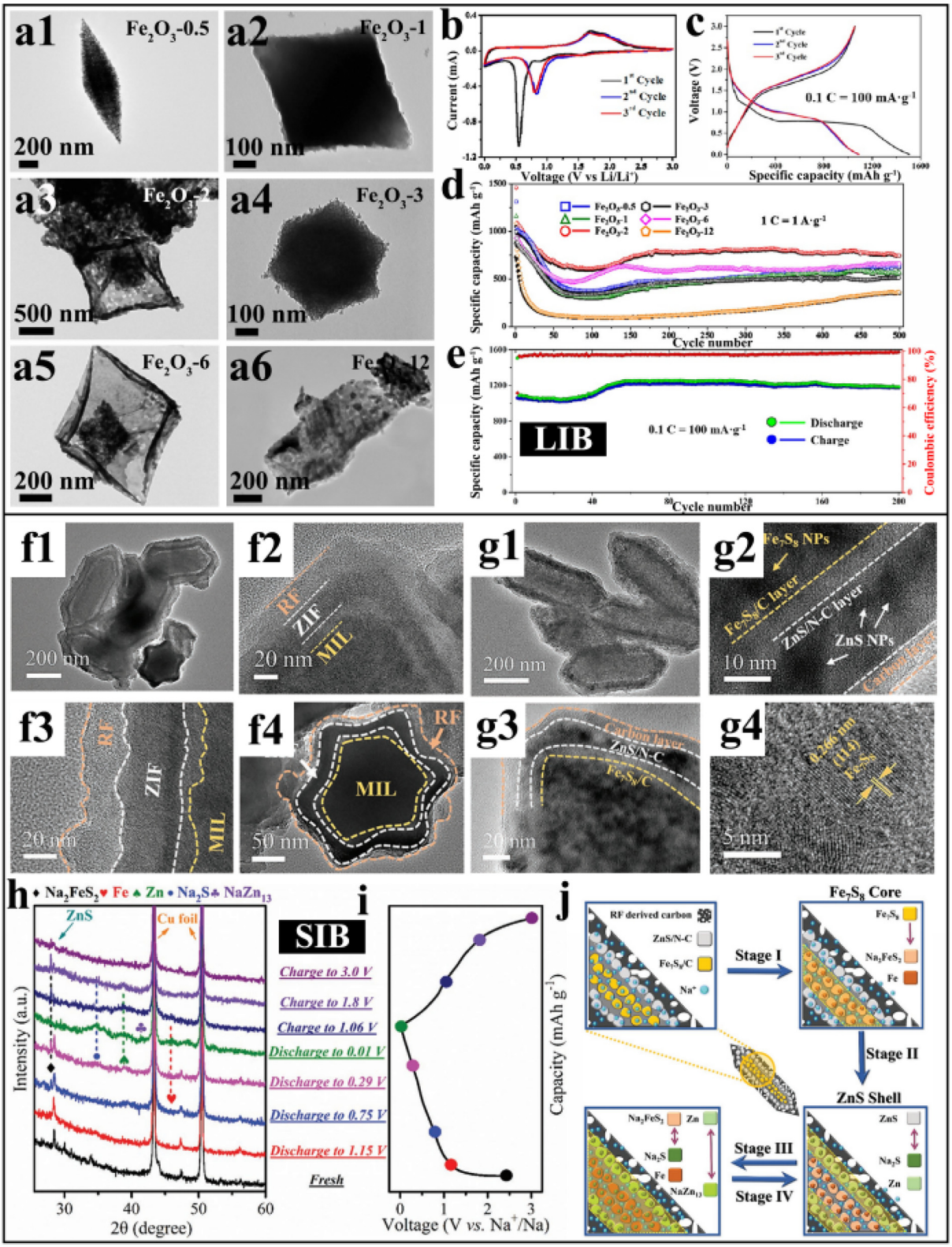

Fig. 23. A1-a6) TEM images of the Fe_2O_3-0.5/1/2/3/6/12. Reproduced with permission from ref. [108]. Copyright 2017, American Chemical Society. b) CV curves, c) Charge-discharge curves d) Cycle performance and e) Coulombic efficiency of Fe_2O_3-2. f1-f4) SEM images of MIL@ZIF@RF. Reproduced with permission from ref. [136]. Copyright 2020, Wiley-VCH GmbH. g1-g4) TEM and HRTEM images of Fe_7S_8/C@ZnS/N-C@C. h-i) *Ex situ* XRD patterns and the corresponding voltage curve of the Fe_7S_8/C@ZnS/N-C@C composite electrode. j) Schematic diagram of the sodium storage mechanism.

nanocomposites can have diverse morphologies and tunable active sites, resulting in ultra-high oxygen reduction activity and long-term stability in ZAB [251].

Except the study of MIB and MAB, MOF-derived nanomaterials have also been applied to zinc-manganese and lithium-sulfur batteries [252,253]. Due to their unique structure and composition

advantages, MOF-derived composites have great potential in the application of electrode materials for rechargeable batteries. However, there are still many unexplored applications, and the advantages of MOFs have not yet been fully exploited.

5.5. Heterogeneous catalysts

A number of works have been reported that the potential applications of MOFs with hollow nanostructures with large surface area, multiphase interfaces, and excellent mass diffusion properties in heterogeneous catalysis. In addition, the synergistic effects arising from the interaction of different shell layers are exploited to modify their properties for specific applications and confined environments to improve stability.

For example, multilayer MOF-on-MOF heterostructures can be fabricated and subjected to a pyrolysis process to achieve solid-to-hollow transition, and the shell number, hollow nanostructure, and metal composition of the resulting metal@NC can be tuned by adjusting the multilayer solid ZIFs [119]. When the multishell hollow Co@NC dodecahedra are employed for the selective hydrogenation of furfural to produce cyclopentanol (CPL), the catalytic activity gradually will be enhanced with increasing shell number (Fig. 24**a**). The multishell hollow structure not only enhances the dispersion of active Co NPs, but also provides a stable multiphase

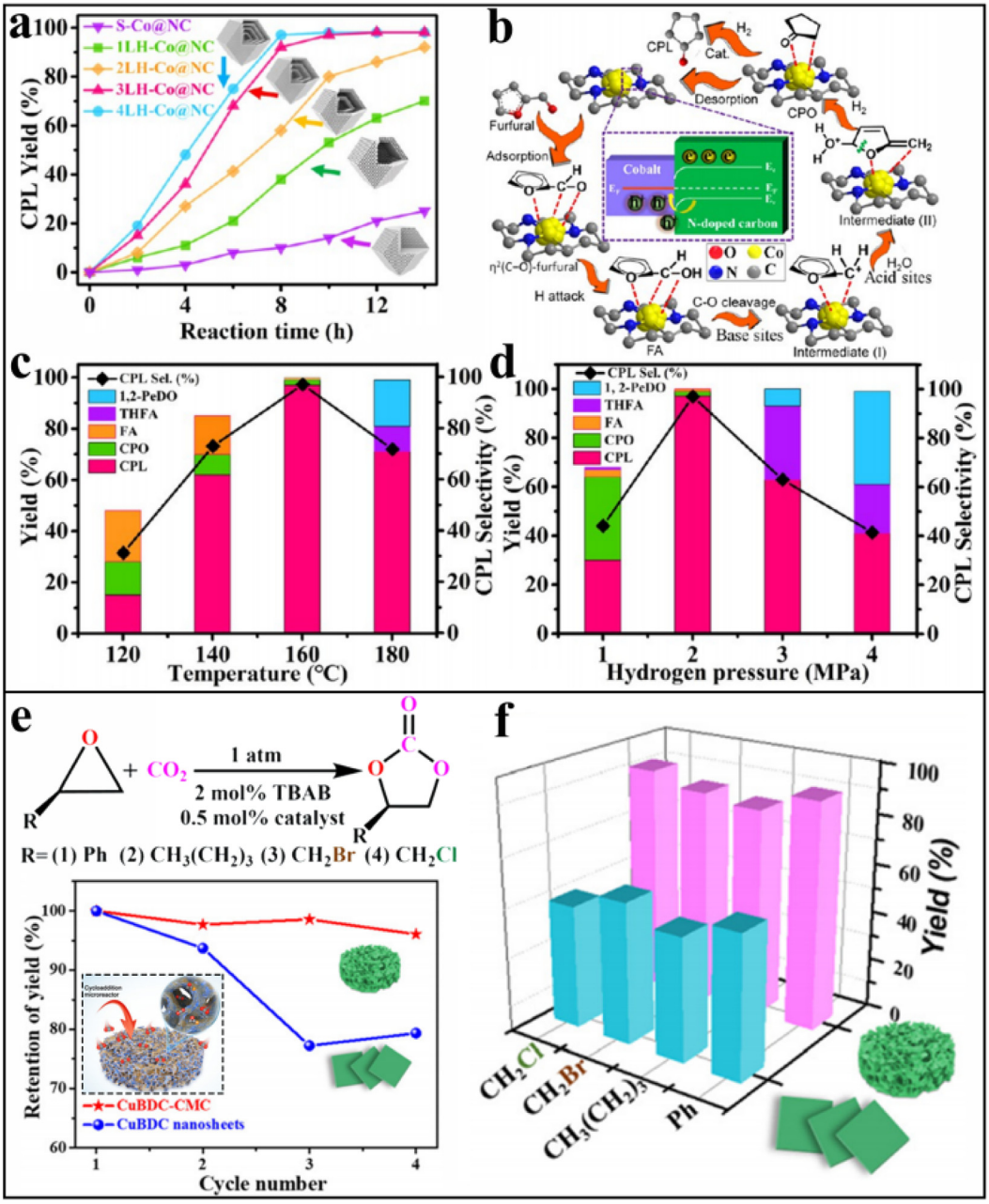

Fig. 24. A) The CPL yields and selectivity of LH-Co@NC. Reproduced with permission from ref. [119]. Copyright 2019, American Chemical Society. b) Mechanism for the hydrogenation of furfural to CPL. c) Influence of reaction temperature and d) H_2 pressure on FFA conversion and product selectivity. e) Retention of the phenyl cyclic carbonate yield in successive cycles and f) yield for cyclic carbonates catalyzed using the CuBDC/CMC micro-reactor. Reproduced with permission from ref. [113]. Copyright 2021, Wiley-VCH GmbH.

heterogeneous environment and improved mass diffusion ability. As shown in Fig. 24**b**, furfural molecules are firstly adsorbed on the surface of Co NPs and further reduced to furfuryl alcohol by dissociated H atoms. Subsequently, CPL is generated by the cleavage of the C-O bond in furfuryl alcohol, the capture of H_2O molecules, the rearrangement reaction of intermediate II, and the complete hydrogenation of cyclopentanone. Obviously, the furfural conversion is also affected by the reaction temperature and hydrogen pressure (Fig. 24**c-24d**).

At the same time, MOFs through morphological modification can be applied as heterogeneous catalysts for cycloaddition reactions. MOFs/aerogel composites have abundant active sites and good mass transfer properties, which provide high reactivity and stability in cycloaddition catalysis [113]. The layered CuBDC/CMC aerogel composites are designed as catalytic micro-reactors due to their high hygroscopicity, mechanical and thermal stability, abundant active sites, and continuous nanostructured coating for the [2 + 3] cycloaddition reaction of CO_2 with four epoxides to generate five-membered cyclic carbonates (Fig. 24**e**). CuBDC nanosheets without support tend to agglomerate during the catalytic process, thus losing a large number of available Cu active sites, while the CMC-supported CuBDC films maintain structural stability throughout the process, thus ensuring high catalytic activity and stability. Meanwhile, the CuBDC/CMC micro-reactor also exhibits better catalytic performance than the CuBDC nanosheet catalyst in other cyclization reactions of different epoxides (Fig. 24**f**).

However, a qualified catalyst should have high recoverable utilization and catalytic selectivity. Based on this, water-stabilized InOF-1 as a carrier is anchored with ultrafine Pd NPs by a two-solvent method [138]. By the synergistic effect, the microporous structure of MOFs improves the selectivity of the target product, while the loaded Pd NPs provide abundant catalytic active sites. Ultimately, the prepared Pd@InOF-1 exhibits a satisfactory size selection effect in the Suzuki-Miyaura coupling reaction with isolated yields up to 90%. Therefore, improving the solution stability, modulating the morphology, and optimizing the pore environment of MOFs becomes a realistic strategy for its application in various organocatalytic reactions.

5.6. Drug delivery

MOFs with porous structures can be used as drug carriers to inhibit drug crystallization by confinement in their nanoscale pores, but rapid hydrolysis in the stomach leads to the immediate release of the drug (Fig. 25**a**) [139]. The current approach to drug delivery using MOFs is mainly the controllable release, where MOFs with long-term chemical stability become regulators of drug release under different stimuli such as medium pH, temperature, and pressure.[140]. The poorly water-soluble drug molecules, such as curcumin (CUR), sulindac (SUL), and triamterene (TAT), are encapsulated by post-synthesis binding, and immersion of MOF-5 crystals in dichloromethane or acetonitrile in excess of the drug, thus showing significant change in the color of the drug after encapsulation (Fig. 25**b**). The drug molecules are immediately released from MOF-5 by hydrolysis decomposition, leading to rapid dissolution and high supersaturation generation in 60 min (Fig. 25**c-25e**). Of note when considering a suitable MOF as an amorphous drug stabilizer and host for rapid release, the main considerations are 1) acceptable toxicity profile, 2) reactive decomposition in an appropriate medium, and 3) suitable pore size to host the drug target.

Research in the treatment of glioblastoma multiforme (GBM) has been hampered by the presence of the highly selective permeability of the blood–brain barrier (BBB). Recently, nanosized particles that mimic viruses have attracted increasing attention in the development of novel drug delivery systems [255]. Fe-based MIL series are chosen as the backbone of the nanoplatform because of its controllable morphology, tunable surface modification, high loading capacity, and versatility, which possesses not only rabies virus (RABV)-like surface proteins, but also RABV-related structures (Fig. 25**f**) [254]. As shown in Fig. 25**g1-25g6**, the presence of water dramatically alters its structure and precisely tailors the morphology and size of MIL series, which can be tuned to closely match the bullet-shaped structure of RABV. MOFs are further functionalized by the lipid bilayer, making the particles more similar to the envelope structure of RABV, thus enhancing BBB penetration and chemotherapy of Glioma (Fig. 25**h**). In short, to achieve the desired effect of drug delivery and therapeutic efficacy, the physiochemical characteristics of viruses need to be taken into account, and the fabrication of bionanocarriers that are highly similar to the structure/morphology and function of viruses may be one of the most effective ways to deliver therapeutic drugs to the target site.

Consequently, in comparison with some common nanocarriers, MOFs for drug delivery have some unique advantages: regular pore structure, large specific surface area, low pharmacological activity, non-toxic, uniform drug loading, and the functionalized surface. Even so, MOF materials for drug delivery still face some severe issues, such as most MOFs are unstable under physiological conditions, so surface modification is needed to slow down the decomposition of MOFs and thus prevent the early release of drugs. Meanwhile, due to the relatively unstable coordination bond between metals and ligands, MOFs are biodegradable and can be widely used in the field of drug delivery.

6. Conclusion and perspectives

Extensive research works have demonstrated that the structure of MOFs determines their function, while the morphology control of crystal materials at multiple dimensions enables the precise fabrication of different hierarchical architectures. Compared with other conventional porous materials, hybrid inorganic–organic MOFs with ultra-large specific surface area, highly ordered structure, and controllable morphology show great potential in terms of environmental protection and energy conservation fields. Moreover, the flexible frameworks allow many desirable structure-related properties to be integrated for extending practical applications. To date, various strategies have been devised, including the use of rationally designed SBUs and multifunctional linkers, the selection of suitable surfactants and reaction solvents, the utilization of diverse substrates, and unprecedented synthetic methods.

Although many methods have been proposed to synthesize the corresponding intricate morphologies and tailored nanostructures based on the various influencing factors of MOFs, the ability to accurately control their sizes and shapes is far from satisfactory. More importantly, the study of morphology-property relationships has not been carried out systematically, and there are still some remaining challenges in the ever-increasing fields of MOF-related research. 1) The understanding of the dynamic coordination principles should be deepened to encompass the kinetic and thermodynamic mechanisms in the formation of MOF crystals as a way to rationally design the structure of MOFs. 2) Investigating the nature of the template and selecting the suitable substrate would provide a good platform for tuning the MOFs. Although the morphology of MOFs could be affected by the templates to a large extent, the homogeneity of the crystals cannot be guaranteed. Hence, post-treatment or functional group modification of these templates is still essential to induce the structural growth of MOFs. 3) Specific crystal structures of bimetallic MOFs need to be elucidated, and atomically accurate structural characterization and computational

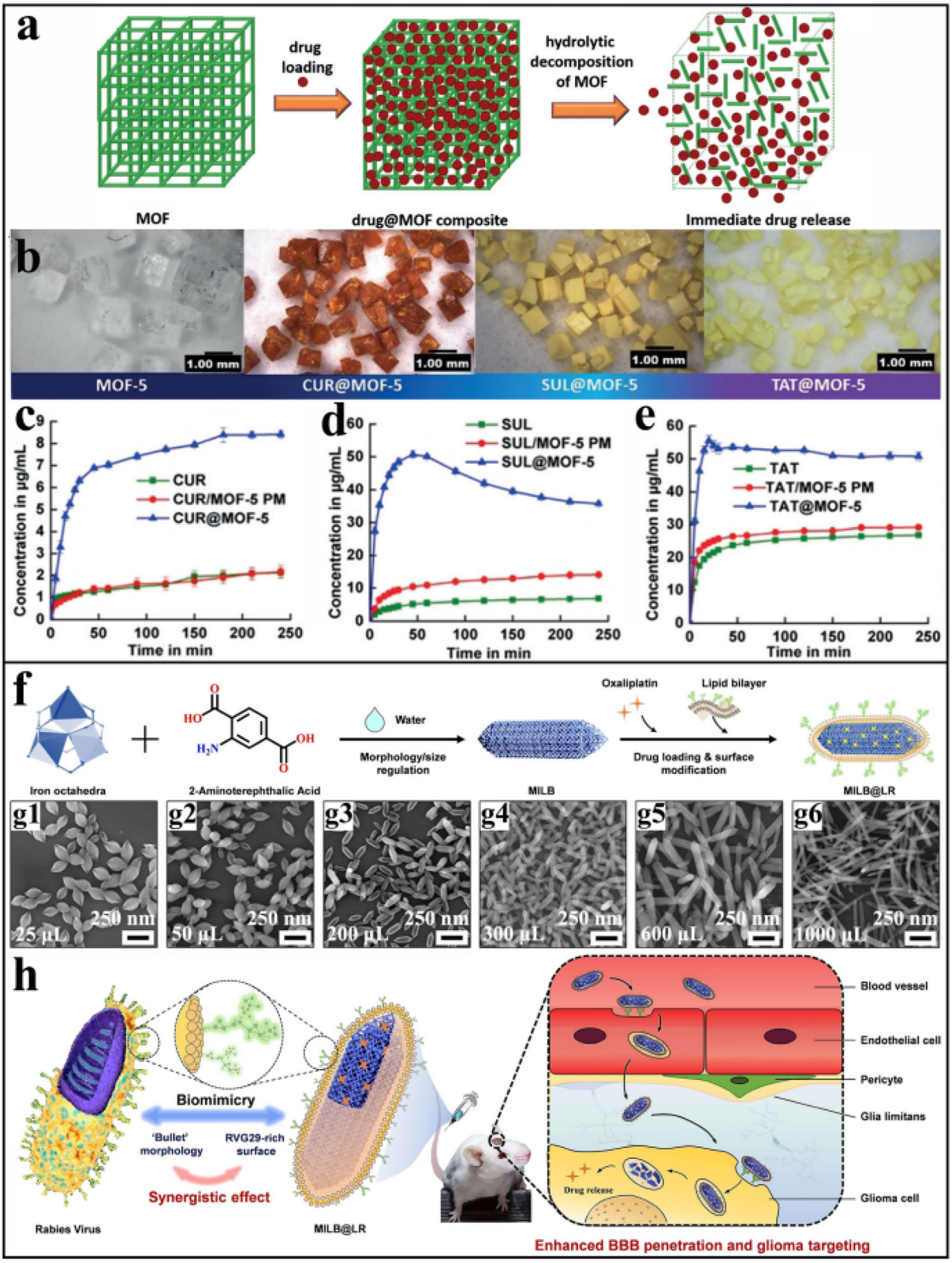

Fig. 25. A) Schematic representation of drug encapsulation and release from MOFs. Reproduced with permission from ref. [139]. Copyright 2019, Wiley-VCH GmbH. b) Optical images of drug@MOF-5 composite crystals. c-e) The drug dissolution rate and supersaturation production of drug@MOF-5 composites. f) Fabrication of MILB@LR. Reproduced with permission from ref. [254]. Copyright 2020, Wiley-VCH GmbH. g1-g6) The morphological evolution of MIL series prepared using different amounts of water. h) Comprehensive RABV-mimic strategy for enhanced BBB penetration and chemotherapy of Glioma.

modeling are necessary to grasp a fundamental understanding of structure–property relationships. 4) In practical applications, MOFs are susceptible to structural collapse and degradation by moisture in the air. Reinforcing the strength of the coordination bond between metal ions and organic ligands, and realizing reversible structural transformation can effectively improve the stability, which is worthy of in-depth research.

However, these above factors are usually interrelated with coordination structures, and the systematic study of morphological effects is extremely challenging. In a word, the structure-directed growth and morphology control of multifunctional MOFs is an effective and versatile approach that offers many valuable opportunities for broader applications. In the future, it is highly anticipated to combine interdisciplinary techniques to fully exploit the advantages of MOF materials for industrial applications, and we have reasons to believe that the prospect of MOF fields is extremely bright.

Data availability

Data will be made available on request.

Declaration of Competing Interest

The authors declare that they have no known competing financial interests or personal relationships that could have appeared to influence the work reported in this paper.

Acknowledgments

This work was financially supported by National Natural Science Foundation of China (52171145, 21601137), Natural Science Foundation of Zhejiang Province (LQ16B010003), Basic Science and Technology Research Project of Wenzhou, Zhejiang Province (G20190007), and the Special Basic Cooperative Research Programs of Yunnan Provincial Undergraduate Universities Association (202101BA070001-042).

References

[1] O.M. Yaghi, G. Li, H. Li, Selective binding and removal of guests in a microporous metal-organic framework, Nature 378 (1995) 703–706.
[2] T.Y. Luo, C. Liu, X.Y. Gan, P.F. Muldoon, N.A. Diemler, J.E. Millstone, N.L. Rosi, Multivariate stratified metal-organic frameworks: diversification using domain building blocks, J. Am. Chem. Soc. 141 (2019) 2161–2168.
[3] H.C. Zhou, S. Kitagawa, Metal-organic frameworks (MOFs), Chem. Soc. Rev. 43 (2014) 5415–5418.
[4] H.C. Zhou, J.R. Long, O.M. Yaghi, Introduction to metal-organic frameworks, Chem. Rev. 112 (2012) 673–674.
[5] H. Furukawa, K.E. Cordova, M. O'Keeffe, O.M. Yaghi, The chemistry and applications of metal-organic frameworks, Science 341 (2013) 1230444.
[6] S. Wang, C.M. McGuirk, A. d'Aquino, J.A. Mason, C.A. Mirkin, Metal-organic framework nanoparticles, Adv. Mater. 2018 (30) (2018) 1800202.
[7] M. Gu, M. Wu, S.C. Wang, C. Chen, D. Xiong, F.Y. Yi, Morphology control of nanoscale metal-organic frameworks for high-performance supercapacitors, Electrochim. Acta 343 (2020).
[8] F. Qi, Z. Sun, X. Fan, Z. Wang, Y. Shi, G. Hu, F. Li, Tunable interaction between metal-organic frameworks and electroactive components in lithium-sulfur batteries: status and perspectives, Adv. Energy Mater. 11 (20) (2021) 2100387.
[9] R. Riccò, O. Linder-Patton, K. Sumida, M.J. Styles, K. Liang, H. Amenitsch, C.J. Doonan, P. Falcaro, Conversion of copper carbonate into a metal-organic framework, Chem. Mater. 30 (2018) 5630–5638.
[10] T. Stassin, S. Rodríguez-Hermida, B. Schrode, A.J. Cruz, F. Carraro, D. Kravchenko, V. Creemers, I. Stassen, T. Hauffman, D.D. Vos, P. Falcaro, R. Resel, R. Ameloot, Vapour-phase deposition of oriented copper dicarboxylate metal-organic framework thin films, Chem. Commun. 55 (2019) 10056–10059.
[11] S. Wongsakulphasatch, F. Nouar, J. Rodriguez, L. Scott, C.L. Guillouzer, T. Devic, P. Horcajada, J.M. Greneche, P.L. Llewellyn, A. Vimont, G. Clet, M. Daturi, C. Serre, Direct accessibility of mixed-metal (III/II) acid sites through the rational synthesis of porous metal carboxylates, Chem. Commun. 51 (2015) 10194–10197.
[12] X.L. Lv, S. Yuan, L.H. Xie, H.F. Darke, Y. Chen, T. He, C. Dong, B. Wang, Y.Z. Zhang, J.R. Li, H.C. Zhou, Ligand rigidification for enhancing the stability of metal-organic frameworks, J. Am. Chem. Soc. 141 (2019) 10283–10293.
[13] J.A. Boissonnault, A.G. Wong-Foy, A.J. Matzger, Core-shell structures arise naturally during ligand exchange in metal-organic frameworks, J. Am. Chem. Soc. 139 (2017) 14841–14844.
[14] X.J. Yu, Y.M. Xian, C. Wang, H.L. Mao, M. Kind, T. Abu-Husein, Z. Chen, S.B. Zhu, B. Ren, A. Terfort, J.L. Zhuang, Liquid-phase epitaxial growth of highly oriented and multivariate surface-attached metal-organic frameworks, J. Am. Chem. Soc. 141 (2019) 18984–18993.
[15] M.J. Kalmutzki, N. Hanikel, O.M. Yaghi. Secondary building units as the turning point in the development of the reticular chemistry of MOFs. Sci. Adv., 4 (2018), p. eaat9180.
[16] F.N. Dai, X.K. Wang, Y.T. Wang, Z.N. Liu, D.F. Sun, Sequential solid-state transformations involving consecutive rearrangements of secondary building units in a metal-organic framework (MOF), Angew. Chem. Int. Ed. 59 (2020) 22372–22377.
[17] L.J. Han, D. Zheng, S.G. Chen, H.G. Zheng, J. Ma, A highly solvent-stable metal-organic framework nanosheet: morphology control, exfoliation, and luminescent property, Small 14 (2018) 1703873.
[18] T. Pan, Y. Shen, P. Wu, Z. Gu, B. Zheng, J. Wu, S. Li, Y. Fu, W. Zhang, F. Huo, Thermal shrinkage behavior of metal-organic frameworks, Adv. Funct. Mater. 30 (2020) 2001389.
[19] K. Li, S. Lin, Y. Li, Q. Zhuang, J. Gu, Aqueous-phase synthesis of mesoporous Zr-based MOFs templated by amphoteric surfactants, Angew. Chem. Int. Ed. 130 (2018) 3497–3501.
[20] M.C. di Gregorio, M. Elsousou, Q. Wen, L.J.W. Shimon, V. Brumfeld, L. Houben, M. Lahav, M.E. van der Boom, Molecular cannibalism: sacrificial materials as precursors for hollow and multidomain single crystals, Nat. Commun. 12 (2021) 1–9.
[21] K. Ma, K.B. Idrees, F.A. Son, R. Maldonado, M.C. Wasson, X. Zhang, X. Wang, E. Shehayeb, A. Merhi, B.R. Kaafarani, T. Islamoglu, J.H. Xin, O.K. Farha, Fiber composites of metal-organic frameworks, Chem. Mater. 32 (2020) 7120–7140.
[22] B.Q. Wang, J. Shang, C. Guo, J.Z. Zhang, F.N. Zhu, A.J. Han, J.F. Liu, A general method to ultrathin bimetal-MOF nanosheets arrays via in situ transformation of layered double hydroxides arrays, Small 15 (2019) 1804761.
[23] E. Virmani, J.M. Rotter, A. Mahringer, T. von Zons, A. Godt, T. Bein, S. Wuttke, D.D. Medina, On-surface synthesis of highly oriented thin metal-organic framework films through vapor-assisted conversion, J. Am. Chem. Soc. 140 (2018) 4812–4819.
[24] Y.W. Zhao, J.N. Wang, R.J. Pei, Micron-sized ultrathin metal-organic framework sheet, J. Am. Chem. Soc. 142 (2020) 10331–10336.
[25] G.R. Cai, M.L. Ding, Q.Y. Wu, H.L. Jiang, Encapsulating soluble active species into hollow crystalline porous capsules beyond integration of homogeneous and heterogeneous catalysis, Natl. Sci. Rev. 7 (2020) 37–45.
[26] A.Q. Hu, Q.Q. Pang, C. Tang, J.X. Bao, H.Q. Liu, K. Ba, S.H. Xie, J. Chen, J.H. Chen, Y.W. Yue, Y. Tang, Q.W. Li, Z.Z. Sun, Epitaxial growth and integration of insulating metal-organic frameworks in electrochemistry, J. Am. Chem. Soc. 141 (2019) 11322–11327.
[27] Y.W. Sun, D. Yan, Y.Y. Wu, F.Y. Shih, C.H. Zhang, H.X. Luo, S.H. Lin, Y. Liu, Fabrication of twin-free ultrathin NH_2-MIL-125 (Ti) membrane with *c*-preferred orientation using transition-metal trichalcogenides as titanium source, ACS Mater. Lett. 4 (2021) 55–60.
[28] Z.Y. Wang, G. Wang, H.Y. Qi, M. Wang, M.C. Wang, S.W. Park, H.P. Wang, M.H. Yu, U. Kaiser, A. Fery, S.Q. Zhou, R.H. Dong, X.L. Feng, Ultrathin two-dimensional conjugated metal-organic framework single-crystalline nanosheets enabled by surfactant-assisted synthesis, Chem. Sci. 11 (2020) 7665–7671.
[29] S.Z. Wang, S.S. Park, C.T. Buru, H.X. Lin, P.C. Chen, E.W. Roth, O.K. Farha, C.A. Mirkin, Colloidal crystal engineering with metal-organic framework nanoparticles and DNA, Nat. Commun. 11 (2020) 2495.
[30] Y. Liu, J.m. Wang, I. Imaz, D. Maspoch. Assembly of colloidal clusters driven by the polyhedral shape of metal-organic framework particles. J. Am. Chem. Soc., 143 (2021), p. 12943-12947.
[31] Q.H. Sun, K. Zhu, X.L. Ji, D.D. Chen, C. Han, T.T. Li, S.M. Huang, J.J. Qian, MOF-derived three-dimensional ordered porous carbon nanomaterial for efficient alkaline zinc-air batteries, Sci. China Mater. 65 (2022) 1453–1462.
[32] G. Lee, S. Lee, S. Oh, D. Kim, M. Oh, Tip-to-middle anisotropic MOF-on-MOF growth with a structural adjustment, J. Am. Chem. Soc. 142 (2020) 3042–3049.
[33] M.T. Zhao, J.Z. Chen, B. Chen, X. Zhang, Z.Y. Shi, Z.Q. Liu, Q.L. Ma, Y.W. Peng, C. L. Tan, X.J. Wu, H. Zhang, Selective epitaxial growth of oriented hierarchical metal-organic framework heterostructures, J. Am. Chem. Soc. 142 (2020) 8953–8961.
[34] J. Wang, J. Tang, B. Ding, Z. Chang, X.D. Hao, T. Takei, N. Kobayashi, Y. Bando, X.G. Zhang, Y. Yamauchi, Self-template-directed metal-organic frameworks network and the derived honeycomb-like carbon flakes via confinement pyrolysis, Small 14 (2018) 1704461.
[35] Q.H. Yang, C.C. Yang, C.H. Lin, H.L. Jiang, Metal-organic-framework-derived hollow N-doped porous carbon with ultrahigh concentrations of single Zn atoms for efficient carbon dioxide conversion, Angew. Chem. Int. Ed. 131 (2019) 3549–3553.
[36] S.Q. Zhang, J.W. Ye, Y. Sun, J. Kang, J.H. Liu, Y. Wang, Y.C. Li, L.H. Zhang, G.L. Ning, Electrospun fibrous mat based on silver (I) metal-organic frameworks-

polylactic acid for bacterial killing and antibiotic-free wound dressing, Chem. Eng. J. 390 (2020).
[37] T.Y. Yang, L.R. Ge, T.S. Ge, G.W. Zhan, R.Z. Wang, Binder-free growth of aluminum-based metal-organic frameworks on aluminum substrate for enhanced water adsorption capacity, Adv. Funct. Mater. 32 (2022) 2105267.
[38] M. Krishtab, I. Stassen, T. Stassin, A.J. Cruz, O.O. Okudur, S. Armini, C. Wilson, S. De Gendt, R. Ameloot, Vapor-deposited zeolitic imidazolate frameworks as gap-filling ultra-low-k dielectrics, Nat. Commun. 10 (2019) 3729.
[39] A.J. Cruz, I. Stassen, M. Krishtab, K. Marcoen, T. Stassin, S. Rodríguez-Hermida, J. Teyssandier, S. Pletincx, R. Verbeke, V. Rubio-Giménez, S. Tatay, C. Martí-Gastaldo, J. Meersschaut, P.M. Vereecken, S. De Feyter, T. Hauffman, R. Ameloot, Integrated cleanroom process for the vapor-phase deposition of large-area zeolitic imidazolate framework thin films, Chem. Mater. 31 (2019) 9462–9471.
[40] Y.J. Zhang, J. Li, W.Y. Zhao, H.L. Dou, X.L. Zhao, Y. Liu, B.W. Zhang, X.W. Yang, Defect-free metal-organic framework membrane for precise ion/solvent separation toward highly stable magnesium metal anode, Adv. Mater. 34 (2022) 2108114.
[41] T.J. Qiu, S. Gao, Z.B. Liang, D.G. Wang, H. Tabassum, R.Q. Zhong, R.Q. Zou, Pristine hollow metal-organic frameworks: design, synthesis and application, Angew. Chem. Int. Ed. 60 (2021) 17314–17336.
[42] W.H. Wang, H.W. Yan, U. Anand, U. Mirsaidov, Visualizing the conversion of metal-organic framework nanoparticles into hollow layered double hydroxide nanocages, J. Am. Chem. Soc. 143 (2021) 1854–1862.
[43] J. Koo, I.C. Hwang, X.J. Yu, S. Saha, Y. Kim, K. Kim, Hollowing out MOFs: hierarchical micro- and mesoporous MOFs with tailorable porosity via selective acid etching, Chem. Sci. 8 (2017) 6799–6803.
[44] Y. He, Z. Wang, H. Wang, Z. Wang, G. Zeng, P. Xu, D. Huang, M. Chen, B. Song, H. Qin, Y. Zhao, Metal-organic framework-derived nanomaterials in environment related fields: Fundamentals, properties and applications, Coordin. Chem. Rev. 429 (2021) 213618.
[45] W.T. Koo, J.S. Jang, I.D. Kim, Metal-organic frameworks for chemiresistive sensors, Chem 5 (2019) 1938–1963.
[46] S. Wang, Z.M. Gao, G.S. Song, Y.T. Yu, W.X. He, L.L. Li, T.Q. Wang, F.Q. Fan, Y.N. Li, L.Y. Zhang, X.M. Zhang, Y. Fu, W. Qi, Copper oxide hierarchical morphology derived from MOF precursors for enhancing ethanol vapor sensing performance, J. Mater. Chem. C 8 (2020) 9671–9677.
[47] Y.Y. Yi, W. Zhao, Z.H. Zeng, C. Wei, C. Lu, Y.L. Shao, W.Y. Guo, S.X. Dou, J.Y. Sun, ZIF-8@ZIF-67-derived nitrogen-doped porous carbon confined CoP polyhedron targeting superior potassium-ion storage, Small 16 (2020) 1906566.
[48] C. Young, J. Wang, J. Kim, Y. Sugahara, J. Henzie, Y. Yamauchi, Controlled chemical vapor deposition for synthesis of nanowire arrays of metal-organic frameworks and their thermal conversion to carbon/metal oxide hybrid materials, Chem. Mater. 30 (2018) 3379–3386.
[49] Z.X. Chen, Y.Z. Li, B.L. Liu, K. Wang, Y.L. Cao, Solvent-free chemical approach to synthesize Co nanoparticles supported on N-doped porous carbon for efficient electrocatalytic oxygen reduction, ChemCatChem 12 (2020) 2580–2588.
[50] J.H. Lee, S. Jeoung, Y.G. Chung, H.R. Moon, Elucidation of flexible metal-organic frameworks: research progresses and recent developments, Coordin. Chem. Rev. 389 (2019) 161–188.
[51] W.H. Guo, W. Xia, K.T. Cai, Y.X. Wu, B. Qiu, Z.B. Liang, C. Qu, R.Q. Zou, Kinetic-controlled formation of bimetallic metal-organic framework hybrid structures, Small 13 (2017) 1702049.
[52] D. Saliba, M. Ammar, M. Rammal, M. Al-Ghoul, M. Hmadeh, Crystal growth of ZIF-8, ZIF-67, and their mixed-metal derivatives, J. Am. Chem. Soc. 140 (2018) 1812–1823.
[53] Z.J. Zhang, L. Wojtas, M. Eddaoudi, M.J. Zaworotko, Stepwise transformation of the molecular building blocks in a porphyrin-encapsulating metal-organic material, J. Am. Chem. Soc. 135 (2013) 5982–5985.
[54] X.Y. Yang, S. Yuan, L.F. Zou, H. Drake, Y.M. Zhang, J.S. Qin, A. Alsalme, H.C. Zhou, One-step synthesis of hybrid core-shell metal-organic frameworks, Angew. Chem. Int. Ed. 57 (2018) 3927–3932.
[55] S. Choi, W. Cha, H. Ji, D. Kim, H.J. Lee, M. Oh, Synthesis of hybrid metal-organic frameworks of $\{Fe_xM_yM'_{1-x-y}\}$-MIL-88B and the use of anions to control their structural features, Nanoscale 8 (2016) 16743–16751.
[56] P. Mani, N. Mandal, M. Roopesh, H. Gopalakrishnan, A. Datta, S. Mandal, Enhancement in electrical conductivity of a porous indium based metal-organic framework upon I_2 uptake: combined experimental and theoretical investigations, J. Mater. Chem. C 8 (2020) 4836–4842.
[57] M.A. Sinnwell, Q.R.S. Miller, L. Palys, D. Barpaga, L. Liu, M.E. Bowden, Y. Han, S. Ghose, M.L. Sushko, H.T. Schaef, W. Xu, M. Nyman, P.K. Thallapally, Molecular intermediate in the directed formation of a zeolitic metal-organic framework, J. Am. Chem. Soc. 142 (2020) 17598–17606.
[58] P.B. Geng, L. Wang, M. Du, Y. Bai, W.T. Li, Y.F. Liu, S.Q. Chen, P. Braunstein, Q. Xu, H. Pang, MIL-96-Al for Li-S batteries: shape or size?, Adv. Mater. 34 (2022) 2107836.
[59] H.J. Lee, Y.J. Cho, W. Cho, M. Oh, Controlled isotropic or anisotropic nanoscale growth of coordination polymers: formation of hybrid coordination polymer particles, ACS Nano 7 (2013) 491–499.
[60] C.N. Gu, Y. Peng, J.J. Li, C.S. Liu, H. Pang, Controllable synthesis of copper ion guided MIL-96 octadecahedron: highly sensitive aptasensor toward alpha-fetoprotein, Appl. Mater. Today 20 (2020).
[61] C. Chen, Y.X. Tuo, Q. Lu, H. Lu, S.Y. Zhang, Y. Zhou, J. Zhang, Z.N. Liu, Z.X. Kang, X. Feng, D. Chen, Hierarchical trimetallic Co-Ni-Fe oxides derived from core-shell structured metal-organic frameworks for highly efficient oxygen evolution reaction, Appl. Catal. B-Environ. 287 (2021).
[62] M. Pan, Y.X. Zhu, K. Wu, L. Chen, Y.J. Hou, S.Y. Yin, H.P. Wang, Y.N. Fan, C.Y. Su, Epitaxial growth of hetero-Ln-MOF hierarchical single crystals for domain- and orientation-controlled multicolor luminescence 3D coding capability, Angew. Chem. Int. Ed. 56 (2017) 14582–14586.
[63] Q.W. Zhang, Z.B. Yang, B.H. Chen, X. Liang, Phase-competition-driven formation of hierarchical FeNiZn-MIL-88B-on-MOF-5 octapods displaying high selectivity for the RWGS reaction, Chem. Commun. 55 (2019) 8450–8453.
[64] X.Y. Yin, X.Y. Zhang, Hierarchical metal-organic frameworks constructed from intergrowth for the adsorption of light hydrocarbons, Mater. Chem. Front. 4 (2020) 3057–3062.
[65] X.K. Song, T.K. Kim, H. Kim, D. Kim, S. Jeong, H.R. Moon, M.S. Lah, Post-synthetic modifications of framework metal ions in isostructural metal-organic frameworks: core-shell heterostructures via selective transmetalations, Chem. Mater. 24 (2012) 3065–3073.
[66] M. Taddei, R.J. Wakeham, A. Koutsianos, E. Andreoli, A.R. Barron, Post-synthetic ligand exchange in zirconium-based metal-organic frameworks: beware of the defects!, Angew. Chem. Int. Ed. 57 (2018) 11706–11710.
[67] L.D. Ji, J. Wang, K.B. Wu, N.J. Yang, Tunable electrochemistry of electrosynthesized copper metal-organic frameworks, Adv. Funct. Mater. 28 (2018) 1706961.
[68] V. Guillerm, T. Grancha, I. Imaz, J. Juanhuix, D. Maspoch, Zigzag ligands for transversal design in reticular chemistry: unveiling new structural opportunities for metal-organic frameworks, J. Am. Chem. Soc. 140 (2018) 10153–10157.
[69] S.S. Zheng, Y. Sun, H.G. Xue, P. Braunstein, W. Huang, H. Pang. Dual-ligand and hard-soft-acid-base strategies to optimize metal-organic framework nanocrystals for stable electrochemical cycling performance. Natl. Sci. Rev., 9 (2022), p. nwab197.
[70] H.J. Lee, J. We, J.O. Kim, D. Kim, W. Cha, E. Lee, J. Sohn, M. Oh, Morphological and structural evolutions of metal-organic framework particles from amorphous spheres to crystalline hexagonal rods, Angew. Chem. Int. Ed. 54 (2015) 10564–10568.
[71] S. Choi, T. Kim, H. Ji, H.J. Lee, M. Oh, Isotropic and anisotropic growth of metal-organic framework (MOF) on MOF: logical inference on MOF structure based on growth behavior and morphological feature, J. Am. Chem. Soc. 138 (2016) 14434–14440.
[72] H. Ji, S. Lee, J. Park, T. Kim, S. Choi, M. Oh, Improvement in crystallinity and porosity of poorly crystalline metal-organic frameworks (MOFs) through their induced growth on a well-crystalline MOF template, Inorg. Chem. 57 (2018) 9048–9054.
[73] L. Feng, K.Y. Wang, T.H. Yan, H.C. Zhou, Porous crystalline spherulite superstructures, Chem 6 (2020) 460–471.
[74] L. Feng, K.Y. Wang, T.H. Yan, H.C. Zhou, Seed-mediated evolution of hierarchical metal-organic framework quaternary superstructures, Chem. Sci. 11 (2020) 1643–1648.
[75] S. Peng, B.L. Bie, Y. Sun, M. Liu, H.J. Cong, W.T. Zhou, Y.C. Xia, H. Tang, H.X. Deng, X. Zhou, Metal-organic frameworks for precise inclusion of single-stranded DNA and transfection in immune cells, Nat. Commun. 9 (2018) 1293.
[76] L.J. Liu, K. Konstas, M.R. Hill, S.G. Telfer, Programmed pore architectures in modular quaternary metal-organic frameworks, J. Am. Chem. Soc. 135 (2013) 17731–17734.
[77] L.J. Liu, S.G. Telfer, Systematic ligand modulation enhances the moisture stability and gas sorption characteristics of quaternary metal-organic frameworks, J. Am. Chem. Soc. 137 (2015) 3901–3909.
[78] A. Umemura, S. Diring, S. Furukawa, H. Uehara, T. Tsuruoka, S. Kitagawa, Morphology design of porous coordination polymer crystals by coordination modulation, J. Am. Chem. Soc. 133 (2011) 15506–15513.
[79] Y. Gong, W.K. Han, H.S. Lu, Q.T. Hu, H. Tu, P.N. Li, X.D. Yan, Z.G. Gu, Single crystal to single crystal transformation of spin-crossover coordination polymers from 3D frameworks to 2D layers, J. Mater. Chem. C 9 (2021) 5082–5087.
[80] Q. Wen, S. Tenenholtz, L.J.W. Shimon, O. Bar-Elli, L.M. Beck, L. Houben, S.R. Cohen, Y. Feldman, D. Oron, M. Lahav, M.E. van der Boom, Chiral and SHG-active metal-organic frameworks formed in solution and on surfaces: uniformity, morphology control, oriented growth, and postassembly functionalization, J. Am. Chem. Soc. 142 (2020) 14210–14221.
[81] M.C. di Gregorio, L.J.W. Shimon, V. Brumfeld, L. Houben, M. Lahav, M.E. van der Boom, Emergence of chirality and structural complexity in single crystals at the molecular and morphological levels, Nat. Commun. 11 (2020) 380.
[82] D. Wu, K. Zhou, J.D. Tian, C.P. Liu, J.Y. Tian, F.L. Jiang, D.Q. Yuan, J. Zhang, Q.H. Chen, M.C. Hong, Induction of chirality in a metal-organic framework built from achiral precursors, Angew. Chem. Int. Ed. 60 (2021) 3087–3094.
[83] Y. Feng, Z.K. Wang, W.D. Fan, Z.X. Kang, S. Feng, L.L. Fan, S.Q. Hu, D.F. Sun, Engineering the pore environment of metal-organic framework membranes via modification of the secondary building unit for improved gas separation, J. Mater. Chem. A 8 (2020) 13132–13141.
[84] W.D. Fan, X.R. Zhang, Z.X. Kang, X.P. Liu, D.F. Sun, Isoreticular chemistry within metal-organic frameworks for gas storage and separation, Coordin. Chem. Rev. 443 (2021).
[85] R. Ameloot, F. Vermoortele, W. Vanhove, M.B. Roeffaers, B.F. Sels, D.E. De Vos, Interfacial synthesis of hollow metal-organic framework capsules demonstrating selective permeability, Nat. Chem. 3 (2011) 382–387.

[86] D.N. Dybtsev, H. Chun, K. Kim, Rigid and flexible: a highly porous metal-organic framework with unusual guest-dependent dynamic behavior, Angew. Chem. Int. Ed. 43 (2004) 5033–5036.
[87] J. Yao, M. He, H. Wang, Strategies for controlling crystal structure and reducing usage of organic ligand and solvents in the synthesis of zeolitic imidazolate frameworks, CrystEngComm 17 (2015) 4970–4976.
[88] E.J. Carrington, C.A. McAnally, A.J. Fletcher, S.P. Thompson, M. Warren, L. Brammer, Solvent-switchable continuous-breathing behaviour in a diamondoid metal-organic framework and its influence on CO_2 versus CH_4 selectivity, Nat. Chem. 9 (2017) 882–889.
[89] L. He, W. Li, Z.W. Jiang, T.T. Zhao, Y. Li, C.M. Li, C.Z. Huang, Y.F. Li, Novel solvent-triggered transformation of Cu-based metal-organic gels to highly monodisperse metal-organic frameworks with controllable shapes, Chem. Eng. J. 374 (2019) 1231–1240.
[90] J. Hwang, R.Y. Yan, M. Oschatz, B.V.K.J. Schmidt, Solvent mediated morphology control of zinc MOFs as carbon templates for application in supercapacitors, J. Mater. Chem. A 6 (2018) 23521–23530.
[91] D.R. Du Bois, A.J. Matzger, Reagent reactivity and solvent choice determine metal-organic framework microstructure during postsynthetic modification, J. Am. Chem. Soc. 143 (2021) 671–674.
[92] J. Sun, X.B. Yu, S.H. Zhao, H.M. Chen, K. Tao, L. Han, Solvent-controlled morphology of amino-functionalized bimetal metal-organic frameworks for asymmetric supercapacitors, Inorg. Chem. 59 (2020) 11385–11395.
[93] L. Zhang, H.J. Li, H.J. He, Y. Yang, Y.J. Cui, G.D. Qian, Structural variation and switchable nonlinear optical behavior of metal-organic frameworks, Small 17 (2021) 2006649.
[94] G. Lu, S.Z. Li, Z. Guo, O.K. Farha, B.G. Hauser, X.Y. Qi, Y. Wang, X. Wang, S.Y. Han, X.G. Liu, J.S. DuChene, H. Zhang, Q.C. Zhang, X.D. Chen, J. Ma, S.C. Loo, W. D. Wei, Y.H. Yang, J.T. Hupp, F.W. Huo, Imparting functionality to a metal-organic framework material by controlled nanoparticle encapsulation, Nat. Chem. 4 (2012) 310–316.
[95] H. Li, F.C. Meng, S.Y. Zhang, L.G. Wang, M. Li, L. Ma, W.N. Zhang, W.L. Zhang, Z. H. Yang, T.P. Wu, S. Lee, F.W. Huo, J. Lu, Crystal-growth-dominated fabrication of metal-organic frameworks with orderly distributed hierarchical porosity, Angew. Chem. Int. Ed. 132 (2020) 2478–2485.
[96] W.W. Xiong, Q.C. Zhang, Surfactants as promising media for the preparation of crystalline inorganic materials, Angew. Chem. Int. Ed. 54 (2015) 11616–11623.
[97] Q. Huang, Y.Y. Guo, D.D. Chen, L.J. Zhang, T.T. Li, Y. Hu, J.J. Qian, S.M. Huang, Rational construction of ultrafine noble metals onto carbon nanoribbons with efficient oxygen reduction in practical alkaline fuel cell, Chem. Eng. J. 424 (2021).
[98] X. Wang, A.R. Dong, Z.Y. Zhu, L.L. Chai, J.Y. Ding, L. Zhong, T.T. Li, Y. Hu, J.J. Qian, S.M. Huang, Surfactant-mediated morphological evolution of MnCo prussian blue structures, Small 16 (2020) 2004614.
[99] N. Wang, W.J. Ma, Y.C. Du, Z.Q. Ren, B.H. Han, L.J. Zhang, B.J. Sun, P. Xu, X.J. Han, Prussian blue microcrystals with morphology evolution as a high-performance photo-fenton catalyst for degradation of organic pollutants, ACS Appl. Mater. Interfaces 11 (2019) 1174–1184.
[100] Y.C. Tan, H.C. Zeng, Defect creation in HKUST-1 via molecular imprinting: attaining anionic framework property and mesoporosity for cation exchange applications, Adv. Funct. Mater. 27 (2017) 1703765.
[101] F. Yang, H. Mu, C.Q. Wang, L. Xiang, K.X. Yao, L.M. Liu, Y. Yang, Y. Han, Y.S. Li, Y.C. Pan, Morphological map of ZIF-8 crystals with five distinctive shapes: feature of filler in mixed-matrix membranes on C_3H_6/C_3H_8 separation, Chem. Mater. 30 (2018) 3467–3473.
[102] Y.Y. Li, J. Jiang, Y. Fang, Z.L. Cao, D.Y. Chen, N.J. Li, Q.F. Xu, J.M. Lu, TiO_2 nanoparticles anchored onto the metal-organic framework N_H2-MIL-88B(Fe) as an adsorptive photocatalyst with enhanced fenton-like degradation of organic pollutants under visible light irradiation, ACS Sustainable Chem. Eng. 6 (2018) 16186–16197.
[103] K.A. Colwell, M.N. Jackson, R.M. Torres-Gavosto, S. Jawahery, B. Vlaisavljevich, J.M. Falkowski, B. Smit, S.C. Weston, J.R. Long, Buffered coordination modulation as a means of controlling crystal morphology and molecular diffusion in an anisotropic metal-organic framework, J. Am. Chem. Soc. 143 (2021) 5044–5052.
[104] H. Bunzen, M. Grzywa, M. Hambach, S. Spirkl, D. Volkmer, From micro to nano: a toolbox for tuning crystal size and morphology of benzotriazolate-based metal-organic frameworks, Cryst. Growth Des. 16 (2016) 3190–3197.
[105] S.D. Marks, K. Riascos-Rodriguez, R.R. Arrieta-Pérez, A.A. Yakovenko, J. Exley, P.G. Evans, A.J. Hernández-Maldonado, Lattice expansion and ligand twist during CO_2 adsorption in flexible Cu bipyridine metal-organic frameworks, J. Mater. Chem. A 8 (2020) 18903–18915.
[106] S.Y. Zhang, H. Liu, C.C. Sun, P.F. Liu, L.C. Li, Z.H. Yang, X. Feng, F.W. Huo, X.H. Lu, CuO/Cu_2O porous composites: shape and composition controllable fabrication inherited from metal organic frameworks and further application in CO oxidation, J. Mater. Chem. A 3 (2015) 5294–5298.
[107] J.H. Park, J. Paczesny, N. Kim, B.A. Grzybowski, Shaping microcrystals of metal-organic frameworks by reaction-diffusion, Angew. Chem. Int. Ed. 59 (2020) 10301–10305.
[108] W.X. Guo, W.W. Sun, L.P. Lv, S.F. Kong, Y. Wang, Microwave-assisted morphology evolution of Fe-based metal-organic frameworks and their derived Fe_2O_3 nanostructures for Li-ion storage, ACS Nano 11 (2017) 4198–4205.
[109] F.Y. Zhang, J.L. Zhang, B.X. Zhang, L.R. Zheng, X.Y. Cheng, Q. Wan, B.X. Han, J. Zhang, CO_2 controls the oriented growth of metal-organic framework with highly accessible active sites, Nat. Commun. 11 (2020) 1431.
[110] Y.C. Lv, Z.L. Xiong, H.Y. Dong, C. Wei, Y.S. Yang, A. Ren, Z.Z. Yao, Y.B. Li, S.C. Xiang, Z.J. Zhang, Y.S. Zhao, Pure metal-organic framework microlasers with controlled cavity shapes, Nano Lett. 20 (2020) 2020–2025.
[111] J. Wu, J.H. Chen, C. Wang, Y. Zhou, K. Ba, H. Xu, W.Z. Bao, X.H. Xu, A. Carlsson, S. Lazar, A. Meingast, Z.Z. Sun, H.X. Deng, Metal-organic framework for transparent electronics, Adv. Sci. 7 (2020) 1903003.
[112] Y.X. Liu, Y.N. Wei, M.H. Liu, Y.C. Bai, X.Y. Wang, S.C. Shang, C.S. Du, W.Q. Gao, J.Y. Chen, Y.Q. Liu, Face-to-face growth of wafer-scale 2D semiconducting MOF films on dielectric substrates, Adv. Mater. 33 (2021) 2007741.
[113] X.J. Bai, X.Y. Lu, R. Ju, H. Chen, L. Shao, X. Zhai, Y.N. Li, F.Q. Fan, Y. Fu, W. Qi, Preparation of MOF film/aerogel composite catalysts via substrate-seeding secondary-growth for the oxygen evolution reaction and CO_2 cycloaddition, Angew. Chem. Int. Ed. 133 (2021) 711–715.
[114] K. Shen, L. Zhang, X.D. Chen, L.M. Liu, D.L. Zhang, Y. Han, J.Y. Chen, J. Long, R. Luque, Y.W. Li, B.L. Chen, Ordered macro-microporous metal-organic framework single crystals, Science 359 (2018) 206–210.
[115] N. Singh, S. Ahmed, A. Fakim, S. Qutub, O. Alahmed, O. El Tall, O. Shekhah, M. Eddaoudi, N.M. Khashab, In situ assembled ZIF superstructures via an emulsion-free soft-templating approach, Chem. Sci. 11 (2020) 11280–11284.
[116] L. Feng, J.L. Li, G.S. Day, X.L. Lv, H.C. Zhou, Temperature-controlled evolution of nanoporous MOF crystallites into hierarchically porous superstructures, Chem 5 (2019) 1265–1274.
[117] L.L. Chai, Z.Y. Hu, X. Wang, Y.W. Xu, L.J. Zhang, T.T. Li, Y. Hu, J.J. Qian, S.M. Huang, Stringing bimetallic metal-organic framework-derived cobalt phosphide composite for high-efficiency overall water splitting, Adv. Sci. 7 (2020) 1903195.
[118] C. Liu, Q. Sun, L.N. Lin, J. Wang, C.Q. Zhang, C.H. Xia, T. Bao, J.J. Wan, R. Huang, J. Zou, C.Z. Yu, Ternary MOF-on-MOF heterostructures with controllable architectural and compositional complexity via multiple selective assembly, Nat. Commun. 11 (2020) 4971.
[119] H.R. Chen, K. Shen, Y.P. Tan, Y.W. Li, Multishell hollow metal/nitrogen/carbon dodecahedrons with precisely controlled architectures and synergistically enhanced catalytic properties, ACS Nano 13 (2019) 7800–7810.
[120] Y. Katayama, M. Kalaj, K.S. Barcus, S.M. Cohen, Self-assembly of metal-organic framework (MOF) nanoparticle monolayers and free-standing multilayers, J. Am. Chem. Soc. 141 (2019) 20000–20003.
[121] S. Bai, B. Kim, C. Kim, O. Tamwattana, H. Park, J. Kim, D. Lee, K. Kang, Permselective metal-organic framework gel membrane enables long-life cycling of rechargeable organic batteries, Nat. Nanotechnol. 16 (2021) 77–84.
[122] L.L. Zou, M. Kitta, J.H. Hong, K. Suenaga, N. Tsumori, Z. Liu, Q. Xu, Fabrication of a spherical superstructure of carbon nanorods, Adv. Mater. 31 (2019) 1900440.
[123] L. Cao, P.C. Dai, J. Tang, D. Li, R.H. Chen, D.D. Liu, X. Gu, L.J. Li, Y. Bando, Y.S. Ok, X.B. Zhao, Y. Yamauchi, Spherical superstructure of boron nitride nanosheets derived from boron-containing metal-organic frameworks, J. Am. Chem. Soc. 142 (2020) 8755–8762.
[124] C. Avci, I. Imaz, A. Carne-Sanchez, J.A. Pariente, N. Tasios, J. Perez-Carvajal, M. I. Alonso, A. Blanco, M. Dijkstra, C. Lopez, D. Maspoch, Self-assembly of polyhedral metal-organic framework particles into three-dimensional ordered superstructures, Nat. Chem. 10 (2017) 78–84.
[125] M. Tu, D.E. Kravchenko, B. Xia, V. Rubio-Gimenez, N. Wauteraerts, R. Verbeke, I.F.J. Vankelecom, T. Stassin, W. Egger, M. Dickmann, H. Amenitsch, R. Ameloot, Template-mediated control over polymorphism in the vapor-assisted formation of zeolitic imidazolate framework powders and films, Angew. Chem. Int. Ed. 133 (2021) 7631–7636.
[126] X. Zhang, Y. Li, C.V. Goethem, K. Wan, W. Zhang, J.S. Luo, I.F.J. Vankelecom, J. Fransaer, Electrochemically assisted interfacial growth of MOF membranes, Matter 1 (2019) 1285–1292.
[127] A. Carne-Sanchez, I. Imaz, M. Cano-Sarabia, D. Maspoch, A spray-drying strategy for synthesis of nanoscale metal-organic frameworks and their assembly into hollow superstructures, Nat. Chem. 5 (2013) 203–211.
[128] Z.X. Cai, Z.L. Wang, Y.J. Xia, H. Lim, W. Zhou, A. Taniguchi, M. Ohtani, K. Kobiro, T. Fujita, Y. Yamauchi, Tailored catalytic nanoframes from metal-organic frameworks by anisotropic surface modification and etching for the hydrogen evolution reaction, Angew. Chem. Int. Ed. 133 (2021) 4797–4805.
[129] W. Xu, H. Chen, K.C. Jie, Z.Z. Yang, T.T. Li, S. Dai, Entropy-driven mechanochemical synthesis of polymetallic zeolitic imidazolate frameworks for CO_2 fixation, Angew. Chem. Int. Ed. 131 (2019) 5072–5076.
[130] Y. Wang, L. Li, L. Yan, X. Gu, P. Dai, D. Liu, J.G. Bell, G. Zhao, X. Zhao, K.M. Thomas, Bottom-up fabrication of ultrathin 2D Zr metal-organic framework nanosheets through a facile continuous microdroplet flow reaction, Chem. Mater. 30 (2018) 3048–3059.
[131] W.X. Liu, R.L. Yin, X.L. Xu, L. Zhang, W.H. Shi, X.H. Cao, Structural engineering of low-dimensional metal-organic frameworks: synthesis, properties, and applications, Adv. Sci. 6 (2019) 1802373.
[132] D.G. Madden, D. O'Nolan, N. Rampal, R. Babu, C. Camur, A.N. Al Shakhs, S.Y. Zhang, G.A. Rance, J. Perez, N.P.M. Casati, C. Cuadrado-Collados, D. O'Sullivan, N.P. Rice, T. Gennett, P. Parilla, S. Shulda, K.E. Hurst, V. Stavila, M.D. Allendorf, J. Silvestre-Albero, A.C. Forse, N.R. Champness, K.W. Chapman, D. Fairen-Jimenez, Densified HKUST–1 monoliths as a route to high volumetric and gravimetric hydrogen storage capacity, J. Am. Chem. Soc. 144 (2022) 13729–13739.

[133] M. Kasula, T. Le, A. Thomsen, M.R. Esfahani, Silver metal organic frameworks and copper metal organic frameworks immobilized on graphene oxide for enhanced adsorption in water treatment, Chem. Eng. J. 439 (2022).
[134] X.X. Lou, F.K. Zhi, X.Y. Sun, F. Wang, X.H. Hou, C.N. Lv, Q. Hu, Construction of co-immobilized laccase and mediator based on MOFs membrane for enhancing organic pollutants removal, Chem. Eng. J. 451 (2023).
[135] L.L. Li, X.C. Kang, M. He, A. Sheveleva, K. Hu, S.J. Xu, Y.Q. Zhou, J. Chen, S. Sapchenko, G. Whitehead, L. Lopez-Odriozola, L.S. Natrajan, E.J.L. McInnes, S. H. Yang, F. Tuna, Evolution of bismuth-based metal-organic frameworks for efficient electroreduction of CO_2, J. Mater. Chem. A 10 (2022) 17801.
[136] D.W. Cao, W.P. Kang, W.H. Wang, A. Sun, Y.Y. Wang, P. Ma, D.F. Sun, Okra-like Fe_7S_8/C@ZnS/N-C@C with core-double-shelled structures as robust and high-rate sodium anode, Small 16 (2020) 1907641.
[137] D.Q. Song, H.Z. Guo, K. Huang, H.Y. Zhang, J. Chen, L. Wang, C. Lian, Y. Wang, Carboxylated carbon quantum dot-induced binary metal-organic framework nanosheet synthesis to boost the electrocatalytic performance, Mater. Today 54 (2022) 42–51.
[138] D.D. Chen, L.S. Wei, Y.H. Yu, L. Zhao, Q.H. Sun, C. Han, J.M. Lu, H.G. Nie, L.X. Shao, J.J. Qian, Z. Yang, Size-selective suzuki-miyaura coupling reaction over ultrafine Pd nanocatalysts in a water-stable indium-organic framework, Inorg. Chem. 61 (2022) 15320–15324.
[139] K. Suresh, A.J. Matzger, Enhanced drug delivery by dissolution of amorphous drug encapsulated in a water unstable metal-organic framework (MOF), Angew. Chem. Int. Ed. 58 (2019) 16790–16794.
[140] M.X. Wu, Y.W. Yang, Metal-organic framework (MOF)-based drug/cargo delivery and cancer therapy, Adv. Mater. 29 (2017) 1606134.
[141] C. Crivello, S. Sevim, O. Graniel, C. Franco, S. Pane, J. Puigmarti-Luis, D. Munoz-Rojas, Advanced technologies for the fabrication of MOF thin films, Mater. Horiz. 8 (2021) 168–178.
[142] M. Usman, M. Ali, B. A. Al-Maythalony, A. S. Ghanem, O. W. Saadi, M. Ali, M. A. Jafar Mazumder, S. Abdel-Azeim, M. A. Habib, Z. H. Yamani, W. Ensinger. Highly efficient permeation and separation of gases with metal-organic frameworks confined in polymeric nanochannels. ACS Appl. Mater. Interfaces, 12 (2020), p. 49992-50001.
[143] C.H. Wang, A. Das, W.Y. Gao, D.C. Powers, Probing substrate diffusion in interstitial MOF chemistry with kinetic isotope effects, Angew. Chem. Int. Ed. 57 (2018) 3676–3681.
[144] C. Tan, M.C. Lee, M. Arshadi, M. Azizi, A. Abbaspourrad, A spiderweb-like metal-organic framework multifunctional foam, Angew. Chem. Int. Ed. 59 (2020) 9506–9513.
[145] K.K. Tu, B. Puertolas, M. Adobes-Vidal, Y.R. Wang, J.G. Sun, J. Traber, I. Burgert, J. Perez-Ramirez, T. Keplinger, Green synthesis of hierarchical metal-organic framework/wood functional composites with superior mechanical properties, Adv. Sci. 7 (2020) 1902897.
[146] J. Zhao, G. He, S. Huang, L.F. Villalobos, M. Dakhchoune, H. Bassas, K.V. Agrawal. Etching gas-sieving nanopores in single-layer graphene with an angstrom precision for high-performance gas mixture separation. Sci. Adv., 5 (2019), p. eaav1851.
[147] R. Makiura, O. Konovalov, Interfacial growth of large-area single-layer metal-organic framework nanosheets, Sci. Rep. 3 (2013) 1–8.
[148] H. Xiao, Z.X. Low, D.B. Gore, R. Kumara, M. Asadnia, Z.X. Zhong, Porous metal-organic framework-based filters: synthesis methods and applications for environmental remediation, Chem. Eng. J. 430 (2022).
[149] Z.H. Yuan, D.D. Meng, Y.Z. Wu, G.Q. Tang, P. Liang, J.H. Xin, D.D. Ye, Raman imaging-assisted customizable assembly of MOFs on cellulose aerogel, Nano Res. 15 (2022) 2599–2607.
[150] D.T. Lee, J.D. Jamir, G.W. Peterson, G.N. Parsons, Water-stable chemical-protective textiles via euhedral surface-oriented 2D Cu-TCPP metal-organic frameworks, Small 15 (2019) 1805133.
[151] C.P. Wang, H.Y. Liu, G. Bian, X.X. Gao, S.C. Zhao, Y. Kang, J. Zhu, X.H. Bu, Metal-layer assisted growth of ultralong quasi-2D MOF nanoarrays on arbitrary substrates for accelerated oxygen evolution, Small 15 (2019) 1906086.
[152] B.Y. Guan, L. Yu, X.W. Lou, Formation of single-holed cobalt/N-doped carbon hollow particles with enhanced electrocatalytic activity toward oxygen reduction reaction in alkaline media, Adv. Sci. 4 (2017) 1700247.
[153] L. Jiao, R. Zhang, G. Wan, W. Yang, X. Wan, H. Zhou, J.L. Shui, S.H. Yu, H.L. Jiang, Nanocasting SiO_2 into metal-organic frameworks imparts dual protection to high-loading Fe single-atom electrocatalysts, Nat. Commun. 11 (2020) 2831.
[154] L. Wang, S.R. Li, Y.Z. Chen, H.L. Jiang, Encapsulating copper nanocrystals into metal-organic frameworks for cascade reactions by photothermal catalysis, Small 17 (2021) 2004481.
[155] M.L. Pang, A.J. Cairns, Y.L. Liu, Y. Belmabkhout, H.C. Zeng, M. Eddaoudi, Synthesis and integration of Fe-soc-MOF cubes into colloidosomes via a single-step emulsion-based approach, J. Am. Chem. Soc. 135 (2013) 10234–10237.
[156] M.L. Hu, M.Y. Masoomi, A. Morsali, Template strategies with MOFs, Coordin. Chem. Rev. 387 (2019) 415–435.
[157] H.L. Huang, J.R. Li, K.K. Wang, T.T. Han, M.M. Tong, L.S. Li, Y.B. Xie, Q.Y. Yang, D.H. Liu, C.L. Zhong, An in situ self-assembly template strategy for the preparation of hierarchical-pore metal-organic frameworks, Nat. Commun. 6 (2015) 8847.
[158] Y.J. Zhao, L.L. Zheng, D. Jiang, W. Xia, X.T. Xu, Y. Yamauchi, J.P. Ge, J. Tang, Nanoengineering metal-organic framework-based materials for use in electrochemical CO_2 reduction reactions, Small 17 (2021) 2006590.
[159] C. Liu, J. Wang, J. Wan, C. Yu, MOF-on-MOF hybrids: synthesis and applications, Coordin. Chem. Rev. 432 (2021) 213743.
[160] K. Ikigaki, K. Okada, Y. Tokudome, T. Toyao, P. Falcaro, C.J. Doonan, M. Takahashi, MOF-on-MOF: oriented growth of multiple layered thin films of metal-organic frameworks, Angew. Chem. Int. Ed. 58 (2019) 6886–6890.
[161] D.D. Chen, Q. Huang, J.Y. Ding, T.T. Li, D. Yu, H.G. Nie, J.J. Qian, Z. Yang, Heteroepitaxial metal-organic frameworks derived cobalt and nitrogen codoped carbon nanosheets to boost oxygen reduction, J. Colloid Interf. Sci. 623 (2022) 1210–1219.
[162] H.H. Zhang, C. Gu, M.S. Yao, S. Kitagawa, Hybridization of emerging crystalline porous materials: synthesis dimensionality and electrochemical energy storage application, Adv. Energy Mater. 12 (2022) 2100321.
[163] S. Lee, S. Oh, M. Oh, Atypical Hybrid metal-organic frameworks (MOFs): a combinative process for MOF-on-MOF growth, etching, and structure transformation, Angew. Chem. Int. Edit. 132 (2020) 1343–1349.
[164] Y.F Gu, Y.N. Wu, L.C. Li, W. Chen, F.T. Li, S. Kitagawa. Controllable modular growth of hierarchical MOF-on-MOF architectures. Angew. Chem. Int. Edit., 129 (2017), p. 15864-15868.
[165] K. Ikigaki, K. Okada, Y. Tokudome, T. Toyao, P. Falcaro, C.J. Doonan, M. Takahashi, MOF-on-MOF: oriented growth of multiple layered thin films of metal-organic frameworks, Angew. Chem. Int. Edit. 131 (2019) 6960–6964.
[166] O. Kwon, J.Y. Kim, S. Park, J.H. Lee, J. Ha, H. Park, H.R. Moon, J. Kim, Computer-aided discovery of connected metal-organic frameworks, Nat. Commun. 10 (2019) 3620.
[167] N. Zhou, F.F. Su, C.P. Guo, L.H. He, Z.K. Jia, M.H. Wang, Q.J. Jia, Z.H. Zhang, S.Y. Lu, Two-dimensional oriented growth of Zn-MOF-on-Zr-MOF architecture: a highly sensitive and selective platform for detecting cancer markers, Biosens. Bioelectron. 123 (2019) 51–58.
[168] D.B. Yu, Q. Shao, Q.J. Song, J.W. Cui, Y.L. Zhang, B. Wu, L. Ge, Y. Wang, Y. Zhang, Y.Q. Qin, R. Vajtai, P.M. Ajayan, H.T. Wang, T.W. Xu, Y.C. Wu, A solvent-assisted ligand exchange approach enables metal-organic frameworks with diverse and complex architectures, Nat. Commun. 11 (2020) 927.
[169] Y.S. Wei, L.L. Zou, H.F. Wang, Y. Wang, Q. Xu, Micro/nano-scaled metal-organic frameworks and their derivatives for energy applications, Adv. Energy Mater. 12 (2021) 2003970.
[170] Z.L. Xu, G.W. Xiao, H.F. Li, Y. Shen, J. Zhang, T. Pan, X. Chen, B. Zheng, J.S. Wu, S. Li, W.N. Zhang, W. Huang, F.W. Huo, Compartmentalization within self-assembled metal-organic framework nanoparticles for tandem reactions, Adv. Funct. Mater. 28 (2018) 1802479.
[171] Y.N. Wu, F.T. Li, W. Zhu, J.C. Cui, C.A. Tao, C.X. Lin, P.M. Hannam, G.T. Li, Metal-organic frameworks with a three-dimensional ordered macroporous structure: dynamic photonic materials, Angew. Chem. Int. Ed. 50 (2011) 12518–12522.
[172] Y.B. He, Z. Chang, S.C. Wu, Y. Qiao, S.Y. Bai, K.Z. Jiang, P. He, H.S. Zhou, Simultaneously inhibiting lithium dendrites growth and polysulfides shuttle by a flexible MOF-based membrane in Li-S batteries, Adv. Energy Mater. 8 (2018) 1802130.
[173] Y. Wang, L.J. Li, H.M. Liang, Y.L. Xing, L.T. Yan, P.C. Dai, X. Gu, G.M. Zhao, X.B. Zhao, Superstructure of a metal-organic framework derived from microdroplet flow reaction: an intermediate state of crystallization by particle attachment, ACS Nano 13 (2019) 2901–2912.
[174] Q. Li, Z.W. Dai, J.B. Wu, W. Liu, T. Di, R. Jiang, X. Zheng, W.Z. Wang, X.X. Ji, P. Li, Z.H. Xu, X.P. Qu, Z.M. Xu, J. Zhou, Fabrication of ordered macro-microporous single-crystalline MOF and its derivative carbon material for supercapacitor, Adv. Energy Mater. 10 (2020) 1903750.
[175] S.X. Sun, X.P. Sun, Y. Liu, J. Peng, Y.G. Qiu, Y. Xu, J.X. Zhang, Q. Li, C. Fang, J.T. Han, Y.H. Huang, 3D hierarchical porous $Co_{1-x}S$@C derived from a ZIF-67 single crystals self-assembling superstructure with superior pseudocapacitance, J. Mater. Chem. A 7 (2019) 17248–17253.
[176] S.E. Habas, H. Lee, V. Radmilovic, G.A. Somorjai, P. Yang, Shaping binary metal nanocrystals through epitaxial seeded growth, Nat. Mater. 6 (2007) 692–697.
[177] Z.B. Liang, Y.X. Wu, J.Q. Cheng, Y.Q. Tang, J.M. Shi, T.J. Qiu, W. Li, S. Gao, R. Zhong, R.Q. Zou, A metal-organic framework nanorod-assembled superstructure and its derivative: unraveling the fast potassium storage mechanism in nitrogen-modified micropores, Small 17 (2021) 2100135.
[178] B.X. Yu, G. Ye, Z. Zeng, L. Zhang, J. Chen, S.Q. Ma, Mussel-inspired polydopamine chemistry to modulate template synthesis of 1D metal-organic framework superstructures, J. Mater. Chem. A 6 (2018) 21567–21576.
[179] F. Qiu, J.R. Edison, Z. Preisler, Y.F. Zhang, G. Li, A. Pan, C.H. Hsu, T.M. Mattox, P. Ercius, C. Song, K. Bustillo, M.A. Brady, E.W. Zaia, S. Jeong, J.B. Neaton, S. Du, S. Whitelam, J.J. Urban, Design rules for self-assembly of 2D nanocrystal/metal-organic framework superstructures, Angew. Chem. Int. Ed. 57 (2018) 13172–13176.
[180] T. Fukushima, S. Horike, H. Kobayashi, M. Tsujimoto, S. Isoda, M.L. Foo, Y. Kubota, M. Takata, S. Kitagawa, Modular design of domain assembly in porous coordination polymer crystals via reactivity-directed crystallization process, J. Am. Chem. Soc. 134 (2012) 13341–13347.
[181] L. Feng, K.Y. Wang, X.L. Lv, T.H. Yan, H.C. Zhou, Hierarchically porous metal-organic frameworks: synthetic strategies and applications, Natl. Sci. Rev. 7 (2020) 1743–1758.
[182] X.R. Wang, Z. Huang, J. Du, X.Z. Wang, N. Gu, X. Tian, Y. Li, Y.Y. Liu, J.Z. Huo, B. Ding, Hydrothermal preparation of five rare-earth (Re = Dy, Gd, Ho, Pr, and Sm) luminescent cluster-based coordination materials: the first MOFs-based ratiometric fluorescent sensor for lysine and bifunctional sensing platform for insulin and Al^{3+}, Inorg. Chem. 57 (2018) 12885–12899.

[183] Z.G. Hu, T. Kundu, Y.X. Wang, Y. Sun, K.Y. Zeng, D. Zhao, Modulated hydrothermal synthesis of highly stable MOF-808(Hf) for methane storage, ACS Sustainable Chem. Eng. 8 (2020) 17042–17053.
[184] Y.S. Wei, M. Zhang, R. Zou, Q. Xu, Metal-organic framework-based catalysts with single metal sites, Chem. Rev. 120 (2020) 12089–12174.
[185] S. Rojas-Buzo, B. Bohigues, C.W. Lopes, D.M. Meira, M. Boronat, M. Moliner, A. Corma, Tailoring lewis/brønsted acid properties of MOF nodes via hydrothermal and solvothermal synthesis: simple approach with exceptional catalytic implications, Chem. Sci. 12 (2021) 10106–10115.
[186] F.J. Claire, M.A. Solomos, J. Kim, G. Wang, M.A. Siegler, M.F. Crommie, T.J. Kempa, Structural and electronic switching of a single crystal 2D metal-organic framework prepared by chemical vapor deposition, Nat. Commun. 11 (2020) 5524.
[187] M. Krishtab, I. Stassen, T. Stassin, A.J. Cruz, O.O. Okudur, S. Armini, C. Wilson, S.D. Gendt, R. Ameloot, Vapor-deposited zeolitic imidazolate frameworks as gap-filling ultra-low-k dielectrics, Nat. Commun. 10 (2019) 3729.
[188] S. Han, R.A. Ciufo, M.L. Meyerson, B.K. Keitz, C.B. Mullins, Solvent-free vacuum growth of oriented HKUST-1 thin films, J. Mater. Chem. A 7 (2019) 19396–19406.
[189] T. Stassin, I. Stassen, J. Marreiros, A.J. Cruz, R. Verbeke, M. Tu, ~H. Reinsch, M. Dickmann, W. Egger, I.F.J. Vankelecom, D.E.D. Vos, R. Ameloot. Solvent-free powder synthesis and MOF-CVD thin films of the large-pore metal-organic framework MAF–6. Chem. Mater., 32 (2020), p. 1784-1793.
[190] K. Khaletskaya, S. Turner, M. Tu, S. Wannapaiboon, A. Schneemann, R. Meyer, A. Ludwig, G.V. Tendeloo, R.A. Fischer, Self-directed localization of ZIF-8 thin film formation by conversion of ZnO nanolayers, Adv. Funct. Mater. 24 (2014) 4804–4811.
[191] I. Stassen, M. Styles, G. Grenci, H.V. Gorp, W. Vanderlinden, S.D. Feyter, P. Falcaro, D.D. Vos, P. Vereecken, R. Ameloot, Chemical vapour deposition of zeolitic imidazolate framework thin films, Nat. Mater. 15 (2016) 304–310.
[192] X. Zhang, K. Wan, P. Subramanian, M.W. Xu, J.S. Luo, J. Fransaer, Electrochemical deposition of metal-organic framework films and their applications, J. Mater. Chem. A 8 (2020) 7569–7587.
[193] W.J. Li, J.F. Feng, Z.J. Lin, Y.L. Yang, Y. Yang, X.S. Wang, S.Y. Gao, R. Cao, Patterned growth of luminescent metal-organic framework films: a versatile electrochemically-assisted microwave deposition method, Chem. Commun. 52 (2016) 3951–3954.
[194] S. Zhou, Y.Y. Wei, L.B. Zhuang, L.X. Ding, H.H. Wang, Introduction of metal precursors by electrodeposition for the in situ growth of metal-organic framework membranes on porous metal substrates, J. Mater. Chem. A 5 (2017) 1948–1951.
[195] M. Kalaj, K.C. Bentz, S. Ayala Jr., J.M. Palomba, K.S. Barcus, Y. Katayama, S.M. Cohen, MOF-polymer hybrid materials: from simple composites to tailored architectures, Chem. Rev. 120 (2020) 8267–8302.
[196] H.Z. Yang, X. Wang, Secondary-component incorporated hollow MOFs and derivatives for catalytic and energy-related applications, Adv. Mater. 31 (2019) 1800743.
[197] Q. Zhang, Z.M. Wu, Y. Lv, Y.L. Li, Y.J. Zhao, R. Zhang, Y.S. Xiao, X.F. Shi, D.R. Zhang, R. Hua, J.L. Yao, J. Guo, R. Huang, Y. Cui, Z.H. Kang, S. Goswami, L. Robison, K. Song, X.H. Li, Y. Han, L.F. Chi, O.K. Farha, G. Lu, Oxygen-assisted cathodic deposition of zeolitic imidazolate frameworks with controlled thickness, Angew. Chem. Int. Ed. 58 (2019) 1123–1128.
[198] R.C. Wei, H.Y. Chi, X. Li, D.W. Lu, Y. Wan, C.W. Yang, Z.P. Lai, Aqueously cathodic deposition of ZIF-8 membranes for superior propylene/propane separation, Adv. Funct. Mater. 30 (2020) 1907089.
[199] D.K. Nguyen, I.M. Schepisi, F.Z. Amir, Extraordinary cycling stability of $Ni_3(HITP)_2$ supercapacitors fabricated by electrophoretic deposition: Cycling at 100,000 cycles, Chem. Eng. J. 378 (2019).
[200] K.D. Lu, T. Aung, N.N. Guo, R. Weichselbaum, W.B. Lin, Nanoscale metal-organic frameworks for therapeutic, imaging, and sensing applications, Adv. Mater. 30 (2018) 1707634.
[201] L. Zhong, J.Y. Ding, J.J. Qian, M.C. Hong, Unconventional inorganic precursors determine the growth of metal-organic frameworks, Coordin. Chem. Rev. 434 (2021).
[202] C. Avci-Camur, J. Troyano, J. Pérez-Carvajal, A. Legrand, D. Farrusseng, I. Imaz, D. Maspoch, Aqueous production of spherical Zr-MOF beads via continuous-flow spray-drying, Green Chem. 20 (2018) 873–878.
[203] J.Y. Shi, P. Zhu, S.F. Zhao, C. Xu, F. Yan, R.Q. Shen, H.M. Xia, H.Y. Jiang, S.Y. Xu, F. Q. Zhao, Continuous spheroidization strategy for explosives with micro/nano hierarchical structure by coupling microfluidics and spray drying, Chem. Eng. J. 412 (2021).
[204] Y.J. Du, J. Gao, L.Y. Zhou, L. Ma, Y. He, X.F. Zheng, Z.H. Huang, Y.J. Jiang, MOF-based nanotubes to hollow nanospheres through protein-induced soft-templating pathways, Adv. Sci. 6 (2019) 1801684.
[205] W. Zhu, Z. Chen, Y. Pan, R. Dai, Y. Wu, Z. Zhuang, D. Wang, Q. Peng, C. Chen, Y. D. Li, Functionalization of hollow nanomaterials for catalytic applications: nanoreactor construction, Adv. Mater. 31 (2019) 1800426.
[206] R.C. Arbulu, Y.B. Jiang, E.J. Peterson, Y. Qin, Metal-organic framework (MOF) nanorods, nanotubes, and nanowires, Angew. Chem. Int. Ed. 57 (2018) 5813–5817.
[207] R. Li, Y.P. Yuan, L.G. Qiu, W. Zhang, J.F. Zhu, A rational self-sacrificing template route to metal-organic framework nanotubes and reversible vapor-phase detection of nitroaromatic explosives, Small 8 (2012) 225–230.
[208] C. Avci, V. Guillerm, C. Carbonell, I. Imaz, D. Maspoch, Post-synthetic anisotropic wet-chemical etching of colloidal sodalite ZIF crystals, Angew. Chem. Int. Ed. 54 (2015) 14417–14421.
[209] W.X. Liu, J.J. Huang, Q. Yang, S.J. Wang, X.M. Sun, W.N. Zhang, J.F. Liu, F.W. Huo, Multi-shelled hollow metal-organic frameworks, Angew. Chem. Int. Ed. 56 (2017) 5512–5516.
[210] Y.S. Wei, M. Zhang, M. Kitta, Z. Liu, S. Horike, Q. Xu, A single-crystal open-capsule metal-organic framework, J. Am. Chem. Soc. 141 (2019) 7906–7916.
[211] X.C. Cai, X.R. Deng, Z.X. Xie, S.X. Bao, Y.S. Shi, J. Lin, M.L. Pang, M. Eddaoudi, Synthesis of highly monodispersed Ga-soc-MOF hollow cubes, colloidosomes and nanocomposites, Chem. Commun. 52 (2016) 9901–9904.
[212] T. Panda, S. Horike, K. Hagi, N. Ogiwara, K. Kadota, T. Itakura, M. Tsujimoto, S. Kitagawa, Mechanical alloying of metal-organic frameworks, Angew. Chem. Int. Ed. 56 (2017) 2413–2417.
[213] T.H. Wei, S.H. Wu, Y.D. Huang, W.S. Lo, B.P. Williams, S.Y. Chen, H.C. Yang, Y.S. Hsu, Z.Y. Lin, X.H. Chen, P.E. Kuo, L.Y. Chou, C.K. Tsung, F.K. Shieh, Rapid mechanochemical encapsulation of biocatalysts into robust metal-organic frameworks, Nat. Commun. 10 (2019) 5002.
[214] P.A. Julien, K. Uzarevic, A.D. Katsenis, S.A. Kimber, T. Wang, O.K. Farha, Y. Zhang, J. Casaban, L.S. Germann, M. Etter, R.E. Dinnebier, S.L. James, I. Halasz, T. Friscic, In situ monitoring and mechanism of the mechanochemical formation of a microporous MOF-74 framework, J. Am. Chem. Soc. 138 (2016) 2929–2932.
[215] M. Dinca, J.R. Long, High-enthalpy hydrogen adsorption in cation-exchanged variants of the microporous metal-organic framework $Mn_3[(Mn_4Cl)_3(BTT)_8(CH_3OH)_{10}]_2$, J. Am. Chem. Soc. 129 (2007) 11172–11176.
[216] J. Hou, C.W. Ashling, S.M. Collins, A. Krajnc, C. Zhou, L. Longley, D.N. Johnstone, P.A. Chater, S. Li, M.V. Coulet, P.L. Llewellyn, F.X. Coudert, D.A. Keen, P.A. Midgley, G. Mali, V. Chen, T.D. Bennett, Metal-organic framework crystal-glass composites, Nat. Commun. 10 (2019) 2580.
[217] V. Martinez, B. Karadeniz, S.M. Avdoshenko, M. Roslova, A.A. Popov, Tunable fulleretic sodalite MOFs: highly efficient and controllable entrapment of C_{60} fullerene via mechanochemistry, Chem. Mater. 32 (2020) 10628–10640.
[218] X.C. Li, Z.H. Zhang, W.M. Xiao, S.J. Deng, C. Chen, N. Zhang, Mechanochemistry-assisted encapsulation of metal nanoparticles in MOF matrices via a sacrificial strategy, J. Mater. Chem. A 7 (2019) 14504.
[219] G.J.H. Lim, Y. Wu, B.B. Shah, J.J. Koh, C.K. Liu, D. Zhao, A.K. Cheetham, J. Wang, J. Ding, 3D-printing of pure metal-organic framework monoliths, ACS Materials Lett. 1 (2019) 147–153.
[220] X.W. Zhu, J.M. Yang, X.J. She, Y.H. Song, J.C. Qian, Y. Wang, H. Xu, H.M. Li, Q.Y. Yan, Rapid synthesis of ultrathin 2D materials through liquid-nitrogen and microwave treatments, J. Mater. Chem. A 7 (2019) 5209–5213.
[221] W. Zhang, R. Li, H. Zheng, J.S. Bao, Y.J. Tang, K. Zhou, Laser-assisted printing of electrodes using metal-organic frameworks for micro-supercapacitors, Adv. Funct. Mater. 31 (2021) 2009057.
[222] H.Q. Jiang, S.Y. Jin, C. Wang, R.Q. Ma, Y.Y. Song, M.Y. Gao, X.T. Liu, A.G. Shen, G. J. Cheng, H.X. Deng, Nanoscale laser metallurgy and patterning in air using MOFs, J. Am. Chem. Soc. 141 (2019) 5481–5489.
[223] R.H. Dong, X.L. Feng, Making large single crystals of 2D MOFs, Nat. Mater. 20 (2021) 122–123.
[224] W.M. Liao, J.H. Zhang, S.Y. Yin, H. Lin, X. Zhang, J. Wang, H.P. Wang, K. Wu, Z. Wang, Y.N. Fan, M. Pan, C.Y. Su, Tailoring exciton and excimer emission in an exfoliated ultrathin 2D metal-organic framework, Nat. Commun. 9 (2018) 2401.
[225] J.H. Huang, P.Y. Wu, Controlled assembly of luminescent lanthanide–organic frameworks via post–treatment of 3D–printed objects, Nano-Micro Lett. 13 (2021) 15.
[226] M. Tu, B. Xia, D.E. Kravchenko, M.L. Tietze, A.J. Cruz, I. Stassen, T. Hauffman, J. Teyssandier, S. De Feyter, Z. Wang, R.A. Fischer, B. Marmiroli, H. Amenitsch, A. Torvisco, M.J. Velasquez-Hernandez, P. Falcaro, R. Ameloot, Direct X-ray and electron-beam lithography of halogenated zeolitic imidazolate frameworks, Nat. Mater. 20 (2021) 93–99.
[227] W.D. Fan, X. Wang, X.P. Liu, B. Xu, X.R. Zhang, W.J. Wang, X.K. Wang, Y.T. Wang, F.N. Dai, D.Q. Yuan, D.F. Sun, Regulating C_2H_2 and CO_2 storage and separation through pore environment modification in a microporous Ni-MOF, ACS Sustainable Chem. Eng. 7 (2018) 2134–2140.
[228] J. Dong, D. Zhao, Y. Lu, W.Y. Sun, Photoluminescent metal-organic frameworks and their application for sensing biomolecules, J. Mater. Chem. A 7 (2019) 22744–22767.
[229] H. Daglar, H.C. Gulbalkan, G. Avci, G.O. Aksu, O.F. Altundal, C. Altintas, I. Erucar, S. Keskin, Effect of metal-organic framework (MOF) database selection on the assessment of gas storage and separation potentials of MOFs, Angew. Chem. Int. Ed. 60 (2021) 7828–7837.
[230] G.R. Cai, P. Yan, L.L. Zhang, H.C. Zhou, H.L. Jiang, Metal-organic framework-based hierarchically porous materials: synthesis and applications, Chem. Rev. 121 (2021) 12278–12326.
[231] P. Pachfule, B.K. Balan, S. Kurungot, R. Banerjee, One-dimensional confinement of a nanosized metal organic framework in carbon nanofibers for improved gas adsorption, Chem. Commun. 48 (2012) 2009–2011.
[232] D. Kim, A. Coskun, Template-directed approach towards the realization of ordered heterogeneity in bimetallic metal-organic frameworks, Angew. Chem. Int. Ed. 56 (2017) 5071–5076.
[233] S. Chaemchuen, K. Zhou, N.A. Kabir, Y. Chen, X. Ke, G.V. Tendeloo, F. Verpoort, Tuning metal sites of DABCO MOF for gas purification at ambient conditions, Micropor. Mesopor. Mat. 201 (2015) 277–285.
[234] S.Y. Kim, S. Han, S. Lee, J.H. Kang, S. Yoon, W. Park, M.W. Shin, J. Kim, Y.G. Chung, Y.S. Bae, Discovery of high-performing metal-organic frameworks for on-board methane storage and delivery via LNG-ANG coupling: high-

throughput screening, machine learning, and experimental validation, Adv. Sci. 9 (2022) 2201559.
[235] K. Nath, A. Ahmed, D.J. Siegel, A.J. Matzger, Microscale determination of binary gas adsorption isotherms in MOFs, J. Am. Chem. Soc. 144 (2022) 20939–20946.
[236] Z. Niu, X.L. Cui, T. Pham, P.C. Lan, H. Xing, K.A. Forrest, L. Wojtas, B. Space, S. Ma, A metal-organic framework based methane nano-trap for the capture of coal-mine methane, Angew. Chem. Int. Ed. 58 (2019) 10138–10141.
[237] Z.B. Liang, C. Qu, W.H. Guo, R.Q. Zou, Q. Xu, Pristine metal-organic frameworks and their composites for energy storage and conversion, Adv. Mater. 30 (2018) 1702891.
[238] H. Hong, J.L. Liu, H.W. Huang, C.A. Etogo, X.F. Yang, B.Y. Guan, L. Zhang, Ordered macro-microporous metal-organic framework single crystals and their derivatives for rechargeable aluminum-ion batteries, J. Am. Chem. Soc. 141 (2019) 14764–14771.
[239] S. Sanati, R. Abazari, J. Albero, A. Morsali, H. Garcia, Z.B. Liang, R.Q. Zou, Metal-organic framework derived bimetallic materials for electrochemical energy storage, Angew. Chem. Int. Ed. 60 (2021) 11048–11067.
[240] G.R. Cai, W. Zhang, L. Jiao, S.H. Yu, H.L. Jiang, Template-directed growth of well-aligned MOF arrays and derived self-supporting electrodes for water splitting, Chem 2 (2017) 791–802.
[241] Y.L. Wu, X. Li, Y.S. Wei, Z. Fu, W. Wei, X.T. Wu, Q.L. Zhu, Q. Xu, Ordered macroporous superstructure of nitrogen-doped nanoporous carbon implanted with ultrafine Ru nanoclusters for efficient pH-universal hydrogen evolution reaction, Adv. Mater. 33 (2021) 2006965.
[242] Y.W. Li, M.T. Lu, Y.H. Wu, Q.H. Ji, H. Xu, J.K. Gao, G.D. Qian, Q.C. Zhang, Morphology regulation of metal-organic framework-derived nanostructures for efficient oxygen evolution electrocatalysis, J. Mater. Chem. A 8 (2020) 18215–18219.
[243] Z.J. Zhu, H.J. Yin, Y. Wang, C.H. Chuang, L. Xing, M. Dong, Y.R. Lu, G. Casillas-Garcia, Y. Zheng, S. Chen, Y. Dou, P. Liu, Q. Cheng, H. Zhao, Coexisting single-atomic Fe and Ni sites on hierarchically ordered porous carbon as a highly efficient ORR electrocatalyst, Adv. Mater. 32 (2020) 2004670.
[244] M. Luo, W. Sun, B.B. Xu, H. Pan, Y. Jiang, Interface engineering of air electrocatalysts for rechargeable zinc-air batteries, Adv. Energy Mater. 11 (2021) 2002762.
[245] E. Vijayakumar, S. Ramakrishnan, C. Sathiskumar, D.J. Yoo, J. Balamurugan, H. S. Noh, D. Kwon, Y.H. Kim, H. Lee, MOF-derived CoP-nitrogen-doped carbon@NiFeP nanoflakes as an efficient and durable electrocatalyst with multiple catalytically active sites for OER, HER, ORR and rechargeable zinc-air batteries, Chem. Eng. J. 428 (2022).
[246] L.L. Chai, L.J. Zhang, X. Wang, L.Q. Xu, C. Han, T.T. Li, Y. Hu, J.J. Qian, S.M. Huang, Bottom-up synthesis of MOF-derived hollow N-doped carbon materials for enhanced ORR performance, Carbon 146 (2019) 248–256.
[247] W.F. Zhai, Y.Y. Ma, D. Chen, J.C. Ho, Z.F. Dai, Y.Q. Qu, Recent progress on the long-term stability of hydrogen evolution reaction electrocatalysts, InfoMat. 4 (2022) 12357.
[248] H.F. Li, P. Wu, Y.W. Xiao, M. Shao, Y. Shen, Y. Fan, H.H. Chen, R.J. Xie, W.L. Zhang, S. Li, J.S. Wu, Y. Fu, B. Zheng, W.N. Zhang, F.W. Huo, Metal-organic frameworks as metal ion precursors for the synthesis of nanocomposites for lithium-ion batteries, Angew. Chem. Int. Ed. 59 (2020) 4763–4769.
[249] R.S. Gao, J. Tang, X.L. Yu, S. Tang, K. Ozawa, T. Sasaki, L.C. Qin, In situ synthesis of MOF-derived carbon shells for silicon anode with improved lithium-ion storage, Nano Energy 70 (2020).
[250] C.L. Liu, Y. Bai, W.T. Li, F.Y. Yang, G.X. Zhang, H. Pang, In situ growth of three-dimensional mxene/metal-organic framework composites for high-performance supercapacitors, Angew. Chem. Int. Ed. 61 (2022) e202116282.
[251] M.D. Zhang, Q.B. Dai, H.G. Zheng, M.D. Chen, L.M. Dai, Novel MOF-derived Co@N-C bifunctional catalysts for highly efficient Zn-Air batteries and water splitting, Adv. Mater. 30 (2018) 1705431.
[252] M. Du, P.B. Geng, C.X. Pei, X.Y. Jiang, Y.Y. Shan, W.H. Hu, L.B. Ni, H. Pang, High-entropy prussian blue analogues and their oxide family as sulfur hosts for lithium-sulfur batteries, Angew. Chem. Int. Ed. 61 (2022) e202209350.
[253] W.T. Li, X.T. Guo, P.B. Geng, M. Du, Q.L. Jing, X.D. Chen, G.X. Zhang, H.P. Li, Q. Xu, P. Braunstein, H. Pang, Rational design and general synthesis of multimetallic metal-organic framework nano-octahedra for enhanced Li-S battery, Adv. Mater. 33 (2021) 2105163.
[254] C.Q. Qiao, R.L. Zhang, Y.D. Wang, Q. Jia, X.F. Wang, Z. Yang, T.F. Xue, R.C. Ji, X.F. Cui, Z.L. Wang, Rabies virus-inspired metal-organic frameworks (MOFs) for targeted imaging and chemotherapy of glioma, Angew. Chem. Int. Ed. 59 (2020) 16982–16988.
[255] T.G.W. Edwardson, D. Hilvert, Virus-inspired function in engineered protein cages, J. Am. Chem. Soc. 141 (2019) 9432–9443.